DOE/MC/26372-3863
(DE94004144)
Distribution Category UC-106

Development of Hollow Fiber Catalytic Membrane Reactors for High Temperature Gas Cleanup

Final Report
September 1989 - March 1994

Yi Hua Ma
W. R. Moser
S. Pien
A. B. Shelekhin

Work Performed Under Contract No.: DE-AC21-89MC26372

For
U.S. Department of Energy
Office of Fossil Energy
Morgantown Energy Technology Center
P.O. Box 880
Morgantown, West Virginia 26507-0880

By
Worcester Polytechnic Institute
Chemical Engineering Department
100 Institute Road
Worcester. Massachusetts 01609

July 1994

DISCLAIMER

CONTENTS

I. INTRODUCTION

The technology employed in the Integrated Gasification Combined Cycle (IGCC) permits burning coals with a wide range of sulfur contents. Emissions from the process should be reduced by an order of magnitude below stringent federal air quality regulations for coal-fired plants. The maximum thermal efficiency of this type of process can be achieved by removing sulfur and particulates from the high temperature gas (e.g., 800 °C to 900 °C). High temperature sulfur removal can be accomplished with sorbents or by using membrane reactors. Catalytically active membrane reactors offer an inherent ability to combine reaction, product concentration and separation in a single unit operation. The conversion of H_2S is limited by the thermodynamic equilibrium of the reaction but can, in principle, be improved by the removal of products (e.g., H_2) during reaction. Here, selective removal of hydrogen could be provided by the membrane during reaction so that the reaction is continuously driven toward the product side. As the membrane is more permeable to H_2, the reaction can be shifted to almost complete conversion.

Severe conditions encountered in the IGCC process (e.g., 900 °C, containing of H_2S, CO_2 and H_2O) make it impossible to use polymeric membranes in the process. A list of inorganic membranes that can be employed in the membrane reactor includes Pd metallic membranes, molecular-sieve glass membranes (PPG Industries), porous Vycor glass membranes and porous sol-gel derived membranes such as alumina, zirconia. Alumina and zirconia membranes, however, cannot withstand for a long time at high temperatures in the presence of water vapors. Palladium membranes are a very promising class of inorganic membranes for gas separations that is currently under development. In this project two different types of membranes were used in the design of the membrane reactor - molecular-sieve glass membrane and Vycor glass porous membrane.

The concept of the membrane reactor was under development for three decades [1]. The conversion of an equilibrium reaction can be increased in the membrane reactor if products of the reaction are selectively removed from the reaction zone by means of a semipermeable membrane. To achieve the shift in the equilibrium, at least one reaction product should be more permeable than the reactants. Usually, this condition limits the application of the membrane

reactors to the reactions in which highly permeable gases are produced (e.g., H_2) during the reaction. Hydrogen can be separated by porous or palladium/platinum membranes that are available commercially. For gases that are heavier than H_2, the porous membranes, with selectivity factors not exceeding the Knudsen selectivity factors, cannot provide efficient separation to carry out simultaneous reaction and separation. To overcome this limitation intensive research programs are being carried out, aimed at developing molecular sieve and composite metal membranes that may provide much higher selectivity factors [2-4].

Reactions of dehydrogenation are the most frequently studied gas phase reactions that are used as examples for the demonstration of the membrane reactor superiority over the conventional packed-bed reactors. A process for dehydrogenation of hydrocarbons in membrane reactors with palladium membranes was introduced by Pfefferle [1]. This work was broadened by Gryaznov and coworkers [5-9] where platinum/palladium alloy membranes were used to carry out the reactions of dehydrogenation [6,7] and several hydrogenation reactions [5,8]. Most recently, palladium alloy metallic membranes were intensively studied by several research groups in Japan [10-12]. In all these publications it was displayed that the conversion in the membrane reactors can be increased, compared to the packed bed reactors, in certain cases up to 100%.

Due to high capital investments on the membrane reactors with platinum/palladium alloy membranes no large scale commercialization projects of the membrane reactors have been reported yet. An additional drawback of the metal membranes is their poisoning by sulfuric compounds. This limitation can be overcome if a composite Pt membranes are used [4]. It was shown by Edlund and Pledger [4,13] that the Pt composite membrane can operate for a prolonged time even in the atmosphere of pure H_2S. Porous alumina and silica membranes with pore size range 40-100 Å are also obvious candidates for using in the high temperature membrane reactors because of their chemical and thermal stability. Several publications have been devoted on studies of the membrane reactors with the porous membranes [14-16]. Most of the reported reactions were the dehydrogenation reactions.

The reaction of hydrogen sulfide decomposition in the membrane reactor was intensively studied because of its great environmental importance [4,13,17,18]. Some results, however, cannot be easily interpreted. For example, the hydrogen concentration on the permeate side was compared to the equilibrium conversion on the shell side and was found twice as high [17]. Such

a comparison may not be appropriate in this case. The equilibrium of the H_2S decomposition reaction depends on the pressure and the conversion on the permeate side must be higher as the partial pressure of the reactant on this side is lower.

The **objective** of this project was to develop economically and technically viable catalytic membrane reactors for high temperature, high pressure gaseous contaminant control in IGCC systems. These catalytic membrane reactors decompose H_2S and separate the reaction products. The reactors were designed to operate in the hostile process environment of the IGCC systems, and at temperatures ranging from 500 to 1000 °C.

II. EXPERIMENTAL INSTALLATIONS

2.1 Permeability measurements installation

Two types of experimental installations were used for experimental determinations of the gas permeability in molecular-sieve membranes (Figures 1 and 2). In one installation high accuracy pressure transducers were used to monitor the pressure increase in the downstream chamber. Permeation rates of different gases can then be calculated from the time dependence of the pressure in the downstream chamber. The installation operated at temperatures up to 250 °C (Figure 1). The membrane module was designed as a tube in which seven hollow fibers were glued by Duralco high temperature resistant epoxy cement (stable up to 250 °C) from both sides of the module. The penetrant was supplied from inside the fibers. The permeate was collected at the shell side. Inlet pressure was measured with a Datametrics pressure transducer with an accuracy of ± 1 Torr. Pressure in the downstream permeate chamber was measured with a pressure transducer with an accuracy of ± 0.1 Torr. The data on pressure in the downstream chamber as a function of time were collected and stored in a personal computer. The membrane module was heated with heating tape wrapped around the module. The temperature of the module was controlled with an Omega CN-9000 temperature controller to an accuracy of ± 0.2 °C. The installation was maintained at room temperature, 25 °C. Permeability coefficients were measured in the temperature range 30-250 °C and at pressures up to 2 MPa.

Another installation was designed to analyze the permeability of gas mixtures at temperatures up to 1000 °C (Figure 2). Ten hollow fiber glass membranes were fixed inside the stainless steel module. The feed was supplied from the fibers lumen. Permeability of He and N_2 was studied. When the permeability of pure gases was measured the tube side outlet was blocked and the transmembrane flow was measured with a bubble flowmeter. Temperature dependencies of the permeability was tested in-situ at temperatures up to 1000 °C.

2.2 Membrane reactor installation

Porous glass membranes with 40 Å pore diameter were used in the design of the membrane reactor. The membranes were provided by Asahi Glass Co. and Corning Glass Co. Inside and outside diameters of the membrane were ID/OD=4.5/6.0 mm respectively. Pure

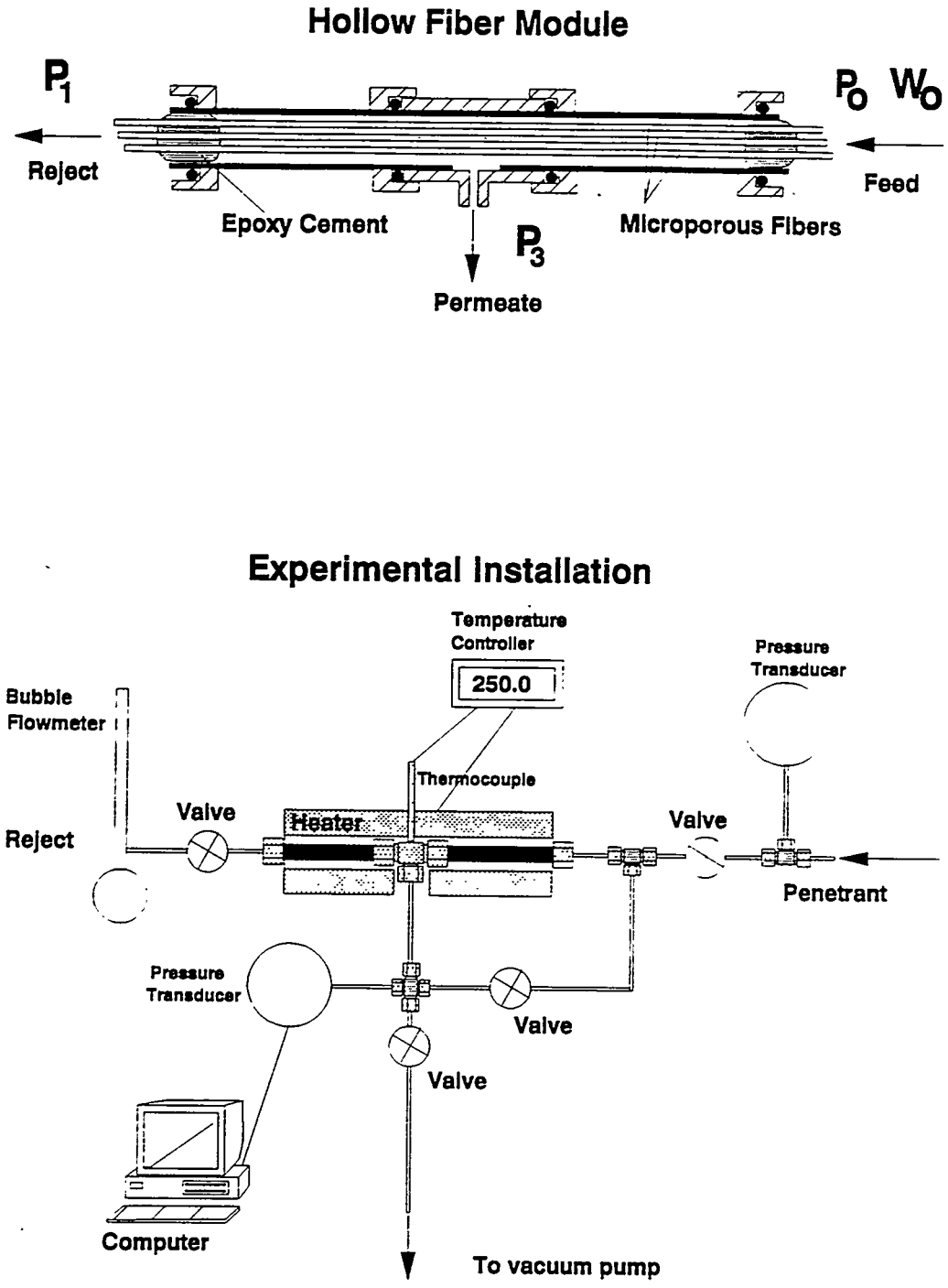

Figure 1. Schematic diagram of the experimental installation for permeability measurements in molecular-sieve hollow fiber glass fibers.

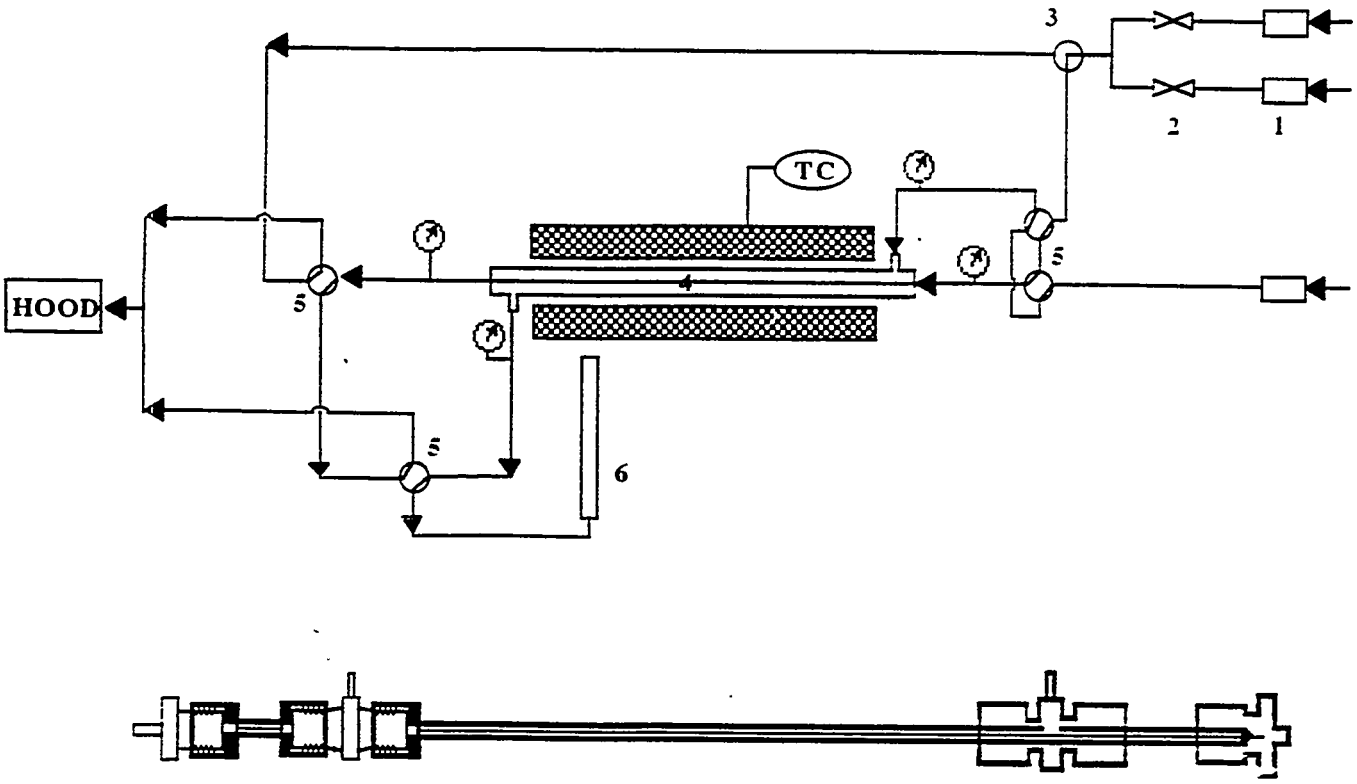

1. Mass Flow Controller 2. Check Valve 3. Three-Way-Valve
4. Hollow Fiber Membrane Reactor 5. Four-Way-Valve 6. Bubble Flow Meter

Figure 2. Experimental installation for high temperature in-situ permeability measurements in hollow fiber glass membranes.

hydrogen sulfide (purity 99.5%), 8.6% H_2S in N_2, 1.1% H_2S in N_2, and 500 ppm H_2S in N_2 gas mixtures were used in the experiments. Molybdenum sulfide (MoS_2) was acquired from Johnson-Matthey and used as the catalyst. The catalyst particles were prepared by compressing the catalyst powder into tablets followed by grinding and sieving.

A schematic diagram of the experimental installation used in this study is presented in Figure 3. Quartz tubes with OD/ID=16/13 mm were used as the reactor shells. One end of the membrane was fixed to the quartz tube with epoxy resin Duralco 4525 (Cotronics) stable up to a temperature of 250 °C. The other end of the membrane was sealed with the same epoxy. The feed gas mixture was supplied on the shell side of the membrane reactor. The furnace was 15 cm long. The porous glass membrane and the quartz tube were 30 cm long. The length of the permeable part of the membrane in the membrane reactor was equal to 22 cm (Figure 4). The temperature in the furnace was controlled by a thermocontroller. The gas composition on the shell and on the tube sides of the membrane reactor was analyzed with the Hewlett Packard HP5890 GC. The pressure in the sampling loop was controlled with a specially designed vacuum gas sampling system to provide reliability and accuracy in a wide range of gas concentrations. The reactor ends were cooled by air flow to prevent overheating and decomposition of the epoxy resin. Flow rates on the feed and shell sides were measured with a bubble flowmeter. The weight of the MoS_2 used in the packed bed was equal to 11 g in both packed bed and membrane reactors. The pressure on the shell side of the membrane reactor was kept at either 2.36 atm (20 psi) or 7.8 atm (100 psi) while the pressure on the tube side of the membrane was kept atmospheric. Before the experimental runs the system was kept at 800 °C in a feed gas flow for 24 hours.

Temperature profile inside the membrane reactor is presented in Figure 5. The packed portion of the membrane reactor was positioned in the hottest zone of the reactor with the temperature variations from 750 °C to 800 °C. The temperature profile inside the membrane tube (tube side) was almost identical to the temperature profile inside the packed bed (shell side) (Figure 5).

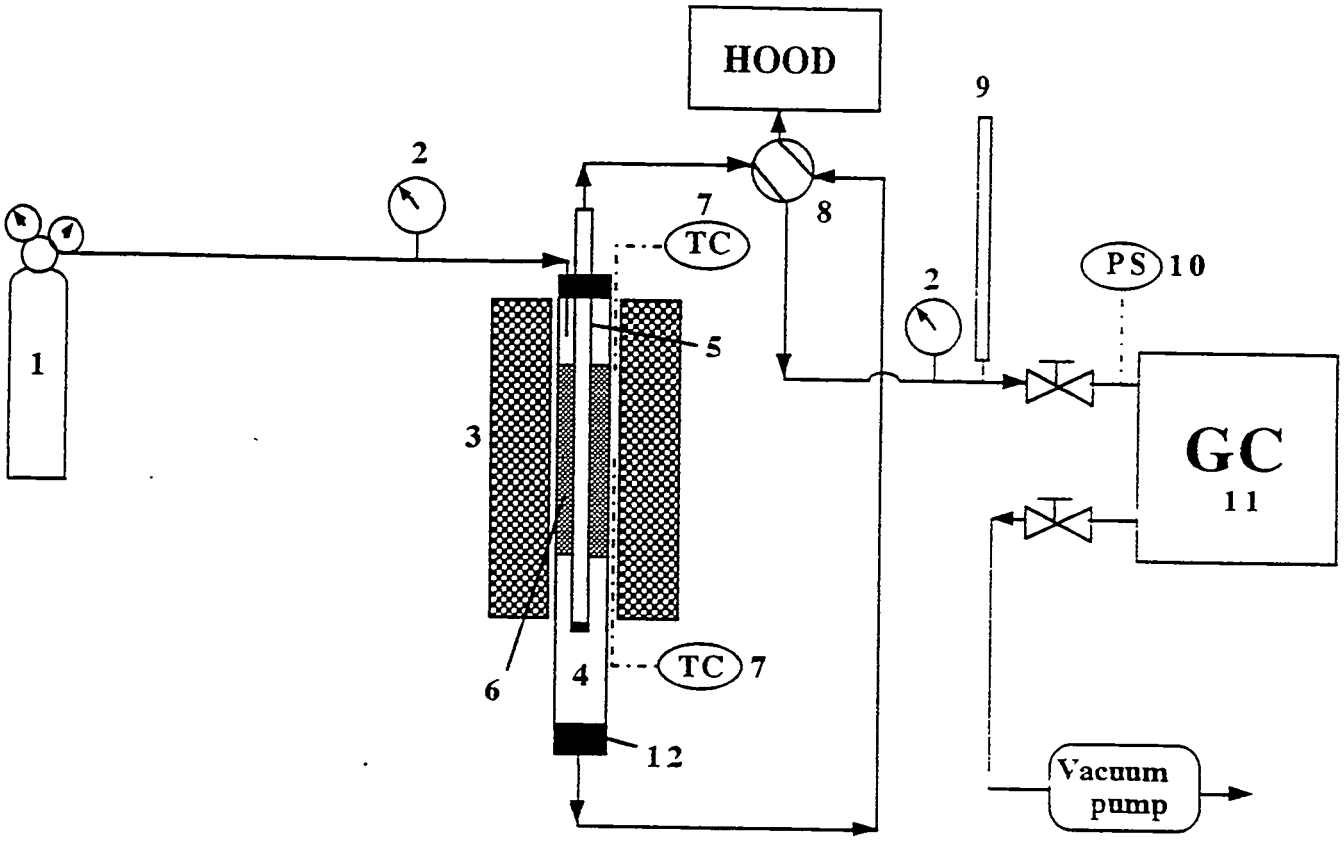

1- Feed. 2- Pressure gage, 3- Furnace, 4- Membrane/packed-bed reactor. 5- Porous Vycor glass membrane. 6- Catalyst (MoS_2), 7- Thermocouple. 8- 4-way-valve, 9- Bubble flow meter. 10- Pressure sensor. 11- Gas chromatograph, 12- Epoxy resin.

Figure 3. Schematic diagram of the membrane reactor experimental installation.

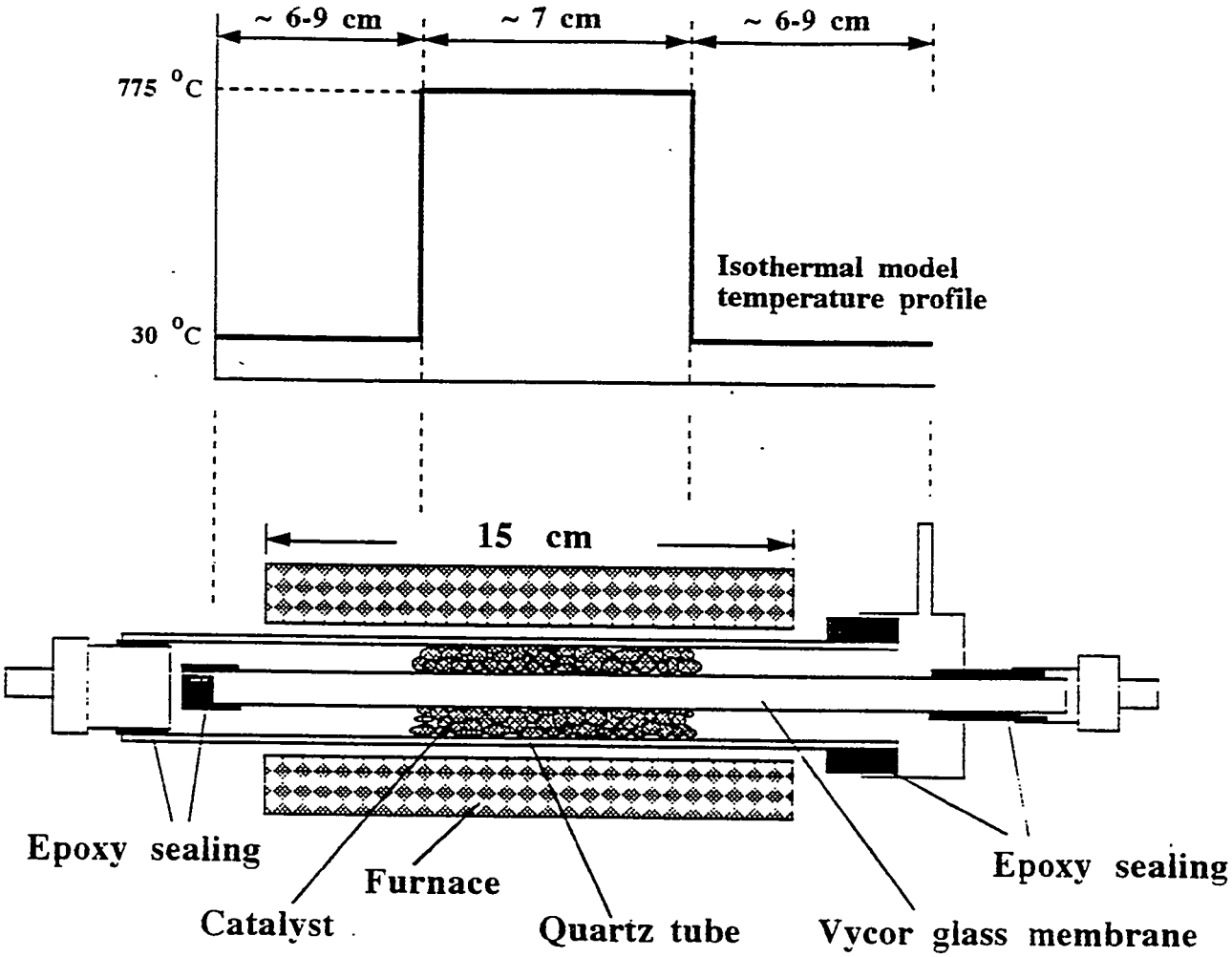

Figure 4. Membrane reactor module.

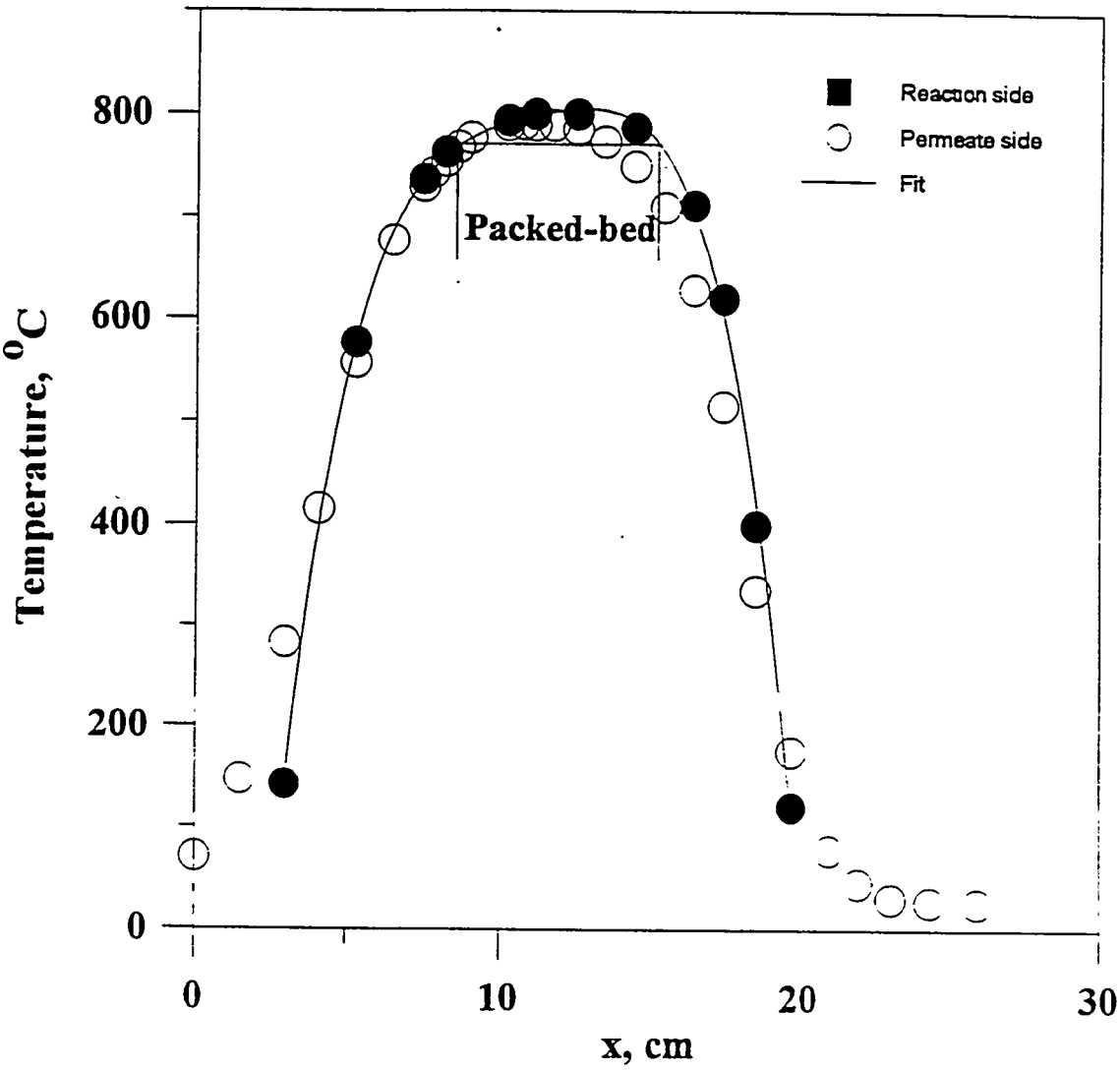

Figure 5. Temperature profile in the membrane reactor.

III. POROUS GLASS MEMBRANES

3.1 Molecular-sieve glass membranes

Major characteristics of the microporous glass membranes are listed in Table 1. Based on adsorption data [31], structural analysis [32], and permeability data [3] it was possible to make an estimate of the pore diameter in the glass membrane (Figure 6). Due to the specifics of the membrane preparation technique, pores with approximate diameter equal to 15 ± 5Å are formed. The diameter was estimated from the data on gas adsorption and surface of the membrane. Further consideration of the previous results suggests that the large pores (~ 15 Å) are interconnected with pore necks which are smaller in diameter (~ 5 Å). Interconnected pores inside the membrane create a tortuous diffusion path. The difference in the pore size between these connections and the larger pores creates an activation barrier for gas diffusion.

3.1.1 Gas concentration in molecular-sieve glass membrane

A mathematical model of gas diffusion in molecular-sieve glass membranes was developed in our previous publications [19].

The total concentration of the gas inside the pores of the microporous glass membrane is determined as

$$C_T = C_a + C_g \qquad (1)$$

where C_T is the total concentration inside the pores, C_a is the concentration in the adsorbed layer, C_g is the concentration in the gas phase inside the pores. At high temperatures, which are of interest for the development of the IGCC process, the total concentration is determined only by the gas phase inside the membrane porous structure, then

$$C_T \approx C_g = \frac{p\ \theta}{RT} \qquad (2)$$

where θ is the porosity of the membrane.

At low temperatures the total concentration inside the pores is determined primarily by the concentration in the adsorbed phase. It was found by Bhandarkar et al. [31] that the

Table 1. Characteristics of the microporous glass membranes [1,2,4-6,14].

Property	*Value*
Pore diameter, d_p	5-20 Å
Surface area	700-1000 m^2/cm^3
Micropore volume	0.11-0.3 cm^3/g
Temperature stability	≈300 °C
Chemical stability	Except in HF
Porosity	15-40 %
Membrane structure	symmetrical
Hollow fiber OD/ID	32/22 μm
Crystallinity	100% amorphous
Chemical composition	SiO_2 + (TiO_2)

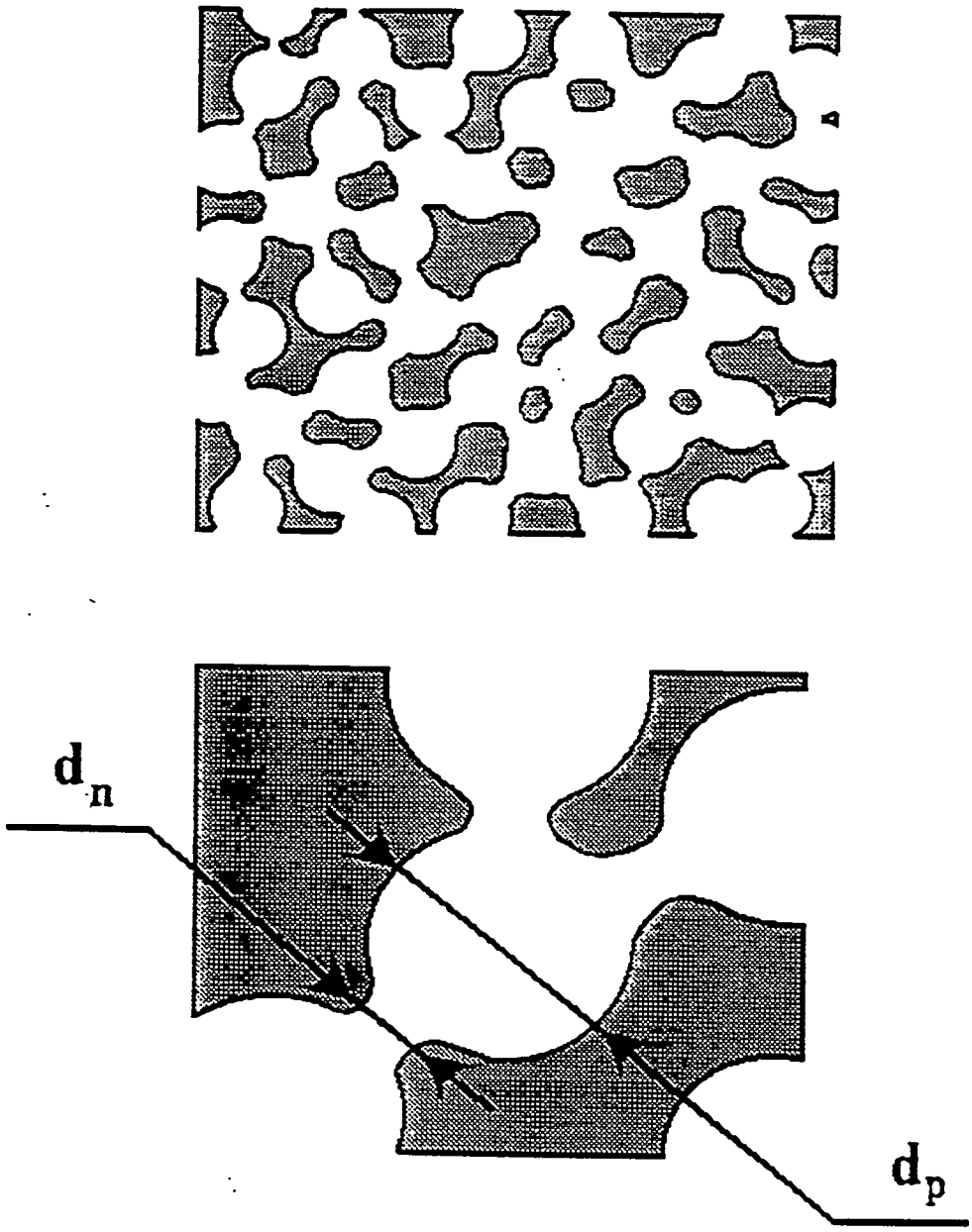

Figure 6. Pore structure of the microporous molecular-sieve glass membrane.

adsorption inside the pores of the molecular-sieve glass membranes is described in accord ingto the Dubinin-Radushkevich model

$$C_T \approx C_a = W\xi/V_m$$

$$W = W_o \exp(-Ae^2/\beta^2)$$

where V_m is the molar volume of the adsorbate in the adsorbed state. ξ is the density of the porous medium, W_o is the limiting pore volume, A and β coefficients.

3.1.2 Diffusion coefficients

If the diffusion proceeds in a medium with some spatial restrictions such as the pore walls, pore openings, etc., the equation for the diffusion coefficient is

$$D = \lambda \rho \bar{u} \qquad (3)$$

where ρ is the probability that the diffusant makes a jump. The jump is of length λ. This probability is governed by geometrical and energetical factors and can be represented in the form

$$\rho = \rho_g \rho_E = \rho_g \exp\left(-\frac{\Delta E}{RT}\right) \qquad (4)$$

where ρ_g is the probability that the gas molecule jumps in the desired direction or the geometric probability, and ρ_E is the probability that the molecule has kinetic energy sufficient to surmount the energy barrier ΔE. If the obstruction in the way of the diffusant molecule is rigid so that the diffusant will bounce off during the collision, then ρ_g can be calculated from

$$\rho_g = \frac{1}{3}\frac{S_n}{S_p} \qquad (5)$$

where S_n is the area of the pore opening that leads to another pore (cross-section of the neck), S_p is the cross-sectional area of the pore. For example, if the diffusant is moving inside a spherical cavity of diameter d_p with a hole on it having diameter d_n, then the probability that the

particle will jump through the hole, ρ_g, is

$$\rho_g = \frac{1}{3}\frac{(\pi d_n^2/4)}{(\pi d_p^2/4)} = \frac{1}{3}\frac{d_n^2}{d_p^2}, \qquad d_n < d_p \tag{6}$$

If the diffusant moves in 3-D space without spatial obstructions then the geometrical probability is $\rho_g = 1/3$. For non-spherical molecules more complex expressions, rather than Equation 5, should be used, taking into account the probability that the non-spherical gas molecule will be oriented in the right way before entering the hole. This phenomenon is known as the shape selectivity of the molecular sieves.

Substituting expressions for the energetical probability ρ_E and the mean free velocity $\bar{u}$ into Equation 12 and taking $\lambda = d_p$, one gets an expression for the diffusion coefficient

$$D = \rho_g d_p \left(\frac{8RT}{\pi M}\right)^{1/2} e^{-\frac{\Delta E}{RT}} \tag{7}$$

For configurational diffusion the diffusion coefficient depends not only on the size of the diffusant but on its shape as well. In principle, configurational diffusion is simply an activated process where the geometrical probability and the activation energy are determined by the geometry of the pore opening. It is also important to note that the representation of the experimental results for the gas diffusion coefficient in the simplified Arrhenius form

$$D = D_o e^{-\frac{\Delta E}{RT}} \tag{8}$$

should only be regarded as an empirical fit of experimental data.

3.1.3 Permeability coefficients

The permeability coefficient in straight pores is

$$P_s = \frac{J_s \cdot L}{\Delta p} \tag{9}$$

where P_s and J_s are the permeability coefficient and the transmembrane flux respectively in straight pores.

For any transport process the driving force is the gradient of the chemical potential

$$J_s = -Bc\frac{\partial \mu}{\partial x} \qquad (10)$$

where B is the mobility, c is the concentration, μ is the chemical potential. Then, the diffusion coefficient is determined by (taking $\mu = \mu^{\circ} + RT\ln p$)

$$D_F = BRT\frac{d\ \ln(p)}{d\ \ln(c)} = D_c\frac{d\ \ln(p)}{d\ \ln(c)} \qquad (11)$$

where D_c is the corrected diffusivity that may or may not depend on the concentration, and D_F is the Fickian diffusivity.

For the adsorbed phase the derivative of the Dubinin Radushkevich adsorption equation is

$$\frac{d\ \ln(p)}{d\ \ln(c)} = \frac{1}{2A/\beta^2 (RT)^2 \ln(p_o/p)} \qquad (12)$$

and the corrected diffusivity in the adsorbed phase is given by

$$D_{ads} = \frac{D_{c,ads}}{\left(2A/\beta^2 (RT)^2 \ln(p_o/p)\right)} \qquad (13)$$

For the gas phase the derivative is

$$\frac{d\ \ln(p)}{d\ \ln(c)} = 1 \qquad (14)$$

and the corrected diffusivity is independent of the pressure ($D_{c,gas} = D_{gas}$). Additionally, a correction coefficient, accounting for the differences between the transmembrane flux in membranes with random porous structures, and the flux in straight channels, should be included in Equation 11.

According to [20] the flux in the porous medium is

$$\frac{J_s}{J}=\frac{\tau}{\theta} \qquad (15)$$

where θ is the porosity, and τ is the tortuosity.

An expression for the total transmembrane flux can be written as follows

$$J=-\left(D_{ads}\frac{dC_{ads}}{dp}+D_{gas}\frac{dC_{gas}}{dp}\right)\frac{\theta}{\tau}\frac{dp}{dx}=-\left(D_{c,ads}\frac{d\ln(p)}{d\ln(C_{ads})}\frac{dC_{ads}}{dp}+\frac{D_{c,gas}}{RT}\right)\frac{\theta}{\tau}\frac{\Delta p}{L} \qquad (16)$$

where $D_{c,ads}$ and $D_{c,gas}$ are the corrected diffusion coefficients in the adsorbed and gas phases respectively, and J is the transmembrane flux across the membrane. The structure of the porous medium need not be defined in Equation 16 because it is being accounted for by the porosity and the tortuosity factor. For example, if the diffusion channels are straight and closely packed, then $\tau=1$ while $\theta=0.95$. Similarly, in the microporous glass membrane with $\theta=0.22$ the tortuosity factor is $\tau=25\pm5$ [20]. In the Vycor glass membrane with $\theta=0.3$ the tortuosity factor is $\tau=5.9\pm0.3$ [21].

Both of the diffusion coefficients, $D_{c,ads}$ and $D_{c,gas}$, are governed by the geometrical and energetical probabilities. Taking these into account, the permeability coefficient can be presented as

$$P=D_{c,ads}\frac{d\ln(p)}{d\ln(C_{ads})}\frac{\theta}{\tau}\frac{dC_{ads}}{dp}+\frac{\theta}{\tau}\frac{D_{c,gas}}{RT} \qquad (17)$$

$$D_{c,ads}=\rho_g d_p\left(\frac{8RT}{\pi M}\right)^{1/2}e^{-\frac{\Delta E_{ads}}{RT}} \qquad (18)$$

$$D_{c,gas}=\rho_g d_p\left(\frac{8RT}{\pi M}\right)^{1/2}e^{-\frac{\Delta E_{gas}}{RT}} \qquad (19)$$

The terms dC_{ads}/dp and 1/RT are analogous to the "solubility" coefficient, which is commonly used to describe the permeability of polymeric membranes. The term 1/RT at 0 °C is equal to 1 m^3(STP)/m^3(pore).atm or θ m^3(STP)/m^3(membrane).atm. As the temperature

increases the "solubility" decreases. For the majority of permanent gases such as H_2, He, N_2, O_2, Ar, etc. the permeability coefficient is simply

$$P=d_p\rho_g\left(\frac{8}{\pi MRT}\right)^{1/2}\frac{\theta}{\tau}e^{-\frac{\Delta E_{gas}}{RT}} \qquad (20)$$

For large straight pores $\Delta E_{gas} \rightarrow 0$, $\rho_g \rightarrow 1/3$ and Equation 20 yields the classical Knudsen formula for the permeability coefficient.

Experimental data on the permeability of different gases were collected and analyzed on the basis of the proposed theoretical approach (Figure 7). It can be seen that the model describes the experimental data with good accuracy and in a wide range of permeability coefficients values ranging from $\sim$1000 Barrer to $\sim$0.01 Barrer. The developed model allows one to predict and explain the separation properties of the molecular-sieve membranes in a wide temperature range [19].

3.1.4 Activation energy of diffusion

In membranes with pore diameters less than 1 nm, overlapping of the gas-solid interaction potential occurs. This interaction originates the potential barrier which is characterized by the activation energy required to overcome it. Several approaches have been proposed to calculate the activation energy in molecular sieves including transition state, molecular dynamics theories [22,23] and some simpler methods in [24]. Ambiguity of the internal porous structure of the molecular-sieve glass membrane is a strong incentive for employing the simpler methods for the estimation of the activation energy of diffusion. One of the simple models for the calculation of the activation energy of diffusion was proposed by Roberts et al. [24]. Interactions between the diffusant and the pore are accounted for with the Lennard-Jones potential. Assuming that the perimeter of the pore neck consists of eight oxygen atoms, then the potential is

$$E_D=8\epsilon/k_{A\text{-}O_2}\left[\left(\frac{\sigma_{A\text{-}O_2}}{r_n}\right)^{12}-\left(\frac{\sigma_{A\text{-}O_2}}{r_n}\right)^{6}\right] \qquad (23)$$

$$\epsilon/k_{A\text{-}O_2}=(\epsilon/k_A\ \ \epsilon/k_{O_2})^{1/2}$$

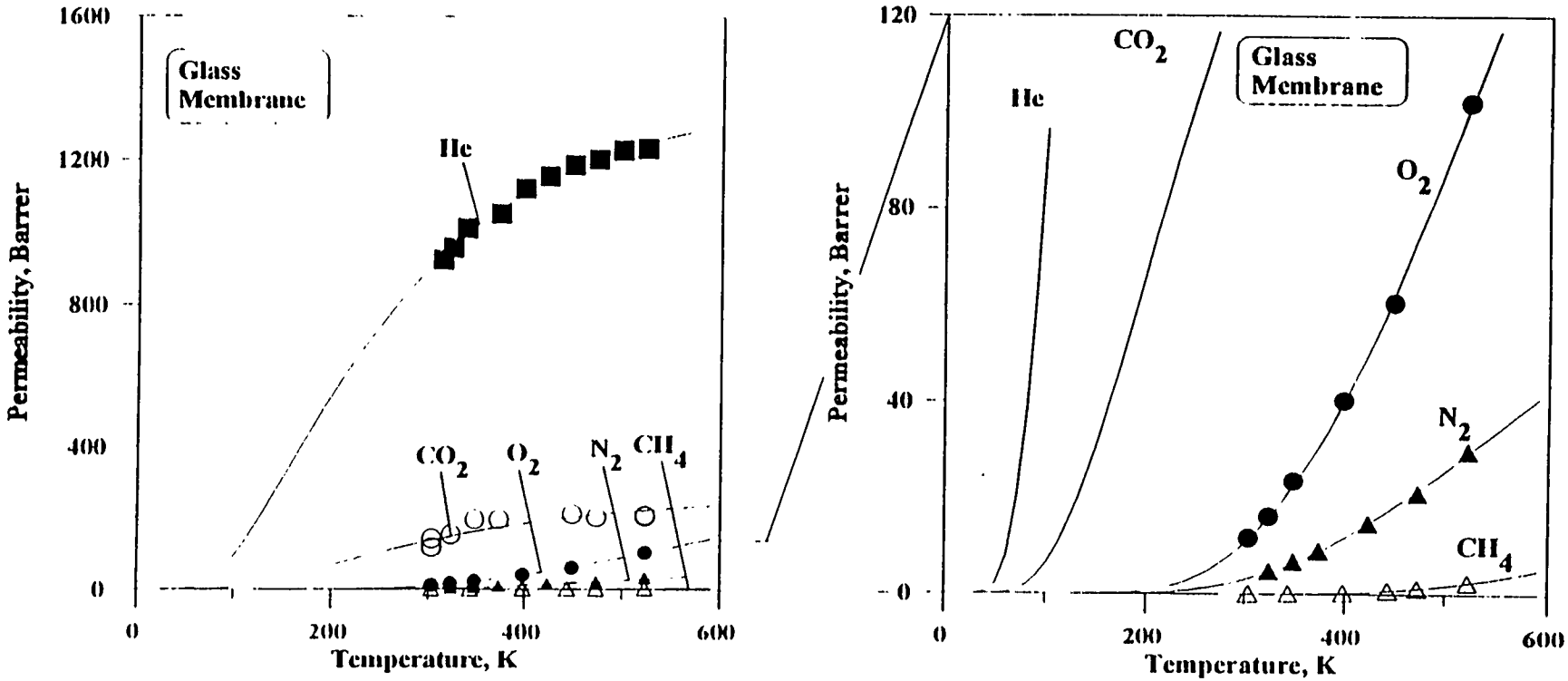

Figure 7 Temperature dependence of the permeability coefficients in the molecular-sieve memrbanes.

$$\sigma_{A-O_2} = (\sigma_A + \sigma_{O_2}) / 2$$

where r_n is the pore neck radius, σ is the distance between the oxygen atom on the neck perimeter and the diffusant, subscript A refers to the diffusant molecule. This approach to the calculation of the activation energy can be used only for the fraction of gas molecules in the gas phase within the porous body. For the adsorbed molecules the activation energy is determined as a difference between the potentials of the adsorbed phase in the pores and in the necks. An example of such an analysis was provided by Xiao and Wei [25]. Figure 8 represents the comparison between experimental and theoretical data for the activation energy of gas diffusion in the molecular-sieve glass membranes. It can be seen that a good agreement was observed between calculated and experimental data.

3.1.5 Selectivity coefficients

An ideal selectivity factor is defined as the ratio of the permeability coefficients

$$\alpha = \frac{P_A}{P_B} = \left(\frac{M_B}{M_A}\right)^{1/2} \exp\left(-\frac{\Delta E_A - \Delta E_B}{RT}\right) \qquad (24)$$

From Equation 24 it follows that only the exponential term depends on the temperature. As the temperature increases this term decreases exponentially and at infinitely high temperature the membrane selectivity is the Knudsen selectivity of the gas separation (Figure 9).

The fact that the selectivity coefficient decreases with temperature is very important because the molecular-sieve glass membranes that were provided by PPG Industries exhibit very high selectivity coefficients only at room temperature. When the temperature increases up to 1000 °C the selectivity coefficients decrease to a value only 2 to 5 times higher than the Knudsen selectivity. It is possible, in principle, to develop a molecular-sieve membrane with a very small pores (of an order of 3 Å) that will provide high selectivity coefficients even at high temperatures. The membranes in this case are probably more suitable to be called dense membranes rather than microporous membranes.

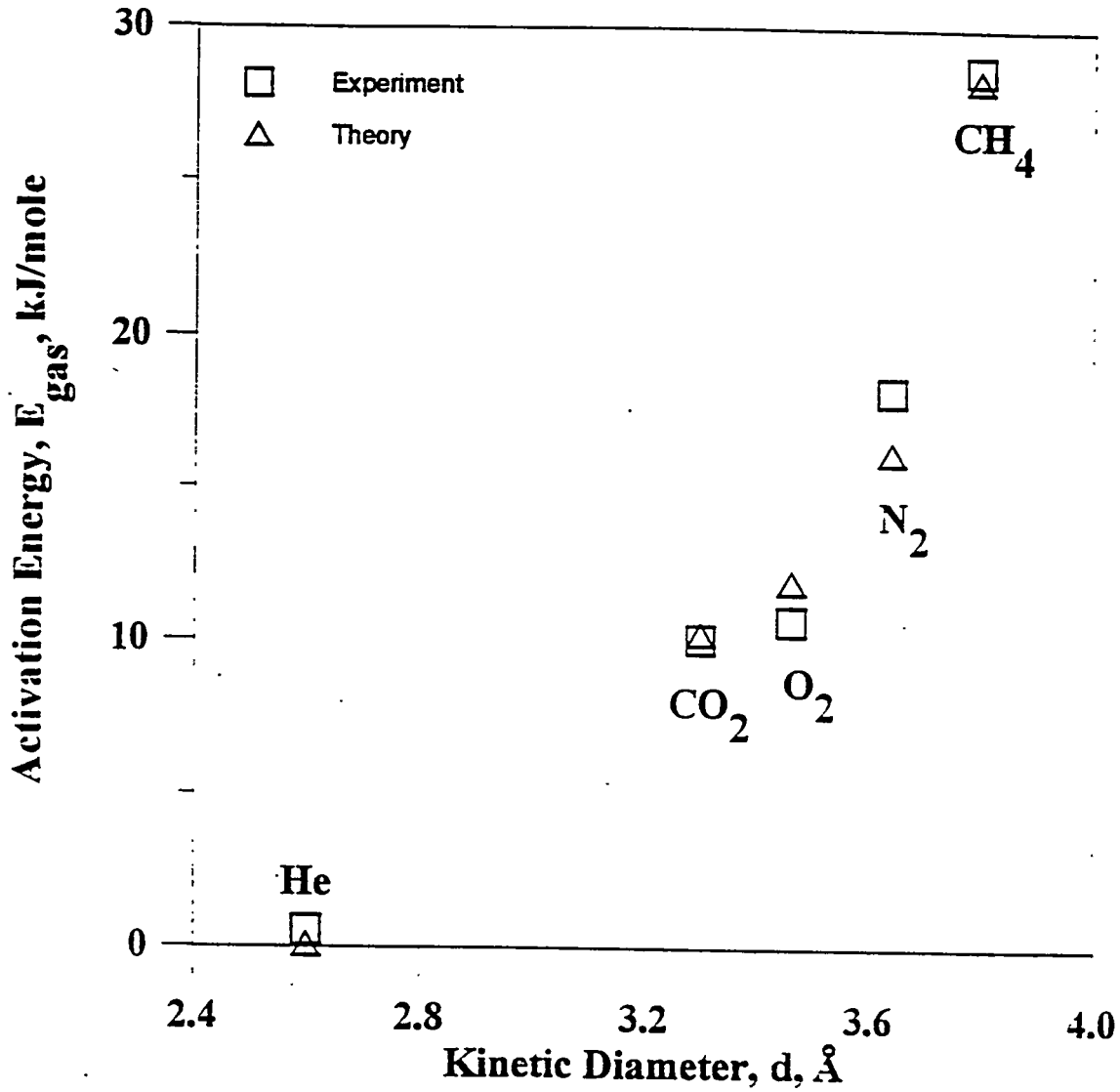

Figure 8. The activation energy of diffusion in the molecular-sieve glass membrane vs. the kinetic diameter.

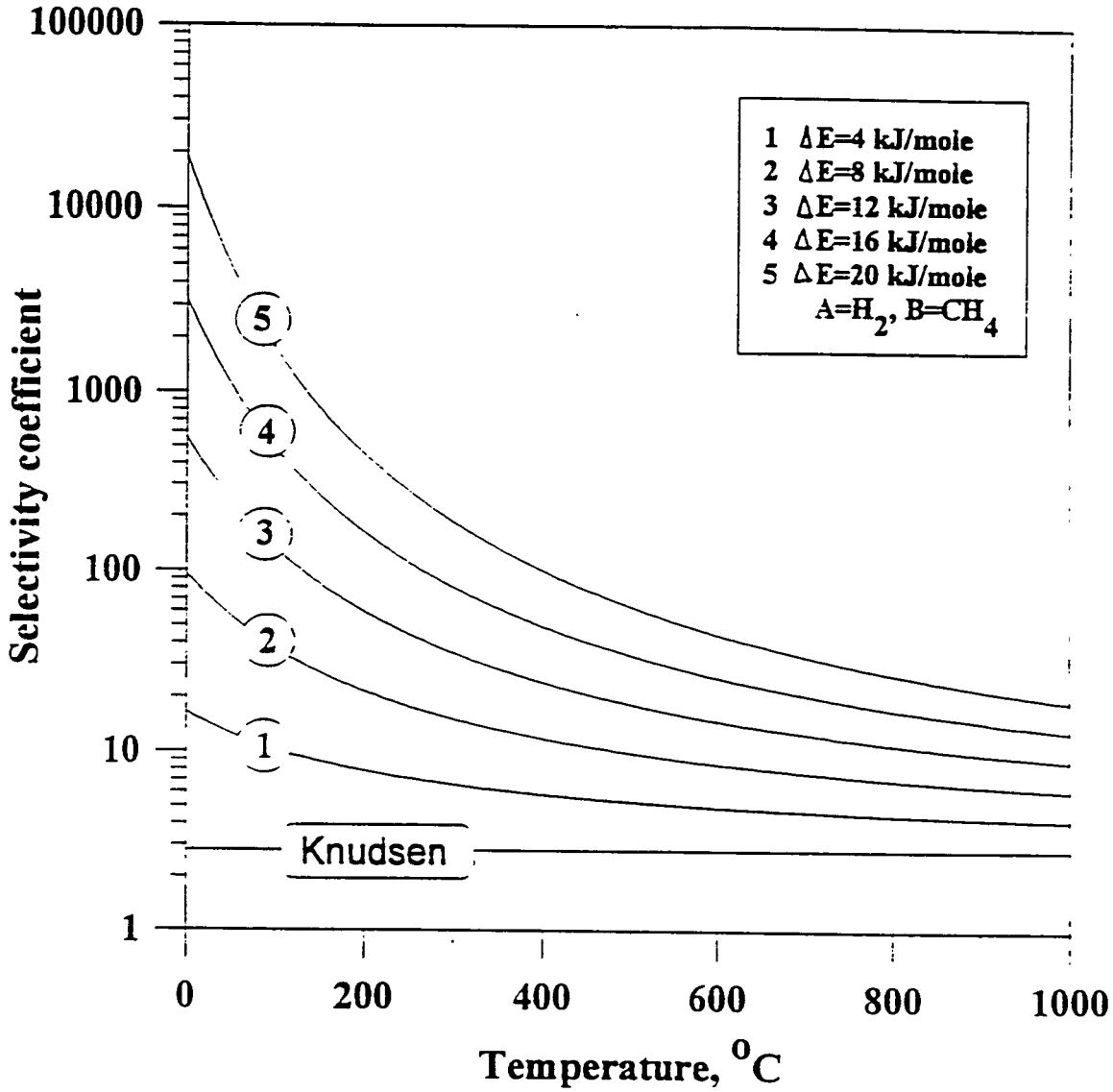

Figure 9. Temperature dependence of the selectivity coefficients in the molecular-sieve glass membrane.

3.1.6 Thermal stability

The developed model of gas diffusion and separation in molecular-sieve membranes assumes that no changes of the internal porous structure occur when the temperature is increased. It was discovered however, that the microporous glass membrane is not stable at temperatures higher than 350 °C. Figure 10 represents a dependence of the transmembrane flow as a function of the temperature in the furnace. The transmembrane flow of He increased when the temperature increased up to 300-350 °C. At temperatures higher than 350 °C the flow rate decreased and was the smallest at T=1000 °C. When the temperature decreased the flow rate through the fiber did not return to its original permeability. During the second heating cycle the permeability decreased at temperatures higher than 350 °C and declined to a very small residual value at 1000 °C.

The reason for the decrease of the permeability of microporous glass membrane is not yet clear. One possible explanation for this fact is that the pore size of the membrane changes due to the excessive surface Gibb's energy of the internal porous structure. The excessive Gibb's energy provides meltdown of the internal porous structure at temperatures that are lower than the melting temperature of silica. Another possible explanation for the permeability changes during the heating of the membrane is a possible presence of the residual B_2O_3 in the glass composition. The melting point of the glass in this case may be lower than the melting point of pure silica.

By developing thin asymmetric membranes with dense layer of silica ($d_p < 3Å$) the temperature stability of the membrane can be improved because the Gibbs free energy in this case is determined by the Gibbs free energy of the thin film rather than comprising small particles of silica.

As it follows from the conducted study of the permeability, selectivity and thermal stability of the molecular-sieve glass membranes they are unsuitable at present time for high temperature (800-1000 °C) IGCC gas cleanup. Further modification of the membrane may make it thermally stable at higher temperatures.

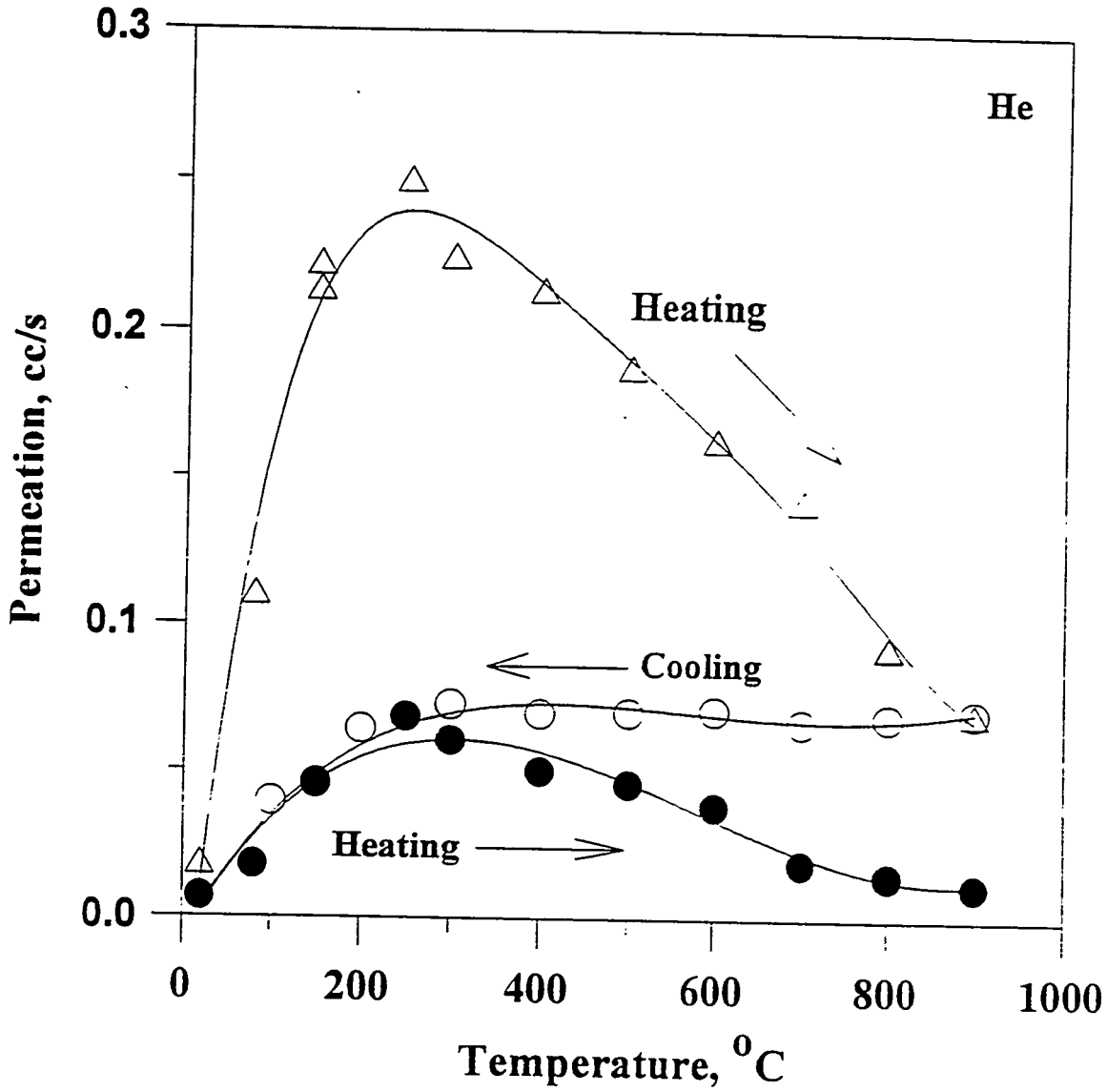

Figure 10. Temperature stability of the molecular-sieve glass membranes.

3.2 Vycor glass membrane

Other possible candidates for the gas separation membrane that can be used presently for the design of the membrane reactor are porous Vycor glass membranes and sol-gel derived membranes. In our study Vycor glass membranes were used for the design of the membrane reactor.

3.2.1 Thermal stability

Figure 11 represents a temperature dependence of the linear shrinkage of the porous Vycor glass membrane after 24 hours treatment at a given temperature in the air. At temperatures greater than 400 °C the membrane began to shrink. At temperatures higher than 800 °C the membrane tube length decreased by more than 10%. No additional changes in the membrane length were observed within the temperature range 1000 °C to 1200 °C, implying that the collapse of the porous structure has been completed. The obtained data on the membrane shrinkage are in a good agreement with the data reported by Kameyama, et al. [18].

3.2.2 Gas permeability and selectivity

Mechanical stability of the membrane at high temperatures does not necessarily mean that the membrane sustained its permeability and selectivity properties as well. Figure 12 illustrates a temperature dependence of the He permeability in the heat treated membranes. First the membranes were kept at a given temperature for 24 hours. After that, the membranes were cooled to the room temperature and the permeability of He was measured in the sample at the room temperature. The permeability of He in the tested membranes was almost unchanged up to the pretreatment temperature of 500 °C. Slight increases in the He permeability were observed in the membranes heat treated at 500-850 °C. When the temperature of pretreatment was higher than 900 °C the He permeability drops drastically and at temperatures of pretreatment higher than 1000 °C the permeability is practically equal to zero. The obtained data are in good agreement with the data on the membrane shrinkage (Figure 11). Apparently, at low temperatures ($T < 850$ °C) only very fine silica particles comprising the porous Vycor glass melt down, and therefore, the pore size within the membrane increases and possibly decreasing the tortuosity factor. As a result of this process the membrane permeability increases up to the

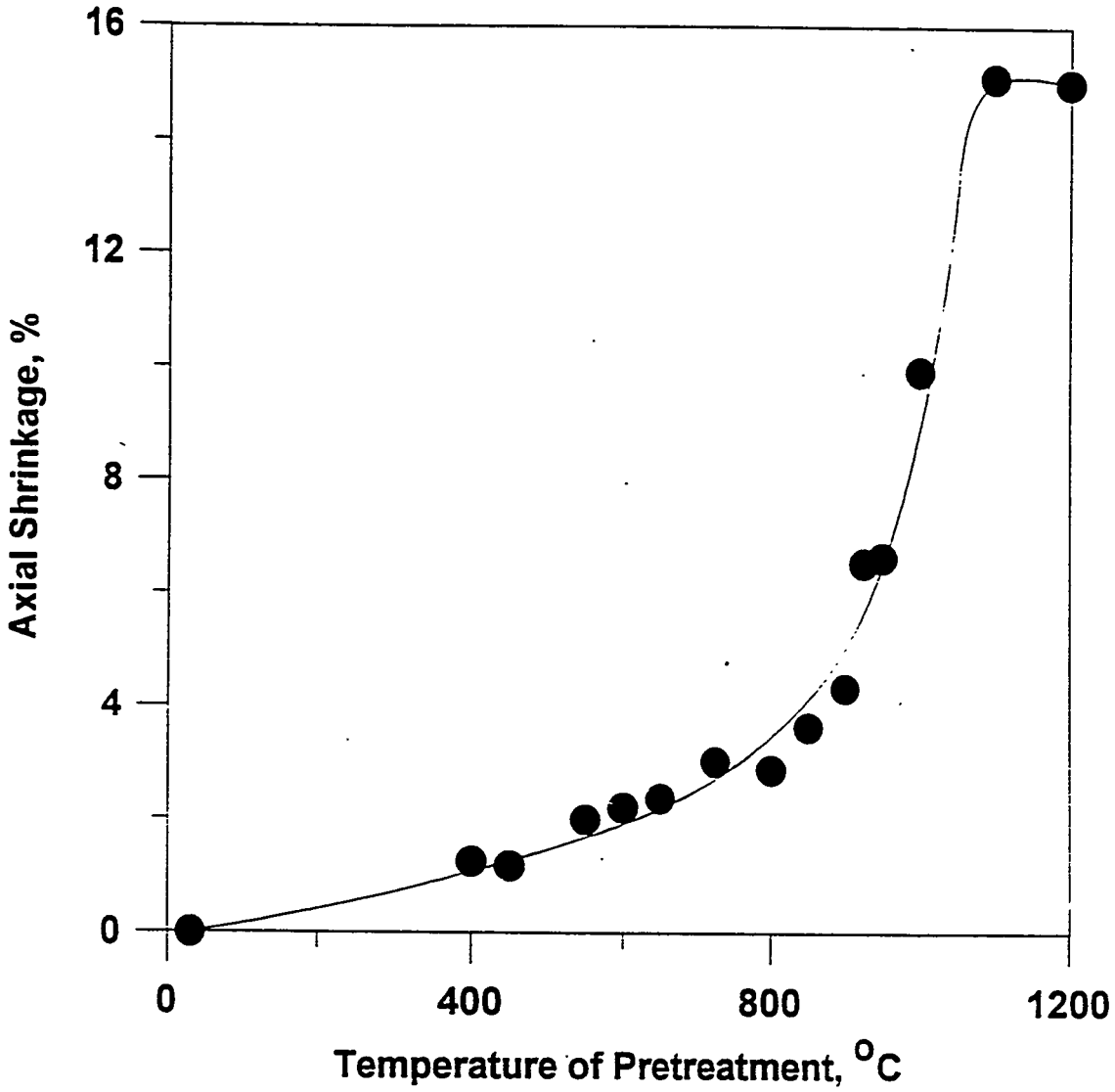

Figure 11. Linear shrinkage of the Vycor glass membrane vs. the temperature of pretreatment.

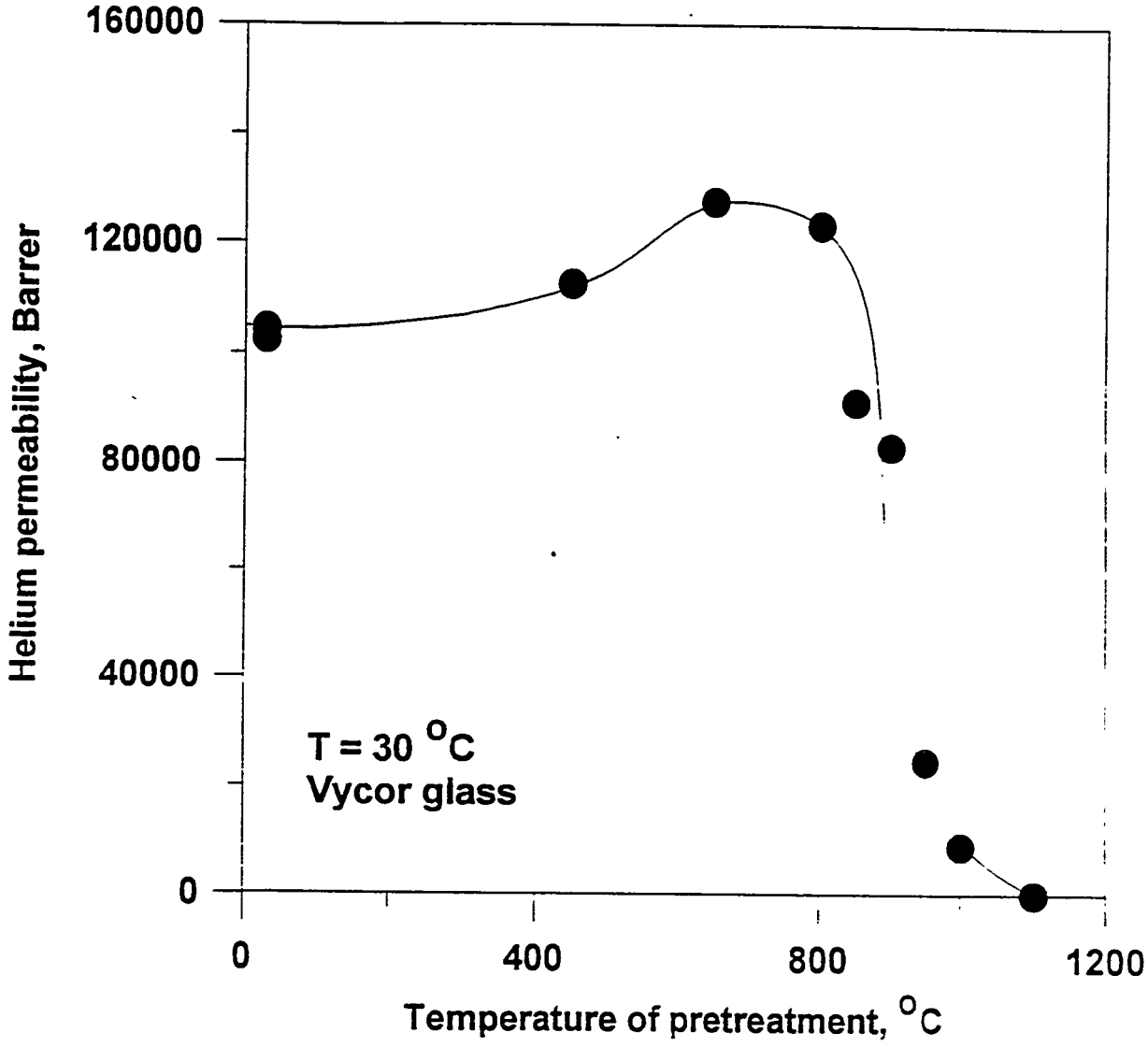

Figure 12. Permeability of He in the Vycor glass membrane versus the temperture of pretreatment.

pretreatment temperature equal to T=850 °C. At temperatures higher than 900 °C larger silica particles melt down blocking some diffusion paths in the membrane. At temperature T > 1000 °C even very large particles coalesce and the porous structure collapses. The membrane becomes impermeable to gases.

In spite of the dramatic changes in the porous structure at high temperature the membrane sustained its selective properties. A temperature dependence of the permeability coefficients in the porous membrane is presented in Figure 13. To prevent the membrane shrinkage during the temperature rise, the membrane was first heat treated at 850 °C for 24 hours and then the permeation experiments were performed. The permeability coefficients of H_2, H_2S, and N_2 decreased when the temperature increased. The observed phenomenon agreed well with the Knudsen mechanism of gas diffusion in porous membranes. At low temperature the permeability coefficient of H_2S was found higher than the permeability coefficient of N_2. However, as the temperature increased the permeability of H_2S decreased faster than the permeability of N_2. At temperatures higher than 600 °C the permeability of H_2S was lower than the permeability of N_2 which is in line with the Knudsen diffusion mechanism. The high permeability of H_2S observed at low temperatures was apparently due to the surface diffusion transport mechanism.

Dependencies of the ideal selectivity factors versus the temperature of the membrane are presented in Figure 14. The selectivity coefficients increased with temperature and reached the maximum value of the Knudsen selectivity at temperatures higher than 500 °C. At high temperatures two factors favor the increase of the selectivity factors with respect to H_2. On one hand the surface flow of highly adsorbable gases such as H_2S decreases. On the other hand the mean free path of gas molecules increases thus decreasing the number of collisions between gas molecules. Therefore, the operating temperature equal to 800 °C provided moderate conversion of the H_2S with the maximum selectivity of separation for the porous membrane. Simultaneously, the membrane retained its mechanical stability. Therefore, all of the reported experiments on the H_2S conversion in the membrane reactor were conducted at 800 °C.

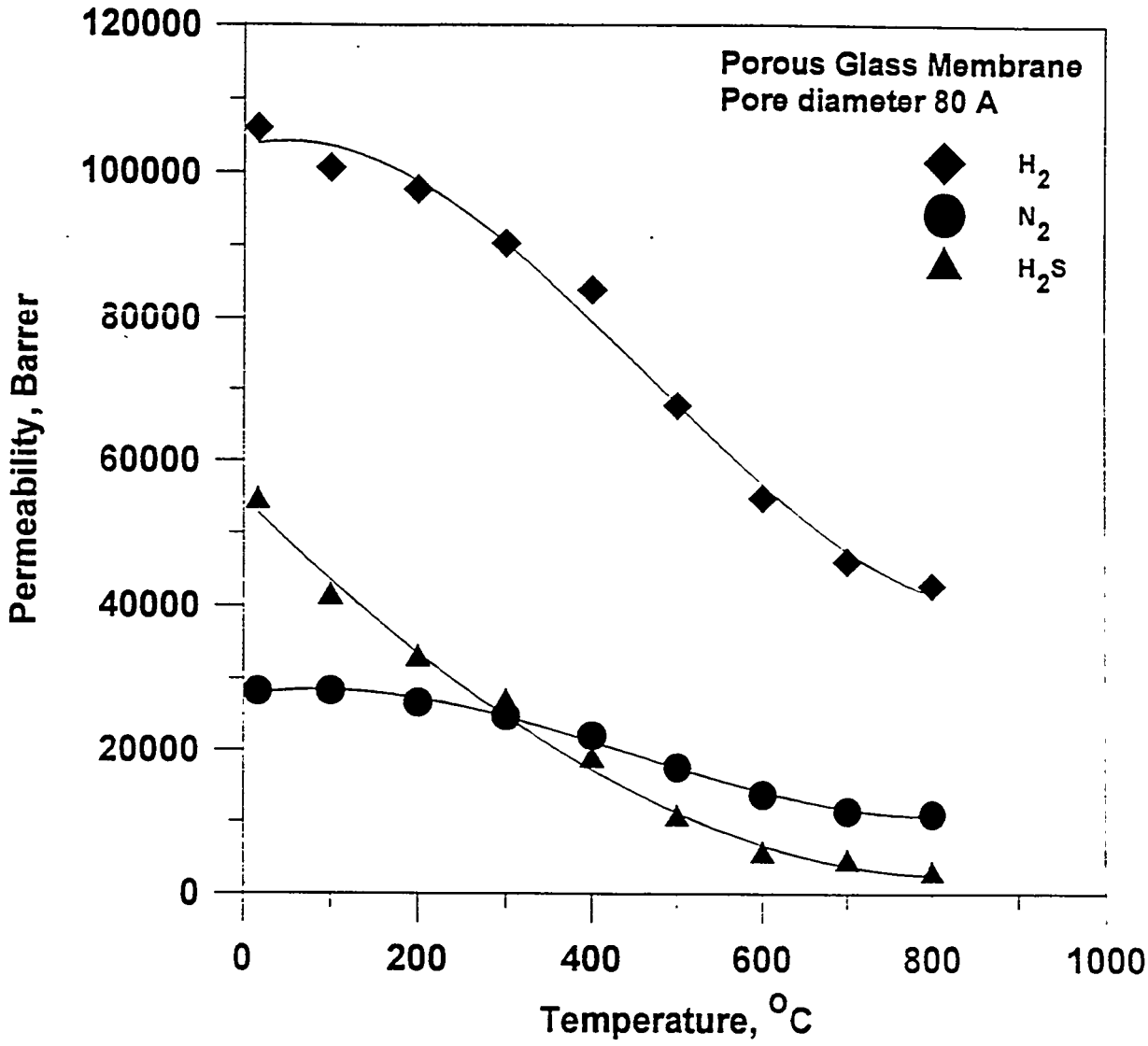

Figure 13. Temperature dependence of H_2, H_2S, S_2 permeability in the Vycor glass membrane.

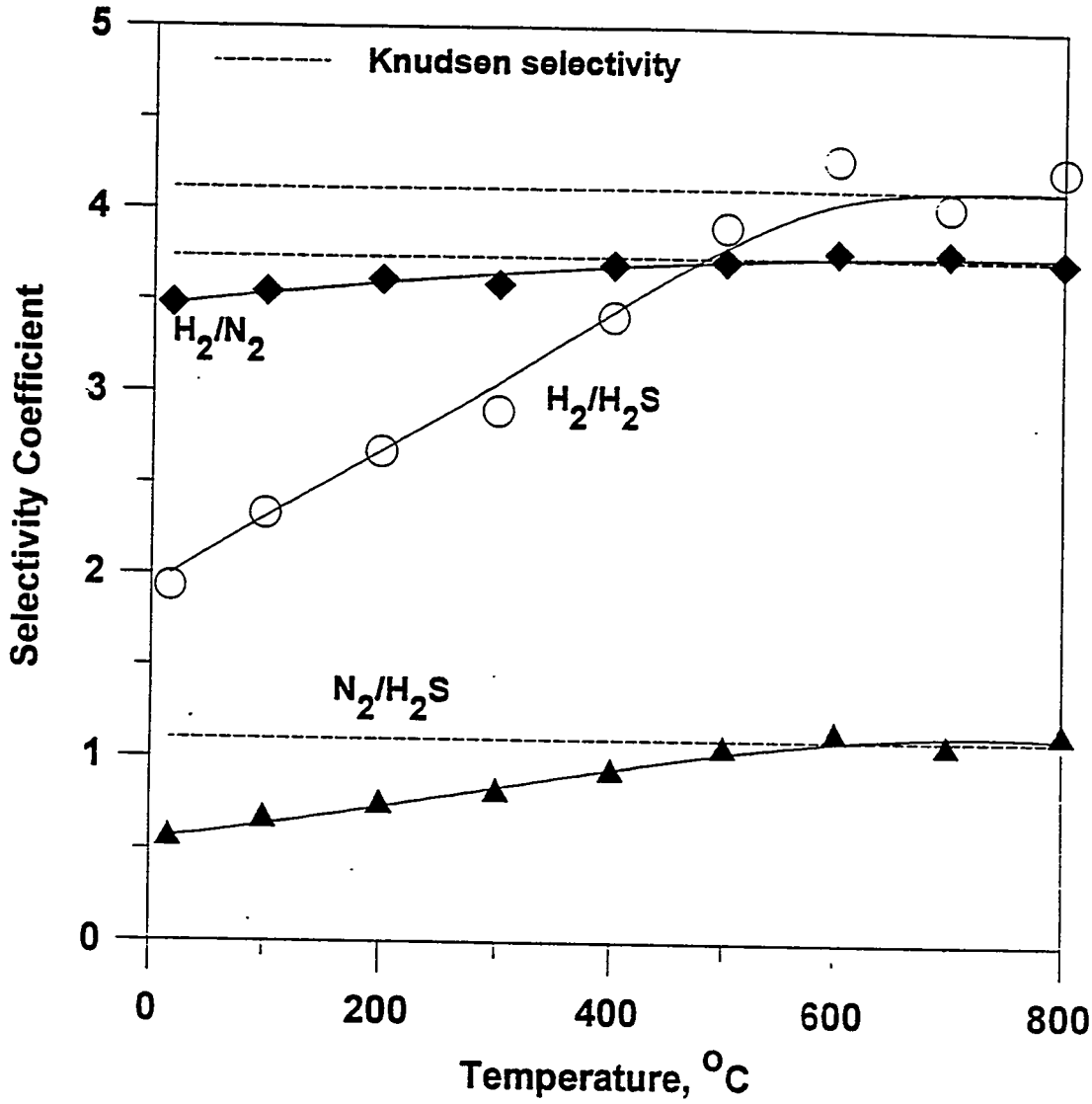

Figure 14. Temperature dependence of selectivity coefficients in the Vycor glass membrane.

IV. THERMODYNAMICS OF H_2S DECOMPOSITION

4.1 Equilibrium conversion of H_2S

Depending on the temperature, the reaction of the H_2S decomposition may be presented as [26]

$$H_2S \rightleftarrows H_2 + S_8 \qquad 717.75\text{-}900K$$

$$2H_2S \rightleftarrows 2H_2 + S_2 \qquad T > 900\ K.$$

The equilibrium constant for the reaction can be calculated according to

$$K_{eq} = e^{-\frac{\Delta G}{RT}}$$

The equilibrium concentration of H_2 in the reaction mixture at different pressures and mixed with inert gases can be calculated from

$$\begin{array}{ccccc} H_2S & \rightleftarrows & H_2 & + & 0.5S_2 \\ a-\xi & & b+\xi & + & 0.5\xi \end{array}$$

$$K_{eq} = \frac{\left[\frac{\xi + b}{a+b+c+0.5\xi}\right]\left[\frac{0.5\xi}{a+b+c+0.5\xi}\right]^{1/2}}{\left[\frac{a-\xi}{a+b+c+0.5\xi}\right]} P^{1/2} \qquad (25)$$

where ξ is the extent of the reaction, a is the moles of H_2S in the feed, b is the moles of H_2 in the feed, c is the moles of the inert gas in the feed, P is the absolute pressure in the reaction vessel.

Equation (25) was solved by the simple Newton iteration method. It follows from Equation 25 that the conversion increases when the absolute pressure decreases. When the amount of the inert gas in the reaction mixture increases the conversion increases as well. Therefore, the conversion on the permeate side of the membrane reactor should always be higher than the conversion on the feed side due to the pressure decrease and/or dilution with the inert sweep gas.

The conversion in the packed bed reactor can be calculated from

$$X_{eq}=\frac{\xi}{a}\cdot 100\%=\frac{C_{PB}^{H_2}-C_{in}^{H_2}}{C_{in}^{H_2S}}\cdot 100\% \qquad (26)$$

where C_{PB}^{H2} is the concentration of H_2 at the reactor outlet, C_{in}^{H2} and C_{in}^{H2S} are the concentrations of H_2 and H_2S in the feed, X_{eq} is the equilibrium conversion.

4.2 Pressure drop in packed beds

To provide the maximum efficiency of the membrane separation, pressure losses along the membrane reactor must be minimized. Pressure drop in the packed bed was calculated according to the semi-empirical equation [27]

$$\left(\frac{[P_{in}-P_{out}]\cdot\rho}{G^2}\right)\left(\frac{d}{L}\right)\left(\frac{\varepsilon^2}{1-\varepsilon}\right)=\frac{150(1-\varepsilon)}{(Gd/\mu)}+1.75 \qquad (27)$$

where P_{in} and P_{out} are the inlet and outlet pressures respectively, G is the mass flow rate, d is the catalyst particle diameter, ρ is the gas density, ε is the void volume, L is the packed bed length, and μ is the gas viscosity. The pressure drop in the packed bed as a function of the catalyst particle size is depicted in Figure 15. One may see that for the packed bed (L=10 cm) the catalyst particles with diameter larger than 0.1 mm must be used to ensure that no significant pressure drop develops along the module. However, the size of the catalyst particles can not be increased infinitely. If the particles of the catalyst are too big, external mass transfer resistance may decrease the reaction rate. The external mass transfer limitation reduces the conversion and therefore hurt the packed bed reactor performance. To prevent high pressure losses along the membrane reactor the catalyst particles of the 0.35 mm size were used. The pressure drop in the packed bed membrane reactor used in this study was less than 5% along the module at pressures higher than 20 psig.

4.3 H_2S conversion in the packed bed reactor

4.3.1 Flow rate dependence

The conversion of H_2S in the packed-bed reactor was studied as a function of the temperature, pressure, and the inlet flow rate in the packed-bed reactor. Figure 16 represents

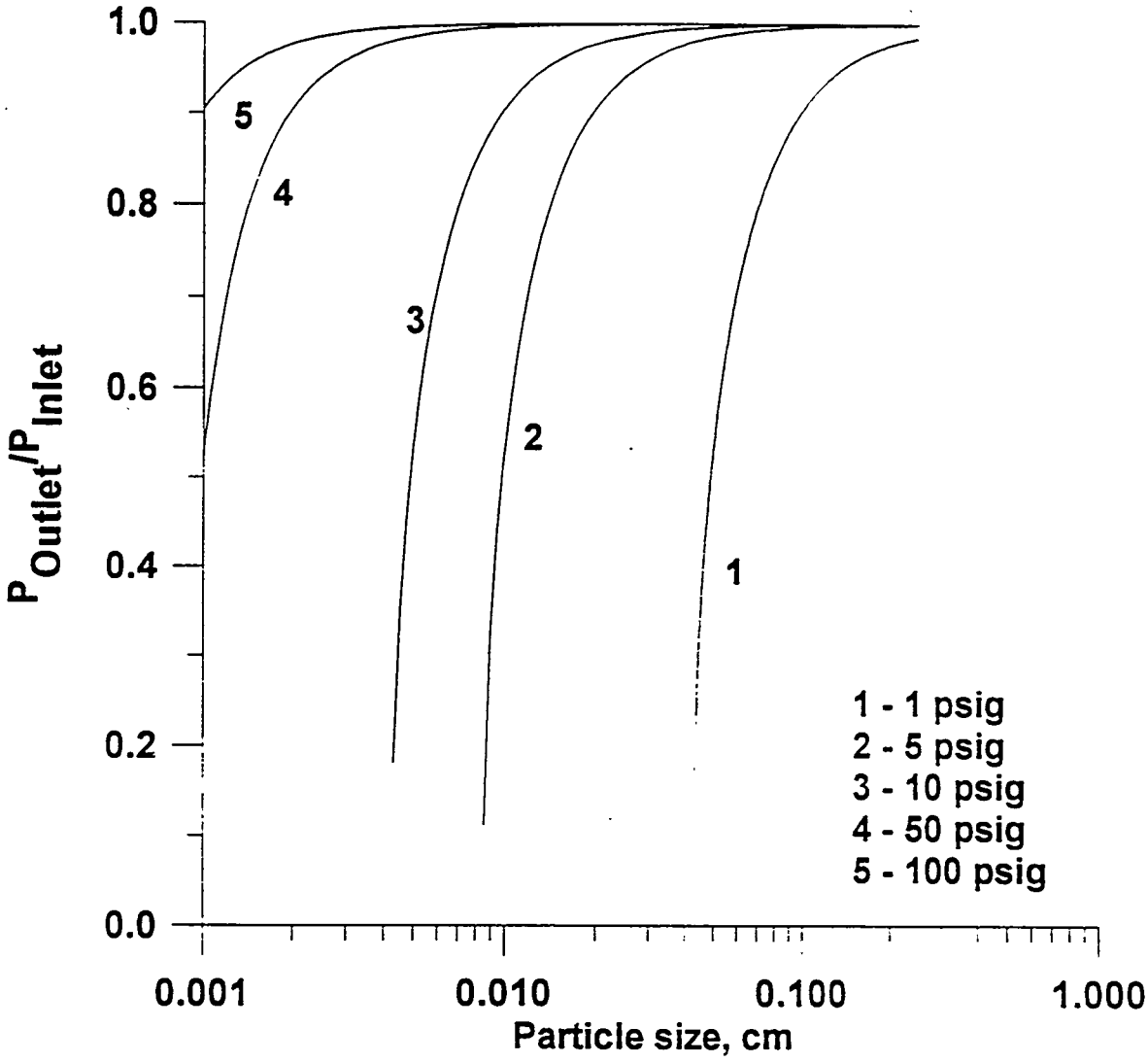

Figure 15 Pressure drop in packed-beds vs. catalyst particle diameter.

a dependence of the H_2S conversion versus the space time in the packed bed reactor. The loads of the MoS_2 catalyst were equal to 2.41 g, 1.57 g, 0.85 g, and 0.32 g. The gas mixture with 1.1% H_2S and N_2 as a balance was used in the experiments. The temperature of the furnace was kept constant at 800 °C. At a constant contact time, H_2S conversion increased with an increase in the amount of the catalyst (Figure 16). Therefore, the conversion rate in the packed-bed might be limited by the external mass transfer limitations. The weight of the catalyst used in the membrane reactor was equal to 11.5 g and was large enough to minimize the effect of the external mass transfer.

4.3.2 Temperature dependence

The temperature dependence of the H_2S conversion in the packed-bed reactor is presented in Figure 17. All of the experimental points were obtained at the same flow rate equal to 5 cm^3/s (at 25 °C, 1 atm). The conversion increased very fast with temperature at $T > 600$ °C. A good agreement was observed between the experimental data obtained in this work and the thermodynamic calculations. The experimental values, however, were systematically less than the values predicted from the theory. The deviation of the experimental data from the theoretical predictions is caused by the temperature profile in the packed bed reactor which will be discussed later.

4.3.3 Pressure dependence

The reaction of the H_2S decomposition is a volume expansion reaction (Equation 25). Therefore, when the absolute pressure in the system increases, the conversion decreases. Figure 18 illustrates a pressure dependence of the H_2S conversion in the packed-bed reactor. The solid line in the figure represents the equilibrium conversion calculated from Equation 25. An agreement between the experimental data and the theoretical predictions is very good at low pressures. In the high pressure region the experimentally observed conversion was less than the equilibrium conversion. This can be explained by the increased influence of the external mass transfer limitations on the overall reaction rate and by the temperature profile in the reactor.

4.4 Catalytic activity of the porous Vycor glass membrane

The main component in the composition of the Vycor glass porous membrane is the amorphous silica. The silica is known for its catalytic activity for the reaction of H_2S decomposition [28,29]. Therefore, the porous Vycor glass membrane may act as a catalytic

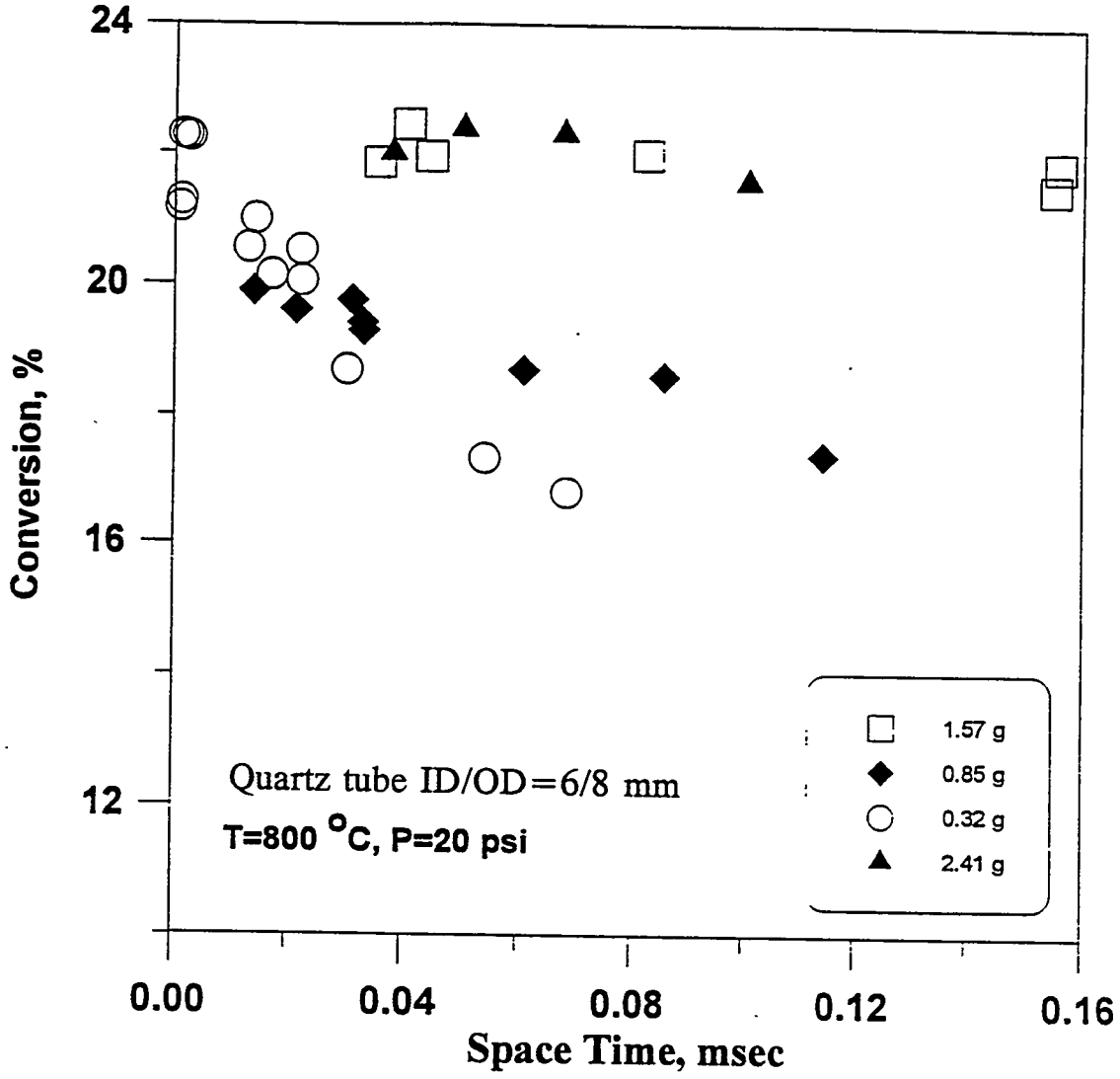

Figure 16. Conversion of H_2S in packed bed reactor vs. space time.

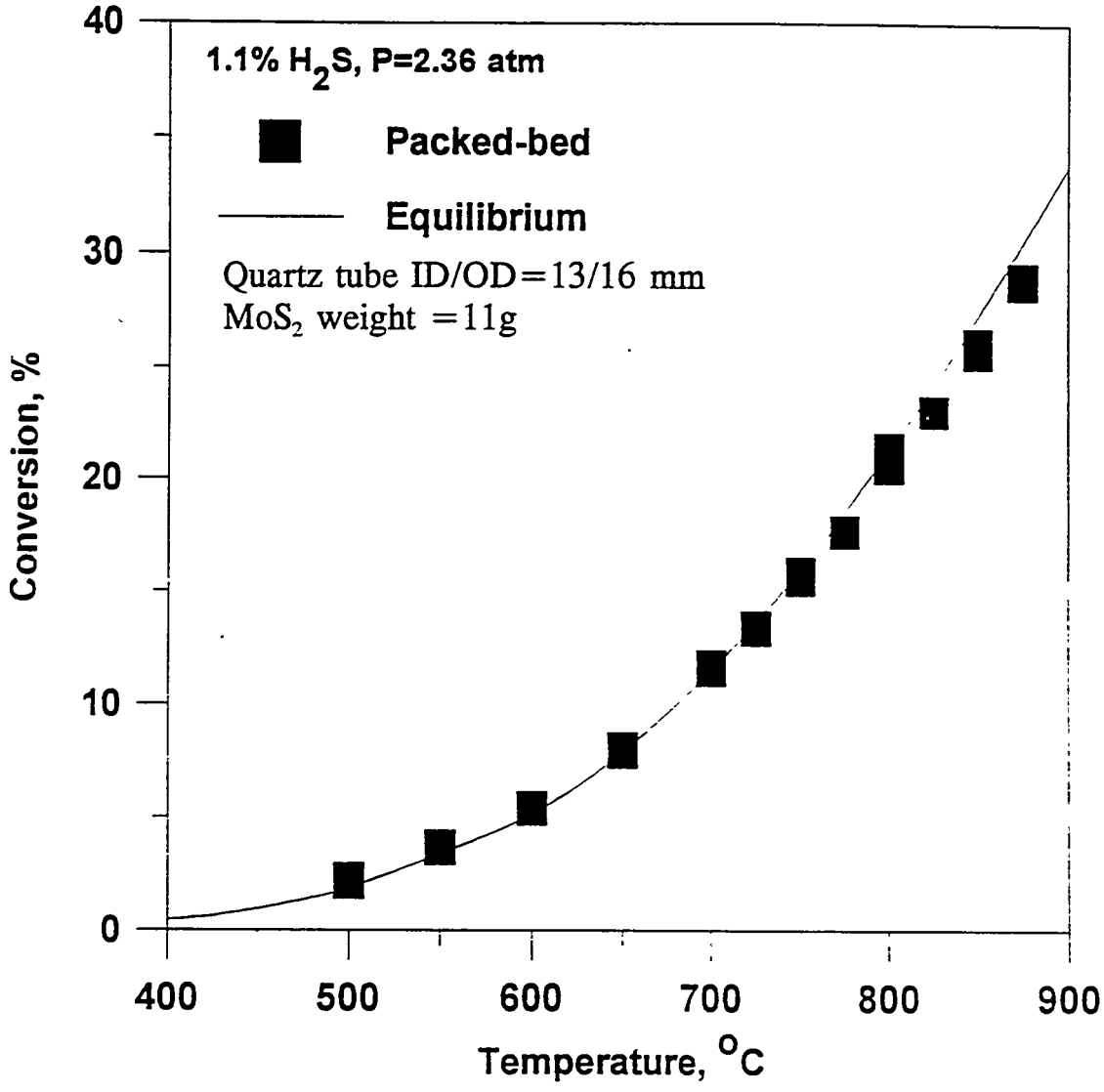

Figure 17 Conversion of H_2S in packed bed reactor vs. temperature.

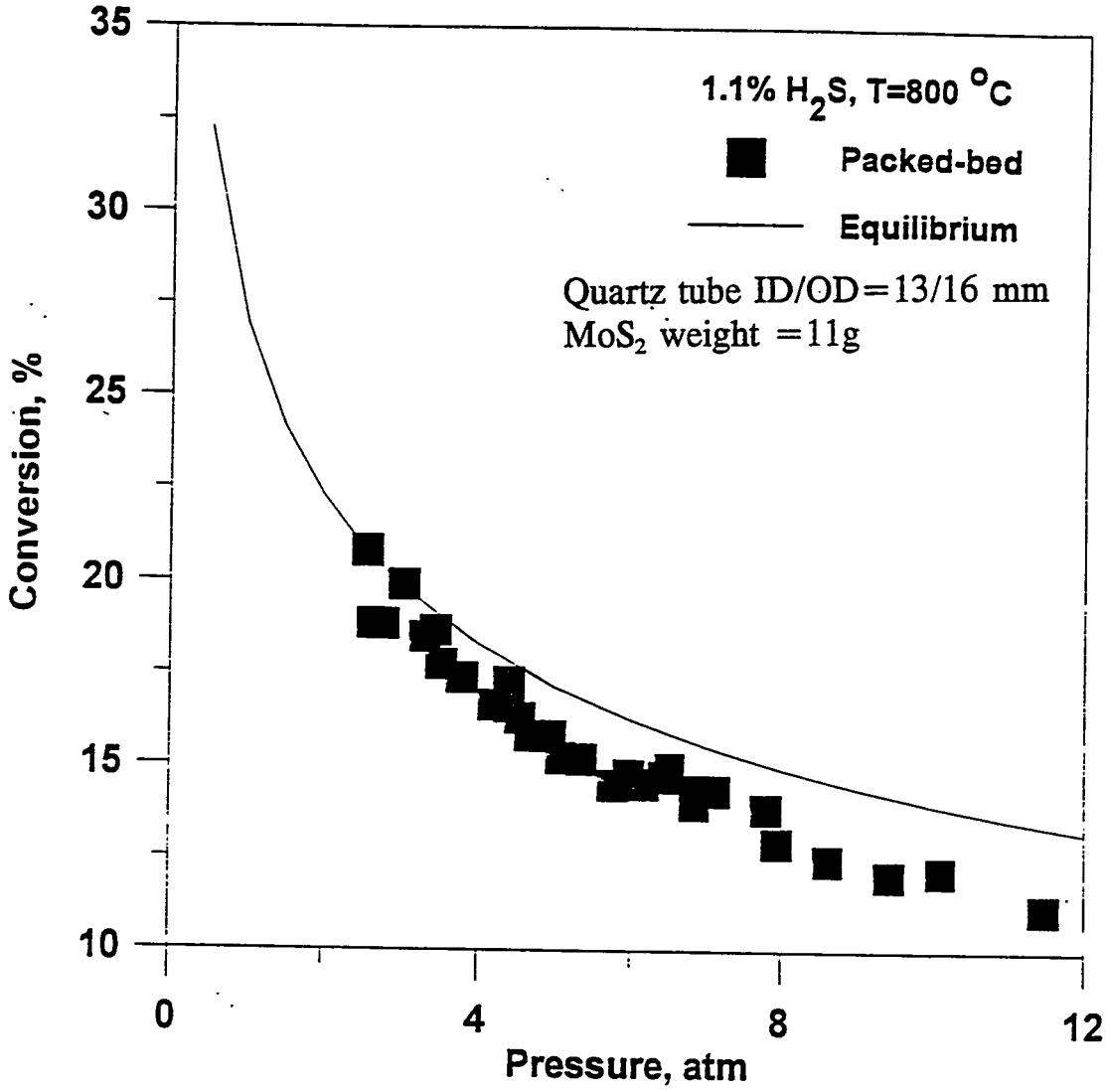

Figure 18. Conversion of H_2S in packed bed reactor vs. pressure.

membrane in the membrane reactor. A dependence of the conversion versus the space time in the fixed bed reactor packed with grounded particles of the Vycor glass membrane is shown in Figure 19. The size of the Vycor glass particles was equal to 0.35 mm. For comparison, the data on the conversion of the H_2S in the fixed bed reactor packed with MoS_2 as a catalyst are also presented in the same figure. The weight of the MoS_2 catalyst was twice the weight of the Vycor glass. The volume of the packed bed was equal in both cases. Within the limits of the experimental error, there was no difference between the conversion in the fixed bed reactors packed with MoS_2 and the Vycor glass. Therefore, the Vycor glass membrane also exhibits the catalytic activity for the H_2S decomposition. The catalytic activity of the Vycor glass membrane should be considered while analyzing the conversion data in the packed bed membrane reactor.

4.5 Kinetics of H_2S decomposition

A thorough analysis of the kinetics of catalytic decomposition of H_2S was presented by Kaloidas and Papayannakos [28,30]. Three different rate expressions based on assumptions of three different kinetic mechanisms were considered (Table 2). All of the three models proposed in [28] are five parameter models. Obviously, the model with five parameters fits the experimental data much better than a less sophisticated two parametric model

$$-r_{H_2S}=k_o e^{-E/RT}\left(p_{H_2S}-\frac{p_{H_2}p_{S_2}^{0.5}}{K_{eq}}\right) \qquad (28)$$

where p_{H2}, p_{H2S}, and p_{S2} are the partial pressures of H_2, H_2S, and S_2 respectively, k_o is the frequency factor, and E is the activation energy. To verify the difference among the three five-parametric models and Equation 28 the reaction rates were calculated at T=800 °C and p=1 atm (Table 3). One may see that the difference between the reaction rates derived from rate expressions (Table 2) and Equation 28 is not statistically significant. Therefore, complexities of the three five-parameter models cannot be justified. In the model calculations conducted in this work Equation 28 was used to calculate the reaction rates for the reaction of H_2S decomposition.

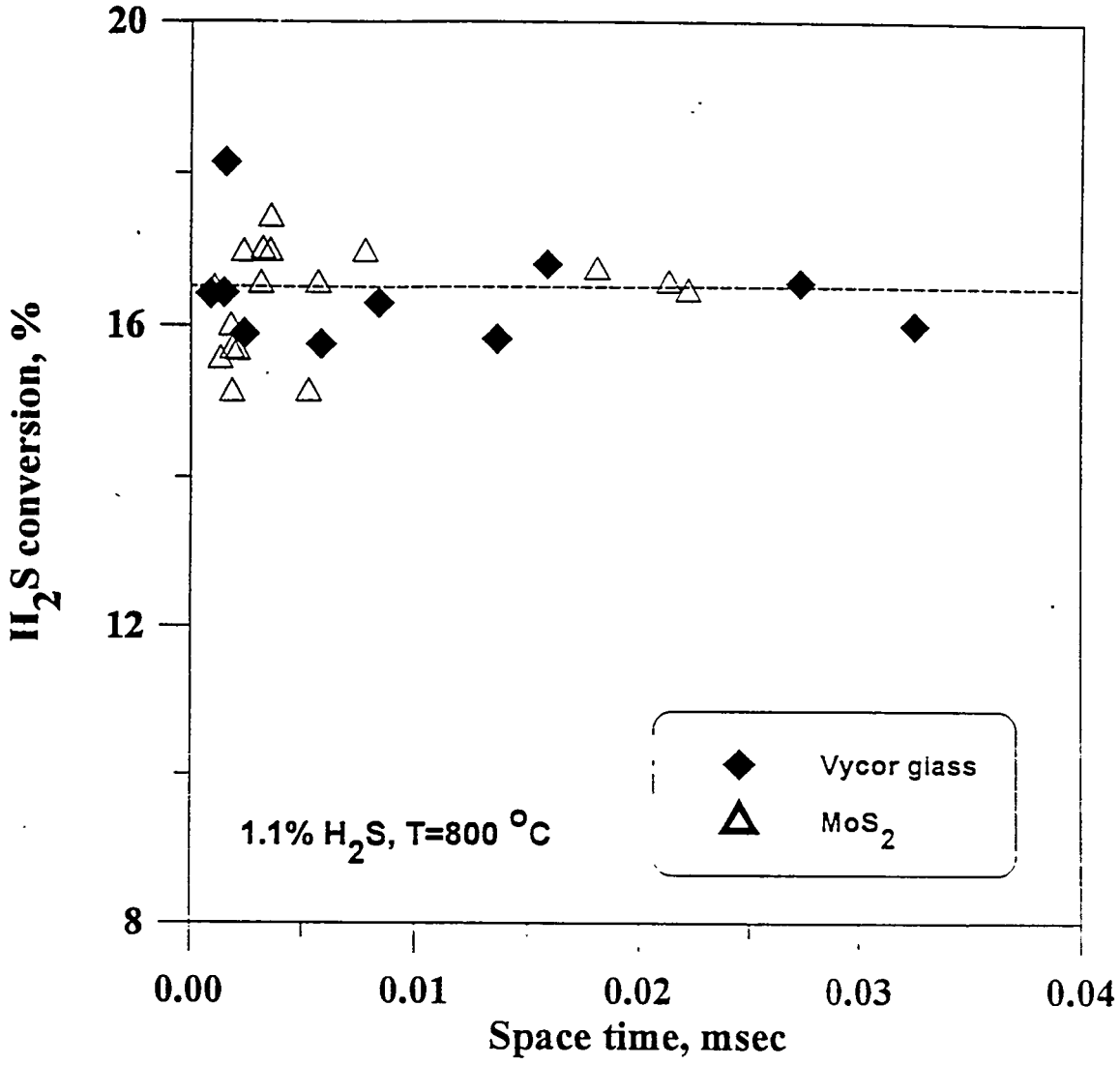

Figure 19. Conversion of H_2S in packed bed reactor vs. space time, τ, μsec for Vycor glass.

TABLE 2. KINETIC MODEL OF H_2S DECOMPOSITION REACTION

I. Homogeneously Catalytic Reaction

(1) $r_1 = k_1 e^{-\frac{E_1}{RT}} (P_{H_2S} - \frac{1}{K_{eq}} P_{H_2} P_{S_2}^{1/2})$

$k_1 = 784.1\ mol/(cm^3\ s\ atm)$
$E_1 = 46.8\ kcal/mol$

II. Heterogeneously Catalytic Reaction

(1) $r_1 = [k_1 e^{-\frac{E_1}{RT}} (P_{H_2S} - \frac{1}{K_{eq}} P_{H_2} P_{S_2}^{1/2})] / [1 + K_{A1} e^{-\frac{E_{A1}}{RT}} P_{S_2}^{1/2} + K_{B1} e^{-\frac{E_{B1}}{RT}} P_{H_2} P_{S_2}^{1/2}]$

$k_1 = 287.9\ mol/(g\ s\ atm)$
$E_1 = 29.48\ kcal/mol$
$K_{A1} = 4.018\ E{+}36\ atm^{-1/2}$
$E_{A1} = 187.8\ kcal/mol$
$K_{B1} = 1.316\ E{-}2\ atm^{-3/2}$
$E_{B1} = -20.3\ kcal/mol$

(2) $r_2 = [k_2 e^{-\frac{E_2}{RT}} (P_{H_2S} - \frac{1}{K_{eq}} P_{H_2} P_{S_2}^{1/2})] / [1 + K_{A2} e^{-\frac{E_{A2}}{RT}} P_{H_2S} + K_{B2} e^{-\frac{E_{B2}}{RT}} P_{S_2}^{1/2}]$

$k_2 = 43.37\ mol/(g\ s\ atm)$
$E_2 = 0.4177\ kcal/mol$
$K_{A2} = 9.75\ E{-}7\ atm^{-1}$
$E_{A2} = -51.50\ kcal/mol$
$K_{B2} = 17.03\ atm^{-1/2}$
$E_{B2} = -24.34\ kcal/mol$

(3) $r_3 = [k_3 e^{-\frac{E_3}{RT}} (P_{H_2S} - \frac{1}{K_{eq}} P_{H_2} P_{S_2}^{1/2})] / [1 + K_{A3} e^{-\frac{E_{A3}}{RT}} P_{H_2S} + K_{B3} e^{-\frac{E_{B3}}{RT}} P_{H_2} P_{H_2S}]$

$k_3 = 23.66\ mol/(g\ s\ atm)$
$E_3 = 31.60\ kcal/mol$
$K_{A3} = 3.547\ E{-}4$
$E_{A3} = -7.918\ kcal/mol$
$K_{B3} = 1.008\ E{+}54\ atm^{-1}$
$E_{B3} = 287.1\ kcal/mol$

III. Rate Equation for Mathematical Modeling

(1) $r_1 = k_1 e^{-\frac{E_1}{RT}} (P_{H_2S} - \frac{1}{K_{eq}} P_{H_2} P_{S_2}^{1/2})$

homogeneousreaction
*
$k_{HOMO} = 800\ mol/(cm^3\ s\ atm)$
$E_{HOMO} = 47\ kcal/mol$

heterogeneousreaction
*
$k_{HETERO} = 300\ mol/(cm^3\ s\ atm)$
$E_{HETERO} = 30\ kcal/mol$

Table 3. The Comparison of Reaction Rate* derived form Different Kinetic Models

Homogeneous (1)	2.15 E-7 mol/(cm^3-s)
Homogeneous (modeling)	1.99 E-7 mol/(cm^3-s)
Heterogeneous (1)	3.92 E-4 mol/(cm^3-s)
Heterogeneous (2)	5.50 E-5 mol/(cm^3-s)
Heterogeneous (3)	7.19 E-5 mol/(cm^3-s)
Heterogeneous (modeling)	3.17 E-4 mol/(cm^3-s)

* The reaction rates were calculated base on a reactant consisting of 92.7% H_2S, 4.9% H_2, and 2.4% S_2 at a reaction condition of 100 psi and 800 °C.

V. DECOMPOSITION OF H_2S IN MEMBRANE REACTOR

5.1 Definition of the stage cut

Due to the volume expansion during the reaction process the volume of the products at the membrane reactor outlet may not be equal to the volume of the feed gas. The stage cut for membrane reactors is defined as the amount of the gas mixture passed through the membrane, F_P, to the total amount of the permeate and reject, F_T (Figure 20):

$$\theta = \frac{F_P}{F_T} \tag{29}$$

At zero stage cut the amount of gas passing along the membrane is infinitely higher than the amount of gas permeated through the membrane. On the other hand, at the stage cut equal to one the total amount of the permeate is equal to the feed amount. In this case the shell side is blocked at the outlet. When the stage cut is equal to one, the membrane does not provide any separation of the reaction gas mixture and operate as a filter. For the reaction of H_2S decomposition, sulfur condenses on the walls of the reactor and collected in a filter trap at the membrane reactor outlet. Therefore, the stage cut, for the reaction of H_2S decomposition, can be determined simply as

$$\theta = \frac{F_P}{F_{Feed}} \tag{30}$$

where F_{Feed} is the feed flow rate.

Total conversion in the membrane reactor is determined in accordance with

$$X_{MR} = \frac{(C_{H_2,T}\theta + C_{H_2,S}(1-\theta)) - C_{H_2,F}}{C_{H_2S,F}} 100\% \tag{31}$$

where b is the concentration of H_2 in the feed. When the catalytic decomposition of H_2S is carried out in the packed bed membrane reactor, the reaction process is accompanied by the simultaneous separation of the gas mixture consisting of H_2, S_2, H_2S. The inert gas N_2 may also be present in the feed. The fastest permeable component in the Vycor glass membrane is H_2. However, all other gases, including diatomic sulfur, permeate across the porous membrane as

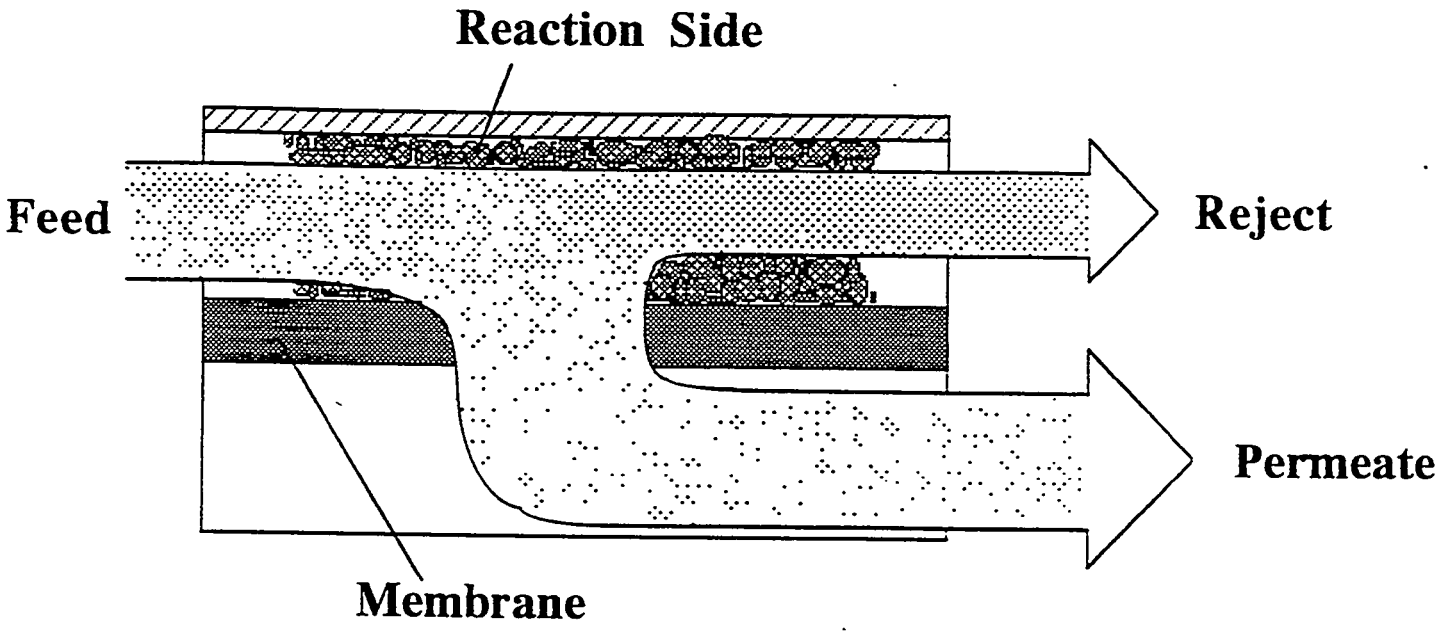

Figure 20. Schematic representation of the stage cut, cocurrent and countercurrent membrane reactors.

well. The preferential diffusion of H_2 across the membrane provides the shift in the equilibrium composition of the gas mixture on the reaction side (the shell side).

Two different process modes were considered in this study including cocurrent and countercurrent membrane reactor configurations (Figure 21). In the cocurrent configuration the permeate and reactant flow unidirectionally while in the countercurrent mode the flows are in the opposite directions.

Another parameter which is important for analysis of the membrane separation processes is the pressure ratio

$$P_r = \frac{P_{dn}}{P_{up}} \qquad (32)$$

The separation of a gas mixture is always more effective when the process is carried at low values of the pressure ratio.

5.2 Decomposition of H_2S in the membrane reactor

Experimental studies of the catalytic decomposition of H_2S in the membrane reactor are summarized in Table 4. Gas mixtures of H_2S in nitrogen with different concentrations (500 ppm to pure H_2S) were used as feed gas mixtures. The decomposition process in the membrane reactor was conducted at either 2.36 atm (20 psi) or 7.8 atm (100 psi) pressure on the reaction side.

5.3 Mathematical model of H_2S decomposition in the membrane reactor

It is well known that the membrane reactor simulation usually involves determination of the kinetic parameters such as the reaction rates for the pertinent reactions. The pressure drop along the membrane reactor should also be specified for an accurate simulation. The temperature profile along the module also affects the conversion in the reactor. In addition, the external mass transfer resistance may decrease the conversion in the packed bed reactor. All of these complicating factors do not necessarily enhance the conversion in the membrane reactor but on the contrary may decrease it. The primary objective in the design of the membrane reactor,

Table 4 Status of the study of H_2S decomposition in the membrane reactor.

COUNTERCURRENT MODE	100%		8.7%		1.1%		500ppm	
	20psi	100psi	20psi	100psi	20psi	100psi	20psi	100psi
	X	X	X	X	X	X		
COCURRENT MODE	100%		8.7%		1.1%		500ppm	
	20psi	100psi	20psi	100psi	20psi	100psi	20psi	100psi
			X	X	X	X	X	X

therefore, must be to eliminate or diminish all of the above mentioned factors. In our study we did not focus on the development of the sophisticated modelling technique but rather on the proper module design that eliminated altogether the above mentioned complications.

To achieve this objective, the size of the catalyst particles was calculated to provide virtually no resistance to the flow in the packed portion of the membrane reactor. The amount of the catalyst and the flow conditions of the experiment were so chosen that the external mass transfer limitations were decreased to the extent when the conversion in the packed bed was determined by the equilibrium of the reaction. The internal diameter of the membrane was also large enough to ensure that the friction losses, that may be quite significant at elevated temperature such as 800 °C, will not result in the significant increase of the pressure drop inside the membrane tube. Selectivity coefficients of the gas separation were measured in situ at 800 °C and found to be equal to the selectivity coefficients calculated based on the Knudsen diffusion model. The surface flow in the porous membrane at 800 °C was negligibly small compared to the Knudsen flow.

As a result of the systematic analysis of the different factors affecting the overall performance of the membrane reactor, it was possible to design the membrane reactor that can be described by a very simple model based on the following assumptions:

* plug flow on the reaction and permeation sides;
* local reaction equilibrium on the reaction and permeation sides:
* ideal Knudsen selectivity of the gas separation.

It was demonstrated that the simplest rate expression can describe the kinetic data well:

$$-r_{H_2S}=k_o e^{-E/RT}\left(p_{H_2S}-\frac{p_{H_2}p_{S_2}^{0.5}}{K_{eq}}\right) \qquad (33)$$

where p_{H2}, p_{H2S}, p_{S2} are the partial pressures of H_2, H_2S, and S_2 respectively, K_{eq} is the equilibrium constant, k_o is the frequency factor, E is the activation energy.

The transmembrane flux is determined in accordance with

$$F_j = \frac{Q_j (p_{Rj} - p_{Pj})}{l} \tag{34}$$

where Q_j is the permeability coefficient, subscripts R and P are the reaction and the permeate sides respectively, l is the membrane thickness.

The following set of differential equations has to be solved in order to calculate the fluxes of the individual gas components and the total conversion in the membrane reactor [15]

(Reaction side)

$$\frac{dJ_{R\ H_2S}}{dx} = r_{H_2S} - \frac{2R_1 F_{H_2S}}{(R_3^2 - R_2^2)} \tag{35}$$

$$\frac{dJ_{R\ S_2}}{dx} = -0.5 r_{H_2S} - \frac{2R_1 F_{S_2}}{(R_3^2 - R_2^2)} \tag{36}$$

$$\frac{dJ_{R\ H_2}}{dx} = -r_{H_2S} - \frac{2R_1 F_{H_2}}{(R_3^2 - R_2^2)} \tag{37}$$

$$\frac{dJ_{R\ N_2}}{dx} = -\frac{2R_1 F_{N_2}}{(R_3^2 - R_2^2)} \tag{38}$$

(Permeate side)

$$\frac{dJ_{P\ H_2S}}{dx} = I_{H_2S} + \frac{2F_{H_2S}}{R_1} \tag{39}$$

$$\frac{dJ_{P\ S_2}}{dx} = -0.5I_{H_2S} + \frac{2F_{S_2}}{R_1} \tag{40}$$

$$\frac{dJ_{P\ H_2}}{dx} = -I_{H_2S} + \frac{2F_{H_2}}{R_1} \tag{41}$$

$$\frac{dJ_{P\ N_2}}{dx} = \frac{2F_{N_2}}{R_1} \tag{42}$$

Here J are the molar rates of the gas components on the reaction (shell) and permeation (tube) sides of the membrane reactor. The initial conditions for the above system of the differential equations are:

(Reaction side)

$$J_{R\ H_2S} = J_{H_2S\ 0} \tag{43}$$

$$J_{R\ S_2} = 0 \tag{44}$$

$$J_{R\ H_2} = J_{H_2\ 0} \tag{45}$$

$$J_{R\ N_2} = J_{N_2\ 0} \tag{46}$$

(Permeate side)

$$J_{P\ H_2S}=0 \quad (47)$$

$$J_{P\ S_2}=0 \quad (48)$$

$$J_{P\ H_2S}=0 \quad (49)$$

$$J_{P\ N_2}=0 \quad (50)$$

Two programs were developed to simulate the conversion in the membrane reactor based on Equations 35-42. In one of the programs the temperature along the membrane module was assumed to change gradually (Figure 5). The experimental temperature profile was fitted by using a polynomial function. The function was then used in the software package to describe the temperature variations of different parameters such as the reaction rate constants, the equilibrium constant, and the permeability. The permeability coefficient was assumed to change with the temperature in accordance with the Knudsen mechanism of gas diffusion. The reaction rate constants were taken from the literature [28,30].

$$k=k_o\exp(-\Delta E/RT)$$

Homogeneous reaction

$k_o=800$ [mol/(cm^3.s.atm)]

$\Delta E=47$ [kcal/mol]

Heterogeneous reaction

$k_o=300$ [mol/(g_{cat}.s.atm)]

$\Delta E=30$ [kcal/mol]

In the membrane reactor the Vycor glass membrane is catalytically active. There are no experimental data on the reaction rate constants for the catalytic decomposition of hydrogen sulfide on amorphous silica. Therefore, for the permeate side of the membrane reactor we used the values of the reaction rate for the homogeneous reaction. It should also be noted that in [28] three different kinetic models for the catalytic decomposition of H_2S were described. Three different sets of frequency factors and the activation energies were calculated based on these

models. The calculated constants produced good fits to the experimental data presented Kaloidas and Papayannakos [28]. However, if the data were used to calculate the reaction rate constants at the temperatures used in our experiments (800 °C, 100 psi, 100%-500 ppm) the different models produced similar values for the reaction rates. Moreover, [28] did not address the question of which model was the best to describe the system. An average of the three sets of the frequency factors and the activation energies was used in the simulations.

In the second model, we assumed that the temperature in the membrane module changed in steps from the room temperature to the average temperature in the membrane reactor equal to 775 °C and then back to the room temperature. Equilibrium conversion was assumed on the permeate and the reaction sides of the membrane reactor. Experimental data for the permeability coefficients at the room temperature and 775 °C were used in the model. The model with a variation of the temperature along the membrane module was named "non-isothermal" model while the other model was named "isothermal".

Both of the models are essentially isothermal models in the sense that in both of them the heat of reaction is not taken into account. The reaction of the H_2S decomposition is an endothermic reaction. It is, therefore, reasonable to assume that at low conversions it would be possible to control the temperature of the reaction mixture by using the external source of heat and the effect of the heat of reaction on conversion is negligible. For the IGCC system no significant heat effects are expected because of a very low concentration of H_2S in the feed (less than 1% H_2S).

The system of equations with the set of initial conditions was solved by using modified Runge-Kutta method. It is important to note that when the reaction rate is very fast, the effect of the stage cut on the conversion does not depend on the inlet flow rates and absolute values of the permeability coefficients, because the reaction mixture is always at the local equilibrium along the membrane reactor. The function depends only on the selectivity factors, pressure ratio across the membrane, and the equilibrium constant.

5.4 Simulation results

5.4.1 Hydrogen concentration in the membrane reactor

A good comparison between the experimental data on H_2 concentration in the membrane

reactor and the model predictions were observed for all of the tested experimental conditions (Figure 21). Both isothermal and non-isothermal models produced a good description of the changes in H_2 concentration in the membrane reactor on the permeate and reaction side. The models correctly describe a decrease in the H_2 concentration with an increase of the stage cut on both the permeate and the reaction sides. The isothermal model in spite of its simplicity provide a better prediction of the concentration dependencies on the stage cut. Apparently, the non-isothermal model underestimates the extent of the H_2S conversion on the permeate side. If the catalytic properties of Vycor glass membrane would be known then the model apparently could describe the reaction/separation processes in the membrane reactor much better. In the absence of such data the isothermal model provides better prediction of the membrane reactor performance. The difference between the experimental data and the theoretical predictions for both models is within 5% range.

Undoubtedly, the operation of the membrane reactor is different from the operation of the conventional packed bed reactor. It can be seen from Figure 21 that the concentration of H_2 on the permeation side far exceeds the equilibrium concentration of H_2 in the packed-bed side of the membrane reactor. At stage cut equal zero the concentration of H_2 on the permeate side is the highest. At the same time when the stage cut $\theta=0$ the concentration of H_2 on the reaction side is equal to the equilibrium concentration in the packed bed reactor at $p=P_{up}$. When the stage cut increases the concentration on both the permeate and the reaction sides of the membrane reactor decreases. At the stage cut $\theta=1$ the concentration of H_2 on the permeate side is determined by the equilibrium because all of the permeate diffuses through the membrane and reacts at the pressure $p=P_{dn}$. In this case, the operation of the membrane reactor in the cocurrent mode is essentially similar to the behavior of the conventional membrane separation modules. The permeate purity is the highest when the stage cut is the lowest. In this case, the average pressure gradient across the membrane is the highest. When the stage cut is high the concentration of highly permeable component decreases because of the dilution with lesser permeable components such as H_2S, S_2, and N_2. Less permeable products at the same time are being accumulated on the reaction side of the membrane reactor thus resulting in a decrease of the H_2 concentration.

The operation pressure on the reaction side may also affect the H_2 concentration

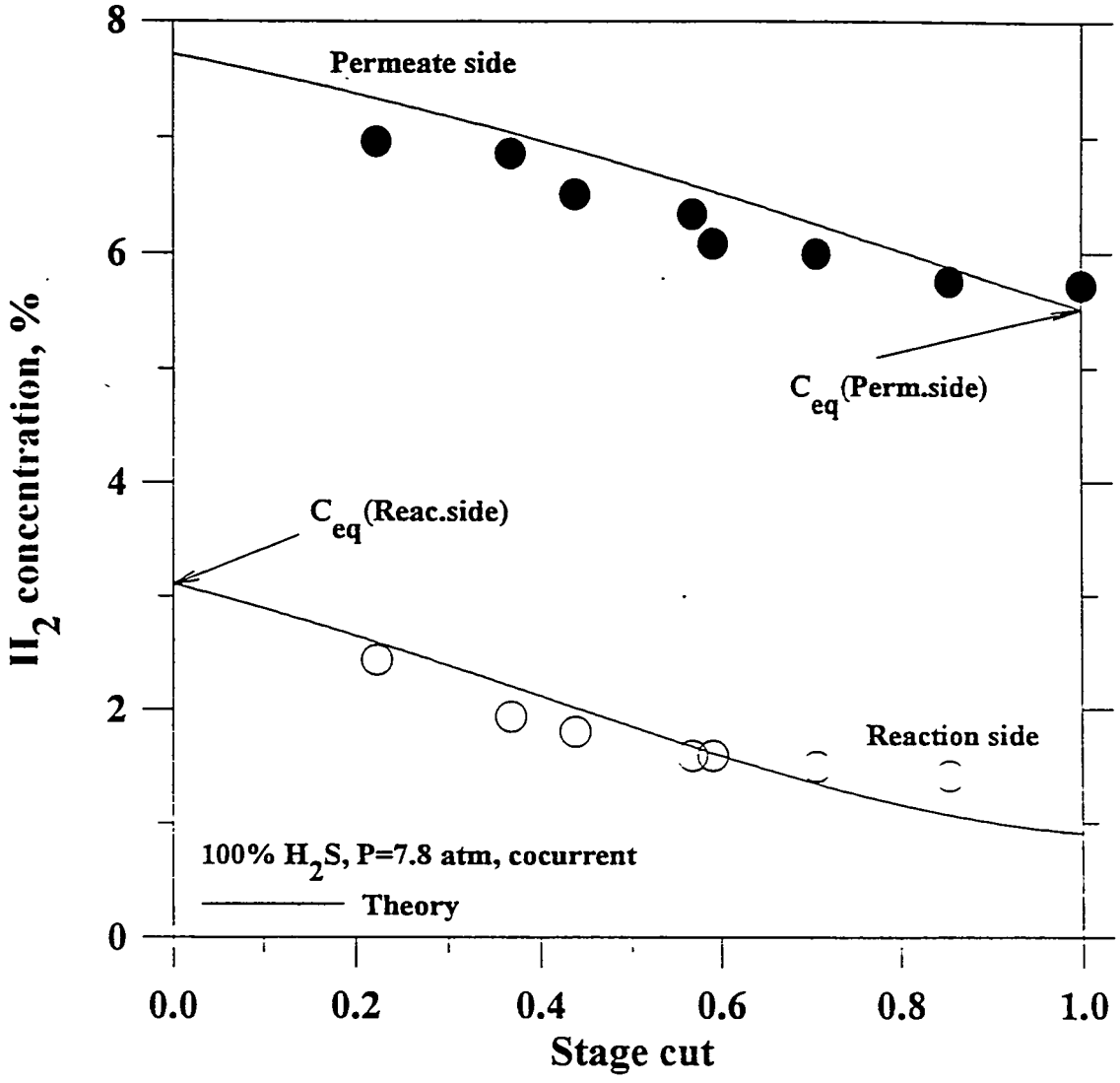

Figure 21(a). Hydrogen concentration at the outlet of the membrane reactor as a function of the stage cut for cocurrent membrane reactor (100% H_2S).

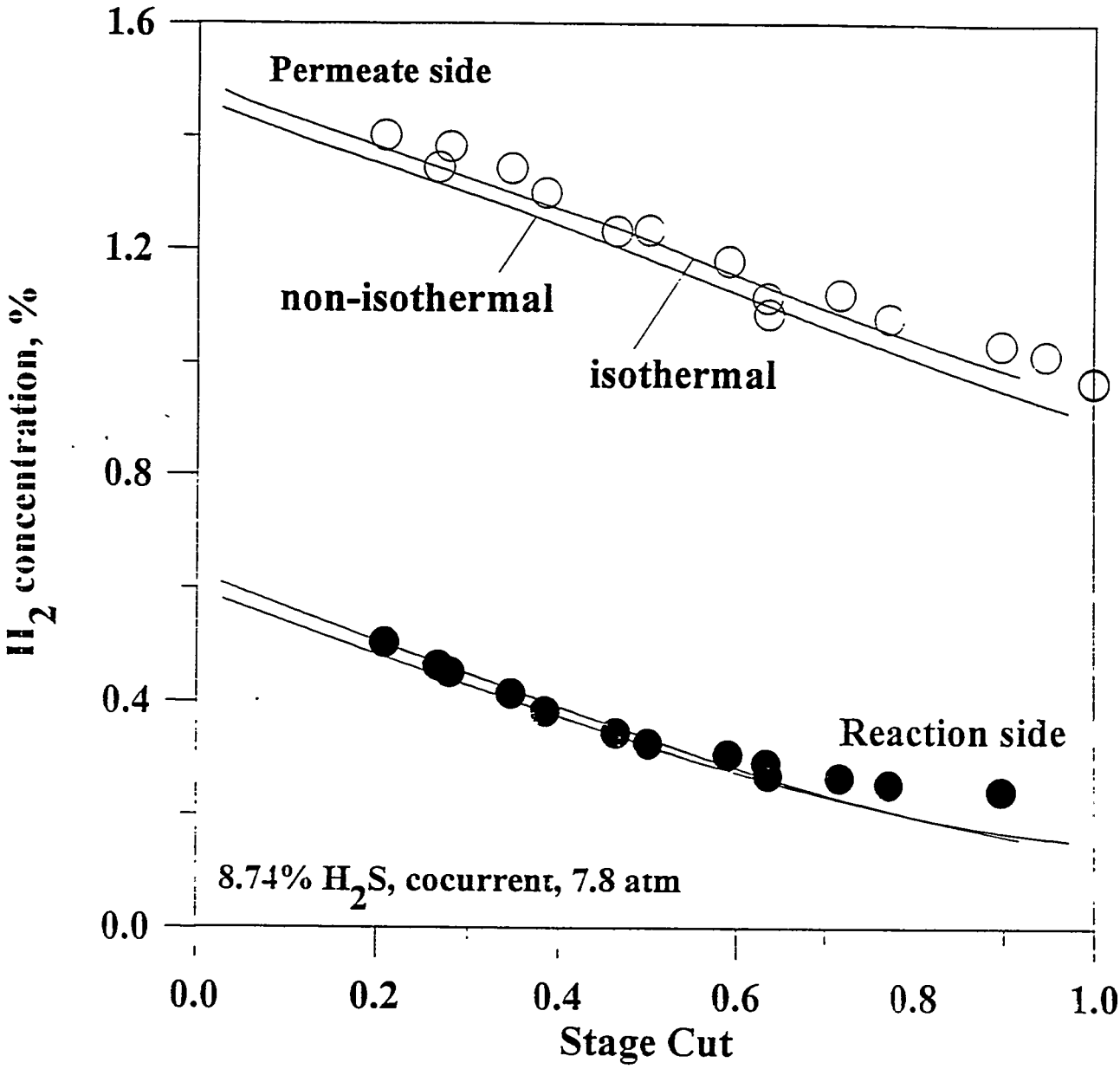

Figure 21(b). Hydrogen concentration at the outlet of the membrane reactor as a function of the stage cut for cocurrent membrane reactor (8.6% H_2S).

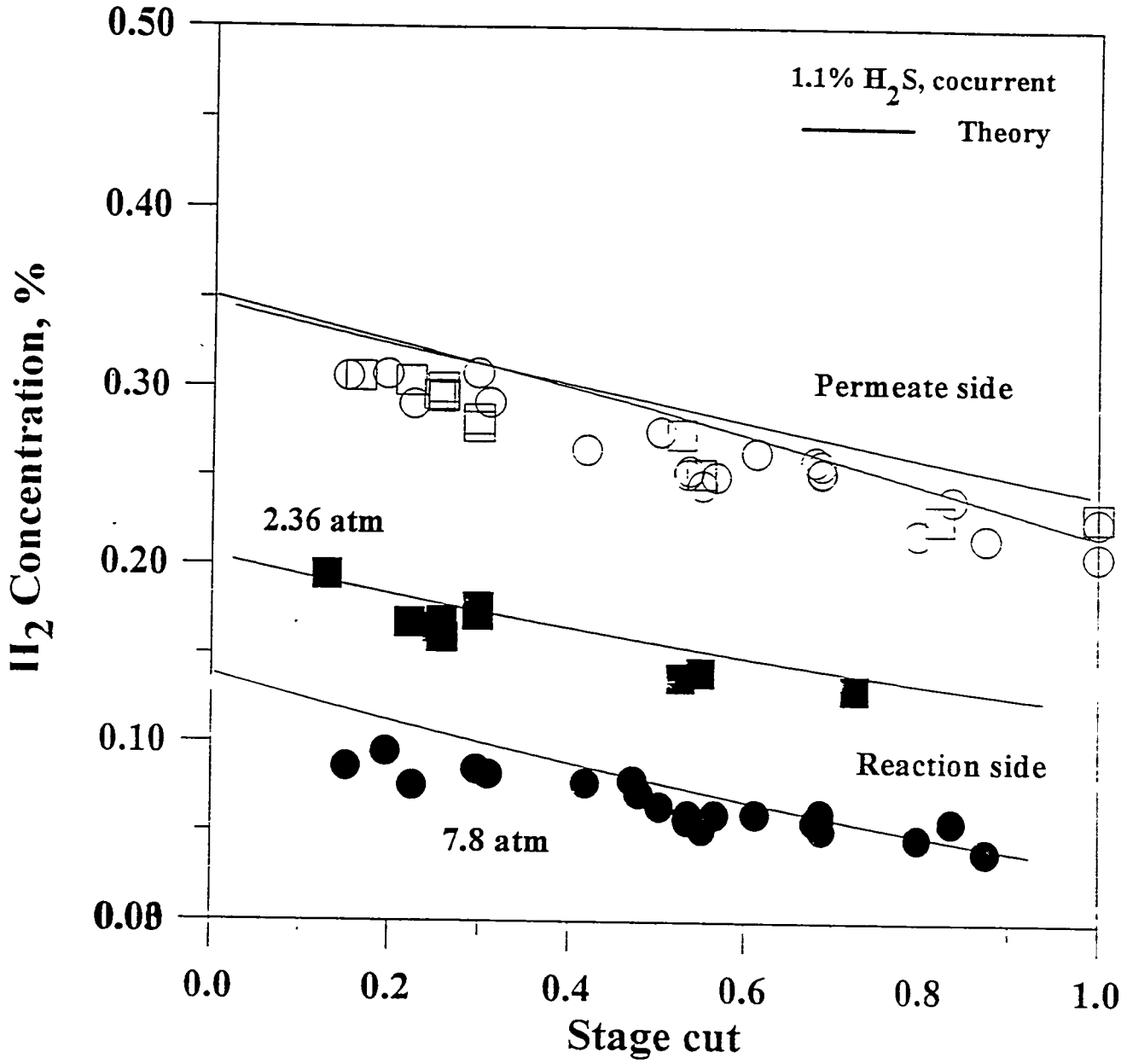

Figure 21(c). Hydrogen concentration at the outlet of the membrane reactor as a function of the stage cut for cocurrent membrane reactor (1.1% H_2S).

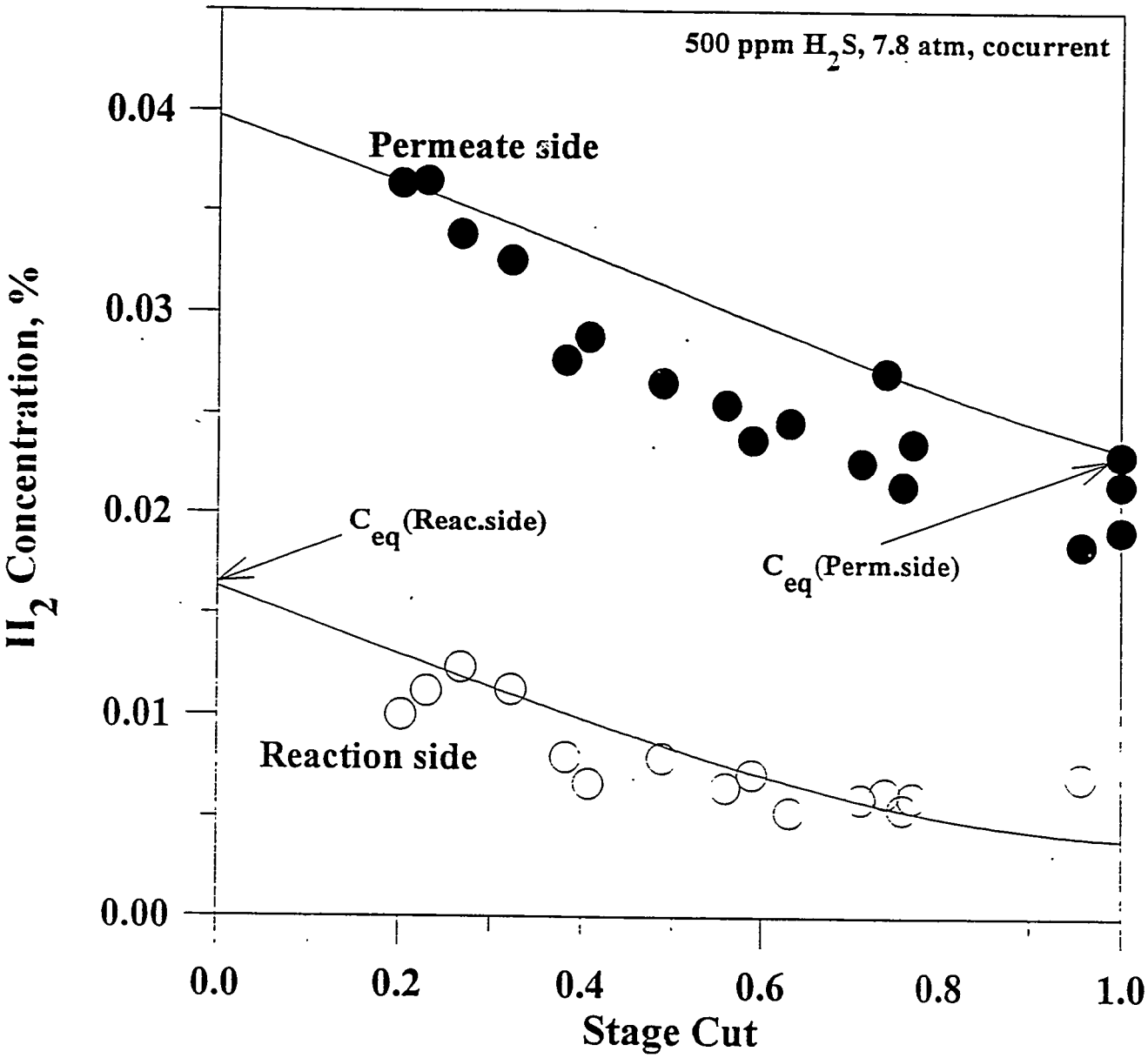

Figure 21(d). Hydrogen concentration at the outlet of the membrane reactor as a function of the stage cut for cocurrent membrane reactor (500 ppm H_2S).

distribution in the membrane reactor. When the absolute pressure on the reaction side increases and the permeate side pressure is fixed, then the pressure ratio P_r decreases. Smaller P_r is advantageous for the membrane separation. However, in the membrane reactor pressure changes result in the changes in the H_2S conversion. When the pressure increases the conversion decreases and the concentration of H_2 on the reaction side decreases. Figure 21 illustrates a decrease of the H_2 concentration on the permeate side at high pressures. When the absolute pressure on the reaction side was raised from 2.36 atm (20 psi) to 7.8 atm (100 psi) the concentration of H_2 on the reaction side decreased by approximately 0.1%. The concentration of H_2 on the permeate side almost did not change due to a better separation of H_2 at low P_r.

5.4.2 Partial pressure of H_2 in the membrane reactor

The separation of H_2 in the membrane reactor can be better explained by considering the dependence of the H_2 partial pressure on the permeate and reaction sides of the membrane reactor (Figure 22). The driving force for the H_2 separation is the H_2 partial pressure gradient across the membrane. The partial pressure of H_2 on the reaction side is the highest when the stage cut is equal to zero. When the stage cut increases the partial pressure on the reaction side slowly decreases due to the stripping of H_2 from the reaction gas mixture. At stage cut equal to one the partial pressures on the permeate and the reaction sides are the same and the membrane function as a simple filter without providing any separation properties. It was demonstrated, that the separation in the membrane reactor is better when the pressure ratio is small. Figure 22 illustrate this point. The difference in the partial pressures is small when the operation pressure is equal to 2.36 atm. Essentially, due to a small difference between the partial pressures on the permeate and the reaction sides, the membrane operation is similar to that of the filter. When the upstream pressure increased to 7.8 atm the H_2 partial pressure gradient increased and the separation in the membrane reactor improved as well. To ensure the highest separation of H_2 in the membrane reactor very low pressure ratios have to be maintained. That can be achieved by increasing the upstream pressure or, more effectively, by decreasing the permeate side pressure with a vacuum pump.

Based on the obtained experimental evidence it can be concluded that the removal of the

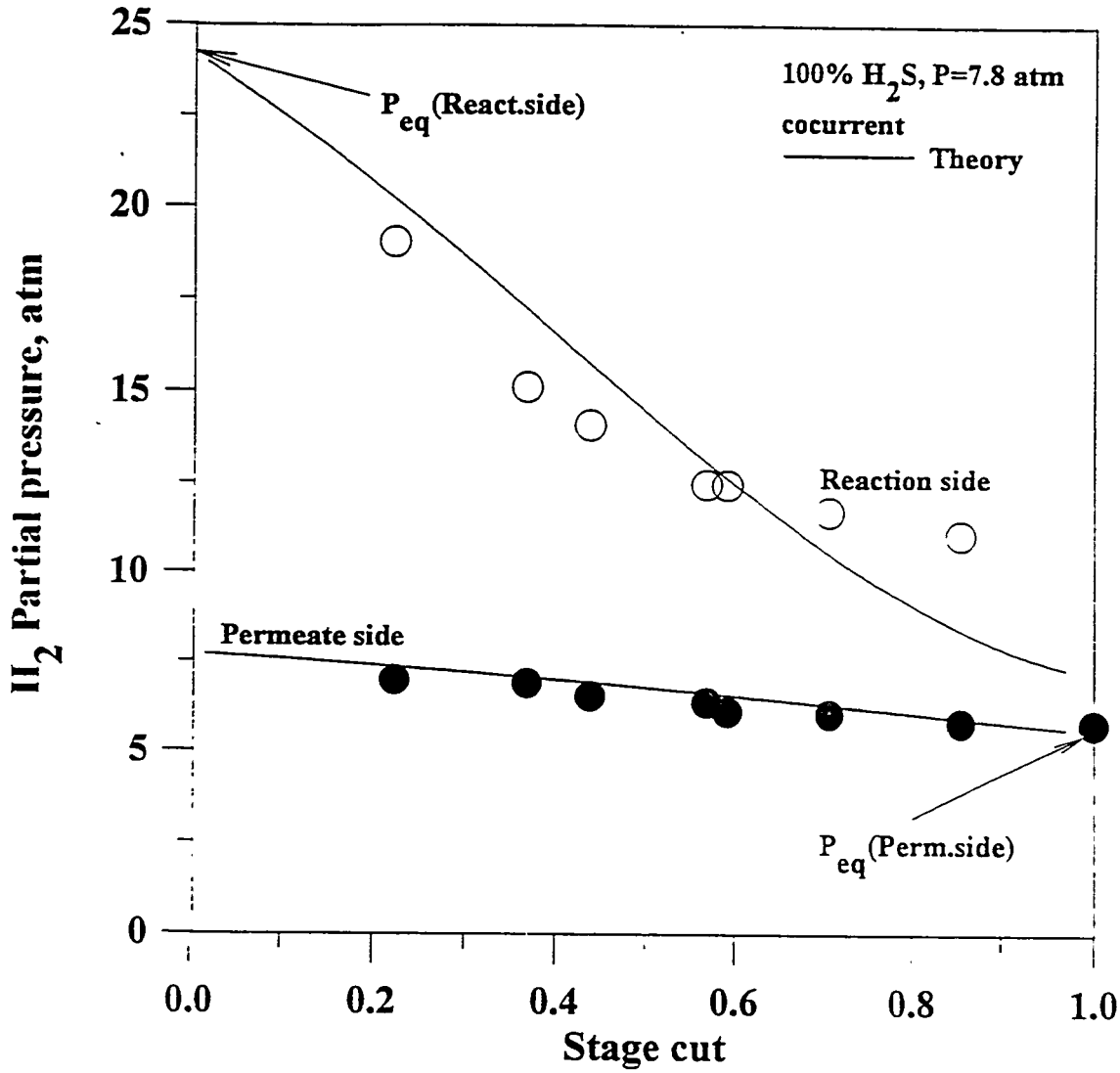

Figure 22(a). Partial pressure of H_2 at the outlet of the membrane reactor as a function of the stage cut for cocurrent membrane reactor (100% H_2S).

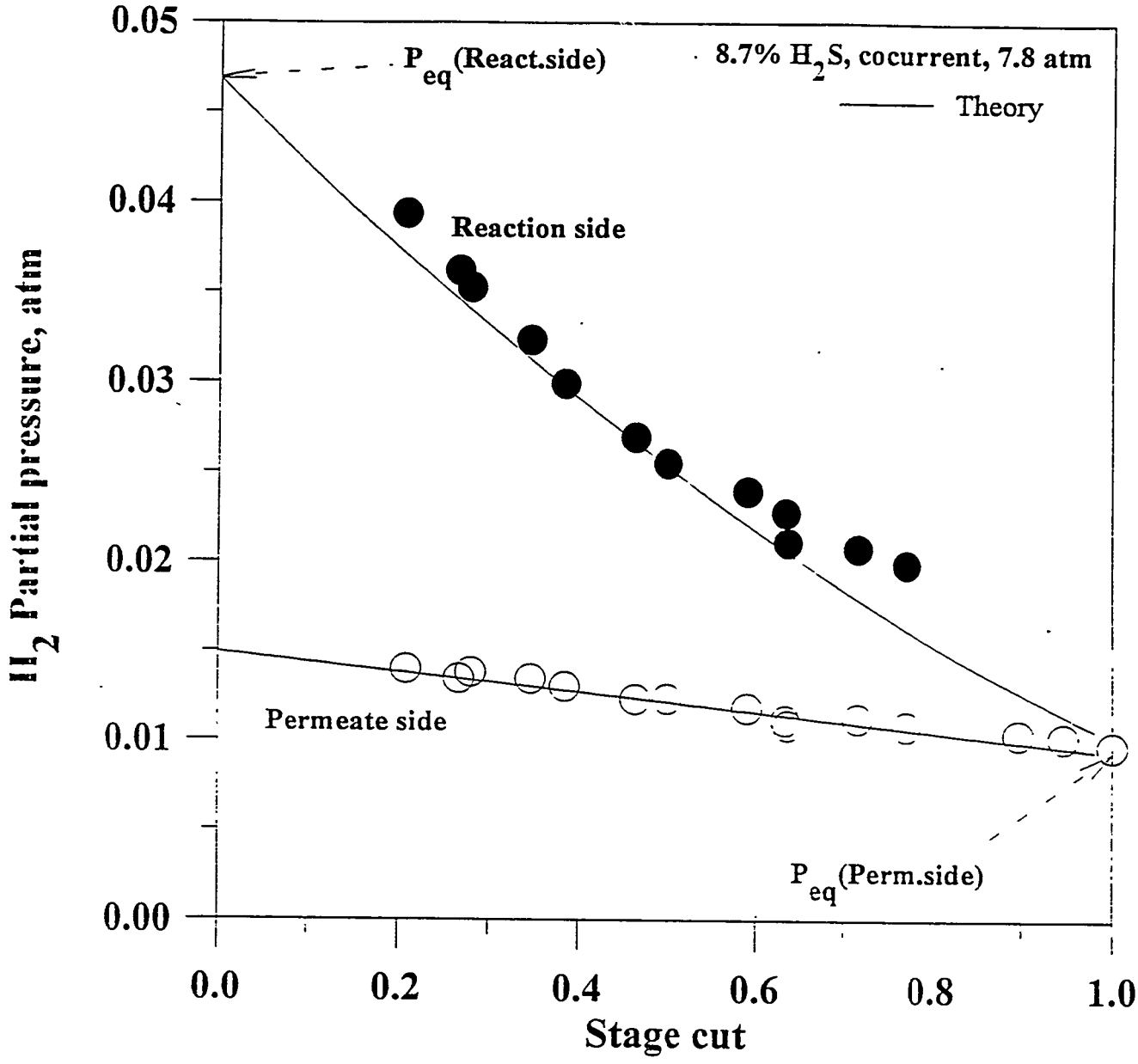

Figure 22(b). Partial pressure of H_2 at the outlet of the membrane reactor as a function of the stage cut for cocurrent membrane reactor (8.6% H_2S).

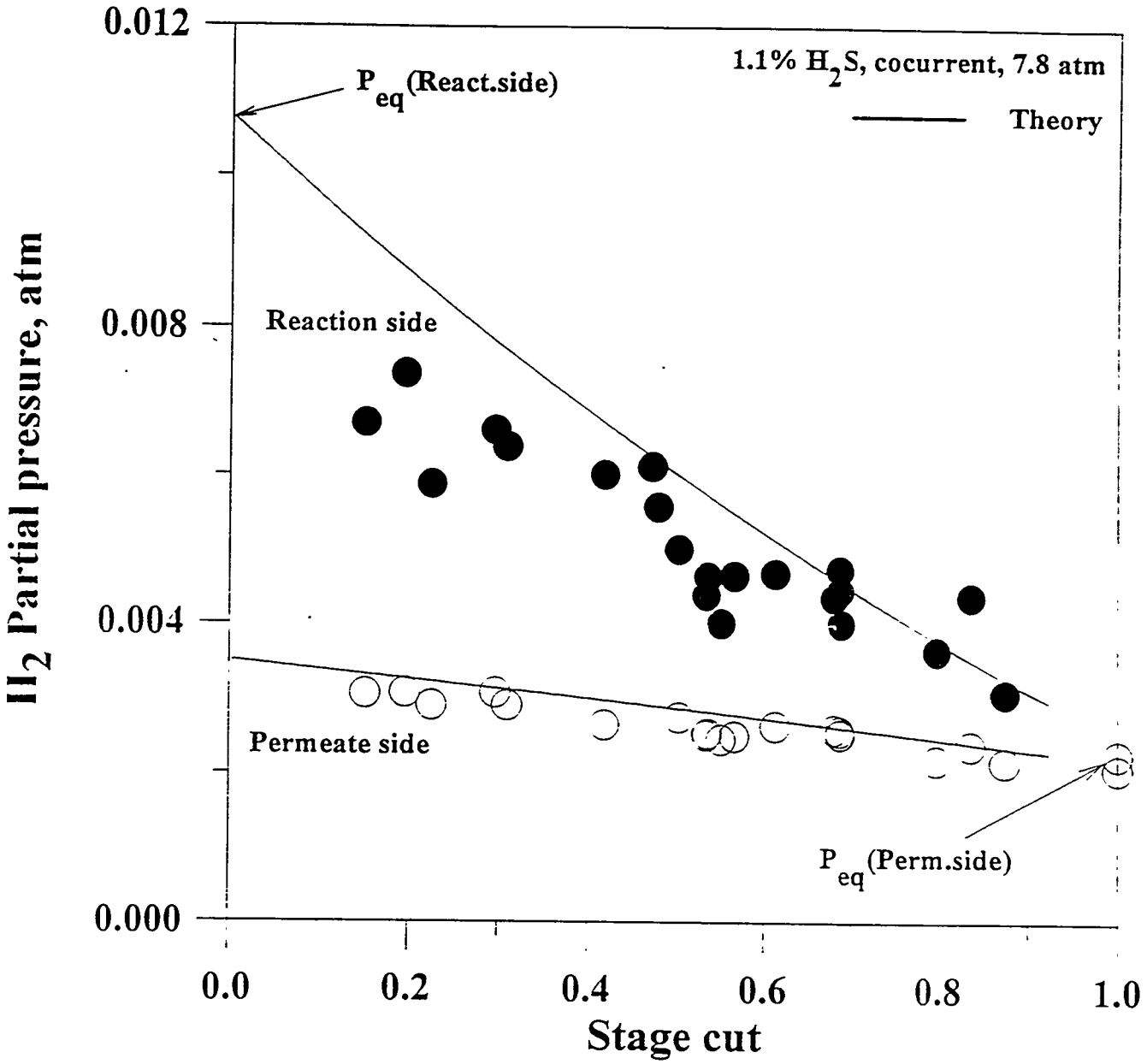

Figure 22(c). Partial pressure of H_2 at the outlet of the membrane reactor as a function of the stage cut for cocurrent membrane reactor (1.1% H_2S).

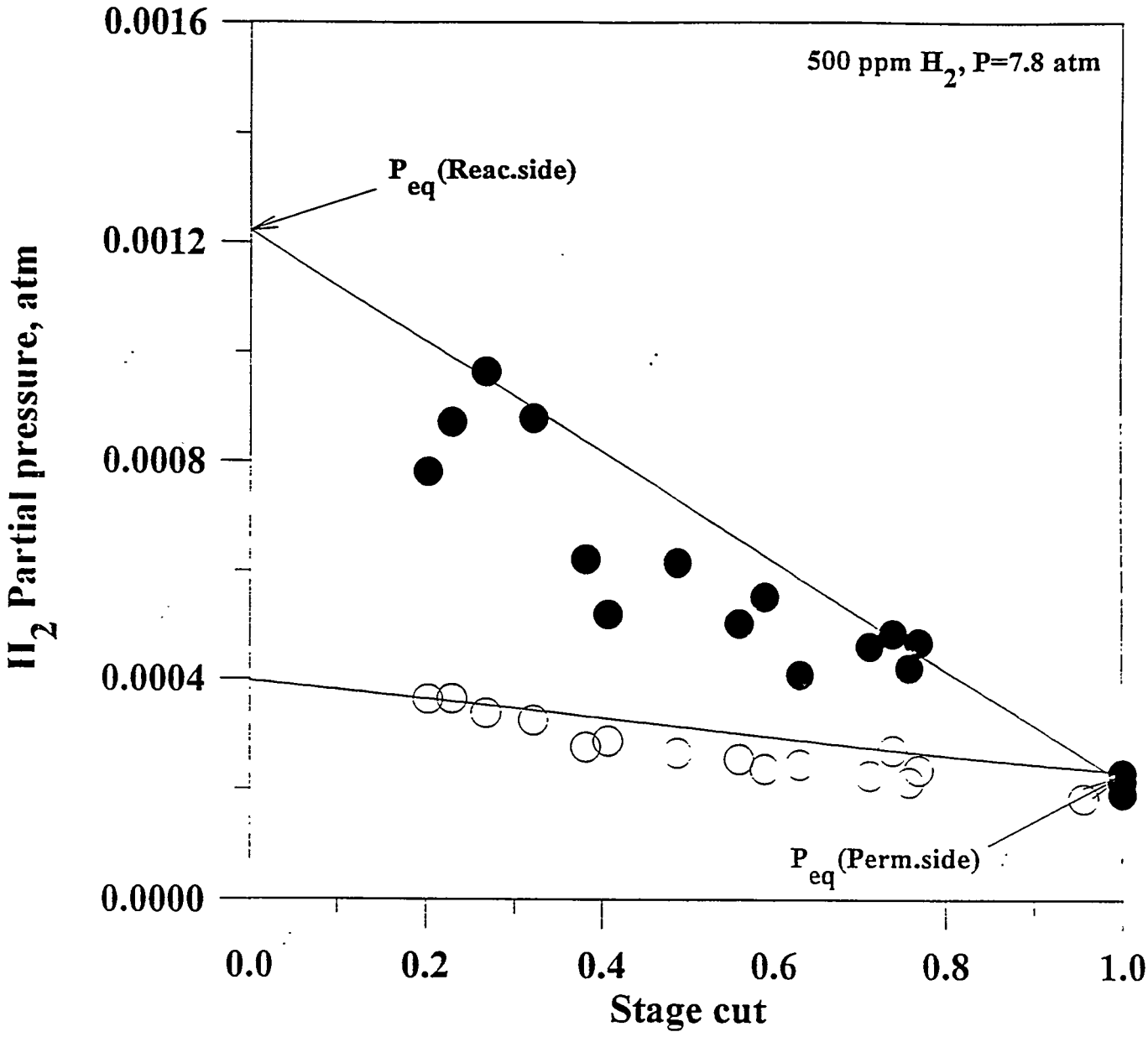

Figure 22(d). Partial pressure of H_2 at the outlet of the membrane reactor as a function of the stage cut for cocurrent membrane reactor (500 ppm H_2S).

highest permeable component from the reaction side occurs during the course of the reaction process in the cocurrent membrane reactor.

5.4.3 The conversion in the membrane reactor

The total conversion as a function of the stage cut regardless of the membrane selectivity is bound by two extremes. At the stage cut close to zero the flow rate on the reaction side considerably exceeds the flow rate on the permeate side. Therefore, even the concentration of H_2 in the cocurrent configuration is the highest, the product $\theta C_{H2,T} \rightarrow 0$ as $\theta \rightarrow 0$. Thus the total conversion at $\theta \rightarrow 0$ is

$$\lim_{\theta \to 0}(X^T) = \frac{\theta C_{H_2}^T + (1-\theta)\, C_{H_2}^S}{C_{H_2S}^F} = \frac{C_{H_2}^S}{C_{H_2S}^F} \qquad (52)$$

which is essentially the expression for the equilibrium conversion in the packed bed reactor at the upstream pressure. For very high stage cuts the influence of the conversion on the reaction side is negligible and the total conversion is

$$\lim_{\theta \to 1}(X^T) = \frac{\theta C_{H_2}^T + (1-\theta)\, C_{H_2}^S}{C_{H_2S}^F} = \frac{C_{H_2}^T}{C_{H_2S}^F} \qquad (53)$$

Therefore. the conversion at high stage cuts is determined by the hydrogen concentration on the permeate side. If a catalyst is present on the permeate side than at $\theta \rightarrow 1$ the total conversion is simply equal to the conversion at the low pressure side of the membrane reactor.

The highest conversion observed in the membrane reactor did not exceed the equilibrium conversion at the low pressure side of the membrane reactor. The conversion increased when the stage cut increased for the cocurrent membrane reactor configuration and both of the models gave reasonable estimate of the changes in the conversion vs. the stage cut (Figure 23). One may notice however, that the isothermal model predicts the conversion in the membrane reactor better than the non-isothermal model. Figure 23 represents the comparison between the experimental data on the H_2S (500 ppm concentration) conversion in the membrane reactor with the theoretical predictions. The experimental error in this case is relatively large because the GC detector under

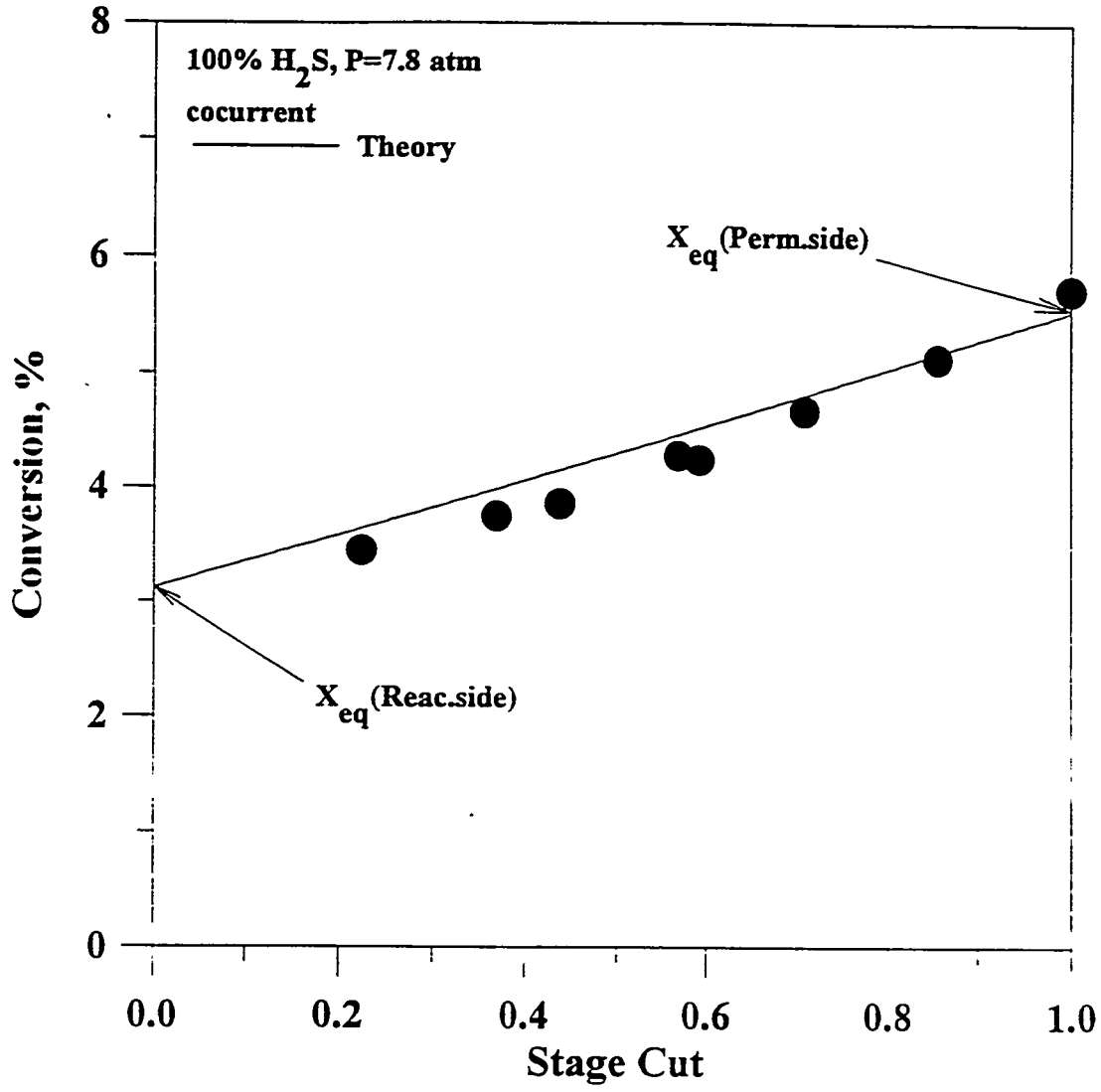

Figure 23(a). Conversion of H_2S in the cocurrent membrane reactor (100% H_2S).

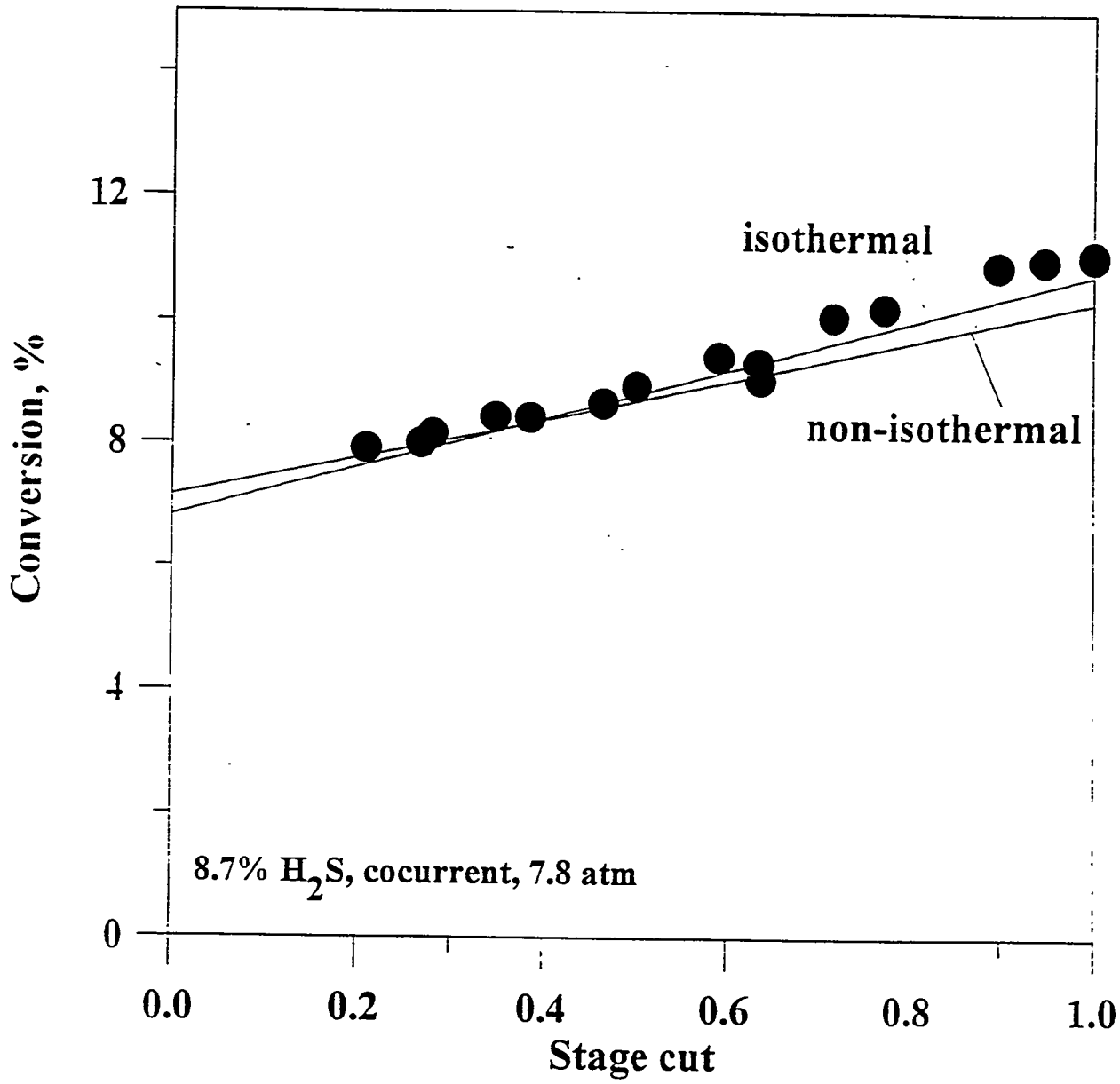

Figure 23(b). Conversion of H_2S in the cocurrent membrane reactor (8.6% H_2S).

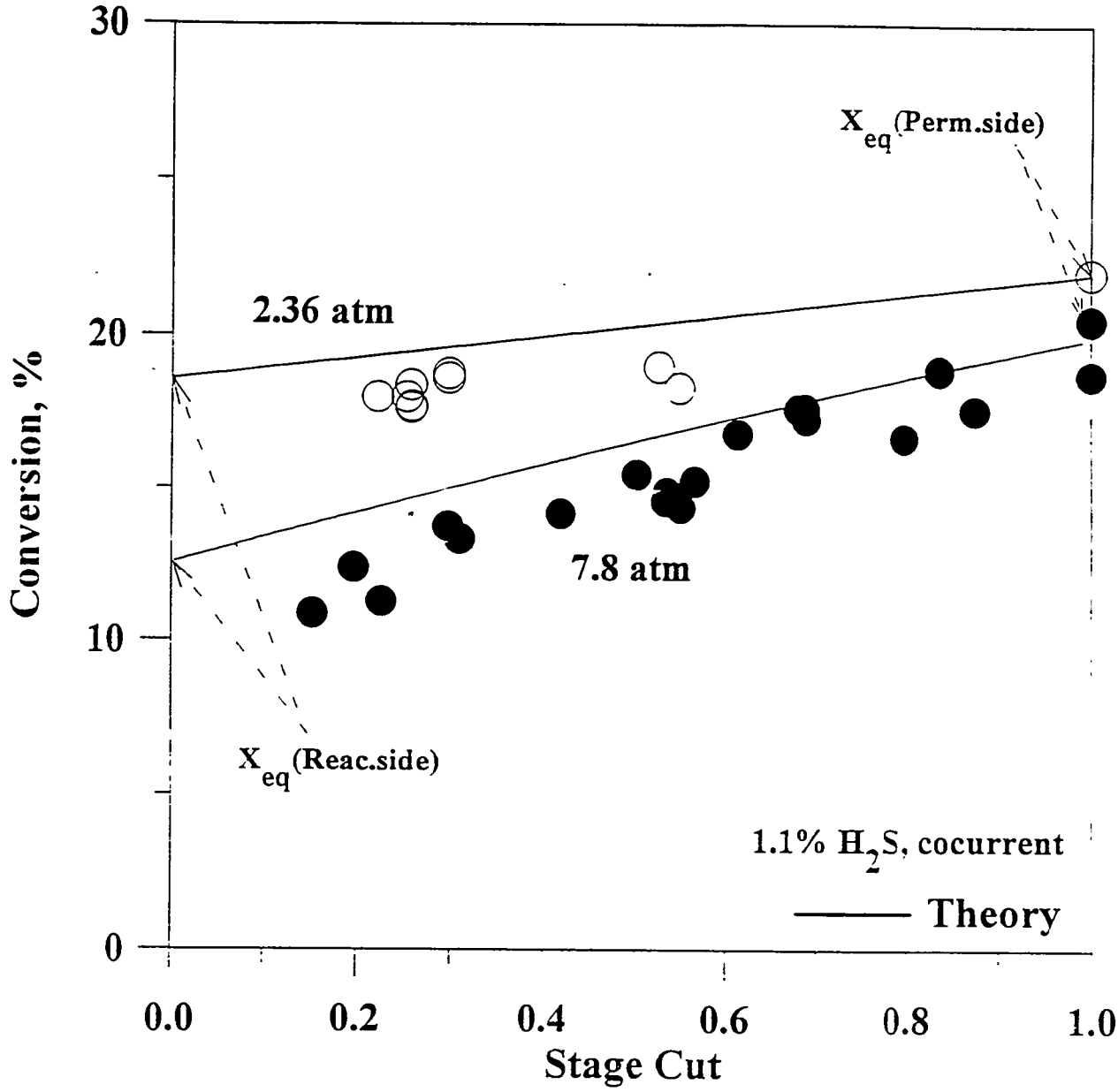

Figure 23(c). Conversion of H_2S in the cocurrent membrane reactor (1.1% H_2S).

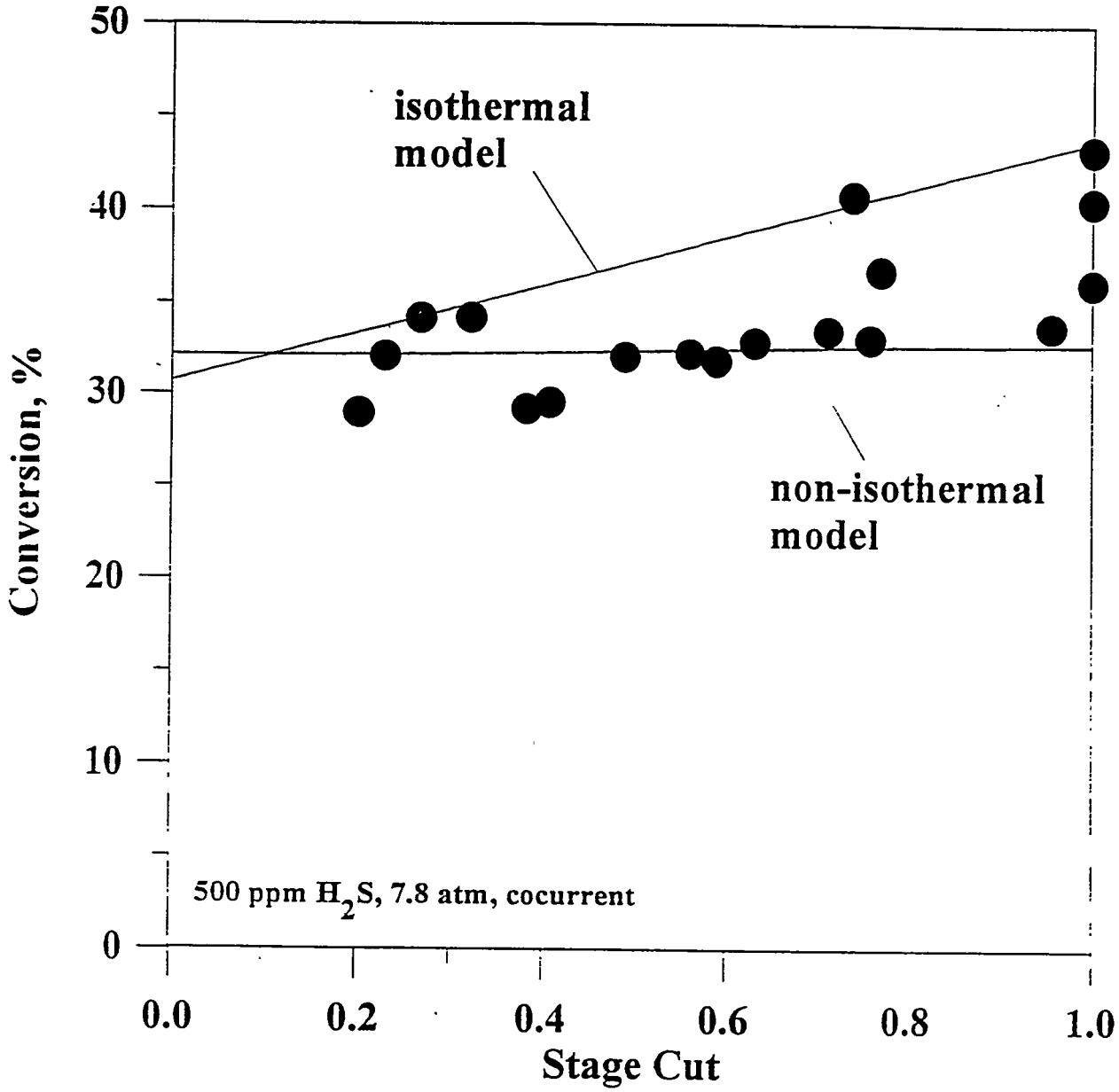

Figure 23(d). Conversion of H_2S in the cocurrent membrane reactor (500 ppm H_2S).

these conditions operates close to its detection limit. The dependence of the H_2 concentration on the reaction side of the membrane reactor is described quite well by both models. The non-isothermal model slightly underestimates the concentration of H_2 on the permeate side. It is probable that the underestimation of the hydrogen concentration on the permeate side was due to the underestimation of the reaction rate constants on the permeate side. The non-isothermal model uses the reaction rate constants for the homogeneous reaction on the permeate side while it would probably be more accurate to use the reaction rates for the heterogeneous reaction on the silica membrane.

5.4.4 Pressure dependence of the conversion in the membrane reactor

It was demonstrated that the isothermal model gives a good description of the conversion in the membrane reactor. Based on this model we can now simulate the optimum conditions for the membrane reactor operation. In addition, we can estimate the performance of the membrane reactor under the conditions of the IGCC process.

Dependencies of the H_2 concentration in the membrane reactor as a function of the stage cut and the pressure gradient across the membrane are presented in Figure 24. It was assumed that the pressure on the permeate side is equal to 1 atm. The concentration of the H_2S in the feed gas stream was equal to 1.1%. The membrane with the Knudsen selectivity (Vycor glass membrane) was used in the experiments and was assumed in the model.

It can be seen (Figure 24) that the hydrogen concentration decreases when the stage cut increases on both the permeate and the reaction sides of the membrane reactor. The concentration of hydrogen on the permeate side however is less affected by the pressure gradient across the membrane. At the same time the concentration of H_2 on the reaction side decreases considerably when the pressure gradient across the membrane increases. Two factors should be taken into account while considering the dependence of the hydrogen concentration on the stage cut at different pressures. First, the reaction of H_2S is a volume expansion reaction. Therefore, when the pressure on the permeate side increases the conversion decreases. On the other hand, when the absolute pressure on the reaction side increases the partial pressure of H_2 on the reaction side increases as well. That results in a better separation of H_2 from the reaction mixture at higher pressure gradients across the membrane. At the pressure difference equal to

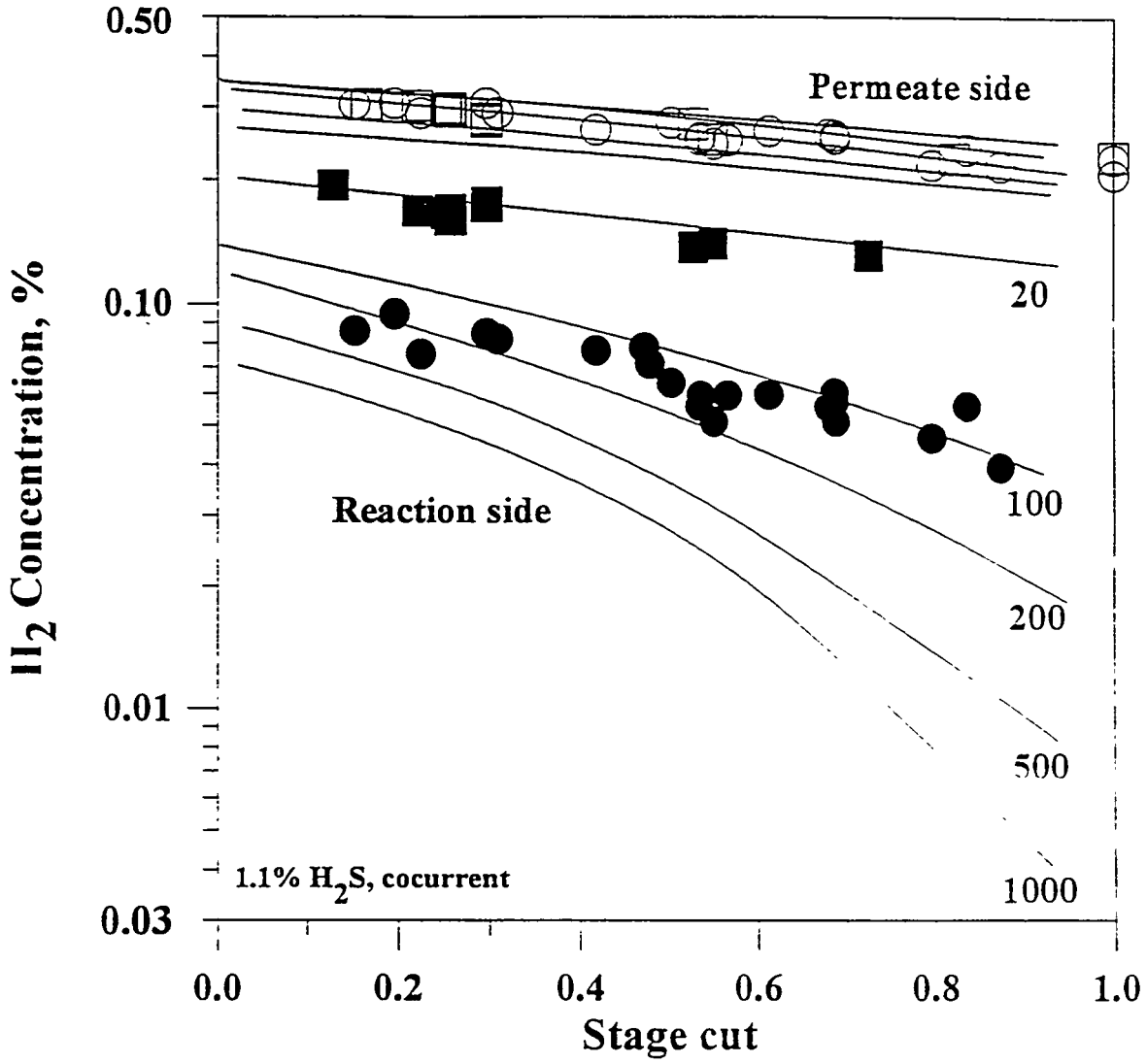

Figure 24. Pressure dependence of H_2 concentration in the cocurrent membrane reactor (1.1% H_2S feed).

1000 psi the hydrogen concentration on the reaction side decreases much steeper with the stage cut than at $\Delta p = 100$ psi. This happens due to a better removal of the H_2 from the reaction mixture.

Dependencies of the total conversion on the stage cut at different pressure gradients are depicted in Figure 25. The conversion always increases when the stage cut increases for the cocurrent membrane reactor configuration. A good agreement between the experimental data collected for $\Delta p = 20$ psi and $\Delta p = 100$ psi and the theoretical predictions was observed. The total conversion at higher pressure drops however is lower than the total conversion at the low pressure drops. The conversion is the lowest when the pressure gradient across the membrane is the highest and is equal to 1000 psi. The conversion decreases when the pressure drop across the membrane increases because of the pressure dependence of the H_2S conversion. Even a high separation performance observed at $\Delta p = 1000$ psi is not sufficient to outweigh the effect of the conversion decrease on the reaction side.

Obviously, the low selectivity characteristics for the Knudsen diffusion mechanism do not provide efficient separation of the reaction gas mixture. Without proper separation of H_2 the enhancement of the conversion cannot be significant. In addition, the concentration of H_2 on the permeate side is too low to be utilized.

5.5 Comparison between cocurrent and countercurrent modes

There is still no sufficient experimental evidence in the literature which of the membrane reactor configurations is more effective - cocurrent or countercurrent [9]. To address this problem the experiments on the H_2S conversion were conducted in both the cocurrent and countercurrent membrane reactor configurations.

In all of the studied cases the H_2 concentration on both the permeate and the reaction sides was found generally lower in the countercurrent configuration than in the cocurrent configuration (Figure 26). It is also interesting to note that the concentration on the permeate side of the membrane reactor is only slightly lower in the countercurrent mode, especially at the high stage cuts. For example in the case of 1.1% H_2S feed at $\theta > 0.5$ the concentration of H_2 is the same for both the cocurrent and countercurrent modes (Figure 26). The difference between

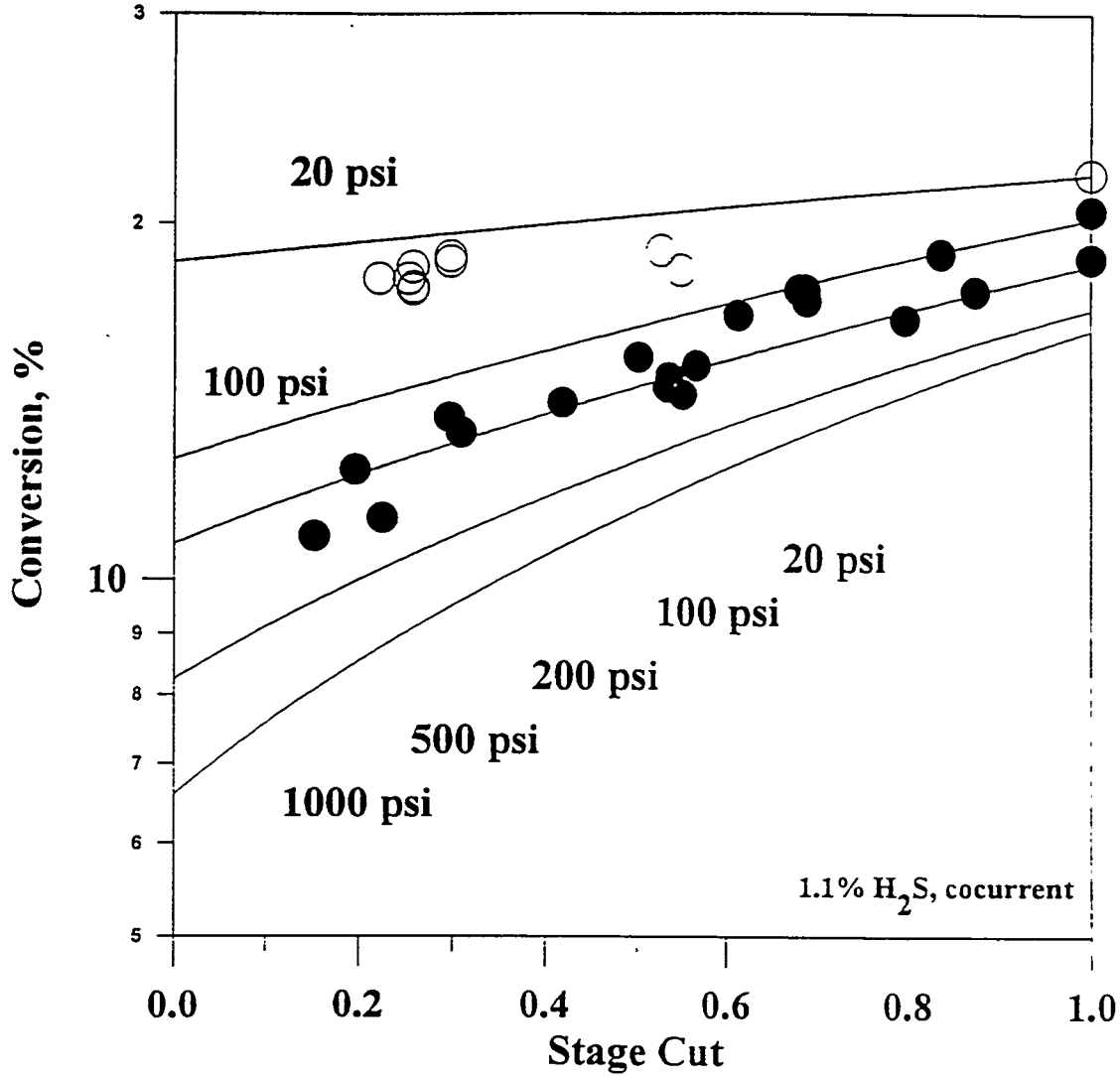

Figure 25. Pressure dependence of H_2S conversion in the cocurrent membrane reactor (1.1% feed).

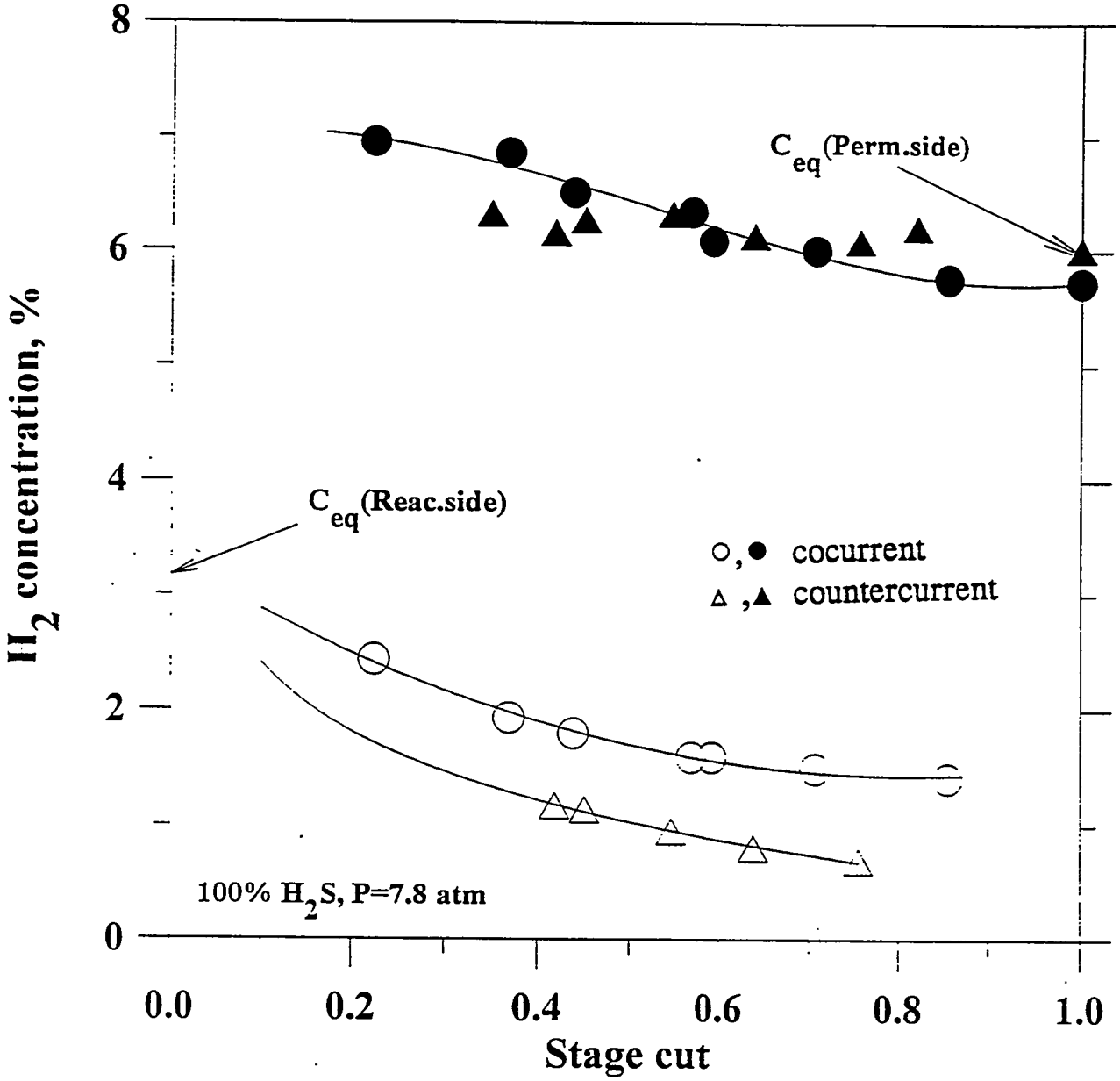

Figure 26(a). Concentration of H_2 in the cocurrent and countercurrent membrane reactors (100% H_2S).

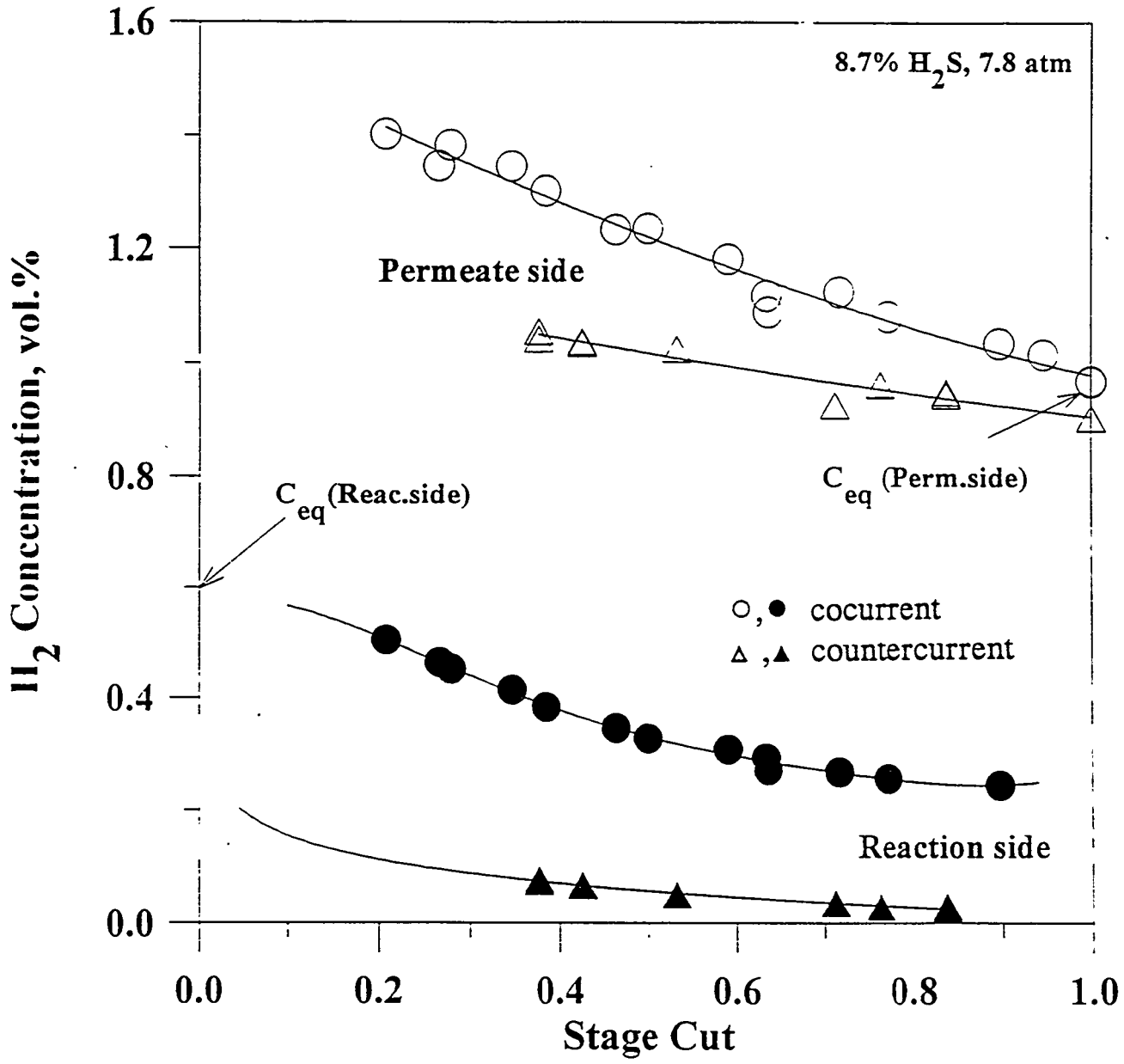

Figure 26(b). Concentration of H_2 in the cocurrent and countercurrent membrane reactors (8.6% H_2S).

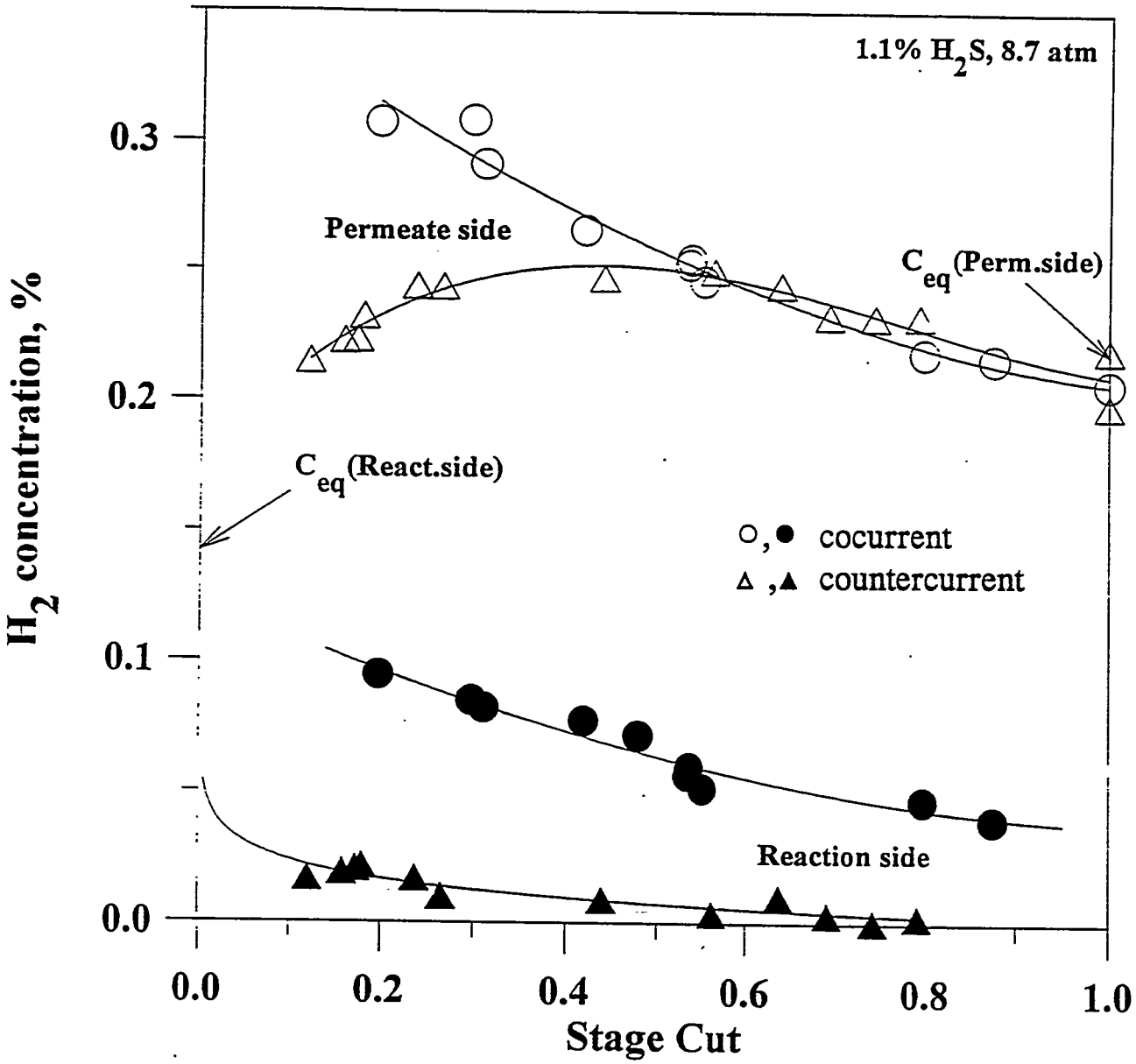

Figure 26(c). Concentration of H_2 in the cocurrent and countercurrent membrane reactors (1.1% H_2S).

the concentrations however is quite significant on the reaction side.

Clear explanation for the observed differences in the concentrations can be obtained from consideration of the partial pressure dependencies on the stage cut (Figures 27). When pure H_2S is used as a feed the partial pressure of H_2 is always higher on the reaction side than on the permeation side in the cocurrent configuration thus providing driving force for continuous H_2 removal from the reaction zone. On the contrary, for the countercurrent configuration at stage cut higher than 0.7 the partial pressure of hydrogen on the permeate side is higher than on the reaction side. Therefore, hydrogen will counterdiffuse to the reaction side and suppress the H_2S decomposition. The situation is presented graphically in Figure 29. The difference between the cocurrent and countercurrent configurations become even more evident when feeds with low content of H_2S were used. For 8.7% H_2S feed gas mixture the partial pressure of H_2 on the reaction side is lower than on the permeate side even at the stage cuts as low as 0.3. Further decrease in the reactant concentration in the feed results in further reductions of the H_2 partial pressure on the reaction side for the countercurrent configuration. Now, even at the stage cut equal to 0.1 the gradient of H_2 partial pressure was in the direction opposite to the transmembrane flow. Thus, for the countercurrent configuration hydrogen diffused back into the reaction stream thus effectively suppressing the conversion on the reaction side.

The unfavorable pattern of H_2 permeation in the countercurrent membrane reactor results in the lower conversions when compared to both the packed-bed reactor and the membrane reactor (Figure 28). The conversion of H_2S in the countercurrent reactor is always lower than the conversion in the cocurrent membrane reactor.The difference between the conversion in the cocurrent and countercurrent membrane reactors is the highest for the feeds with low concentration of the reactant because of the higher sensitivity of the H_2S conversion of the feeds with low concentration of H_2S to the presence of H_2 in the feed stream.

Cocurrent membrane reactor configuration provides higher conversion of H_2S than the countercurrent configuration.

5.6 Optimum conditions for H_2S decomposition

It is a generally accepted point of view that the membrane with an infinite selectivity of

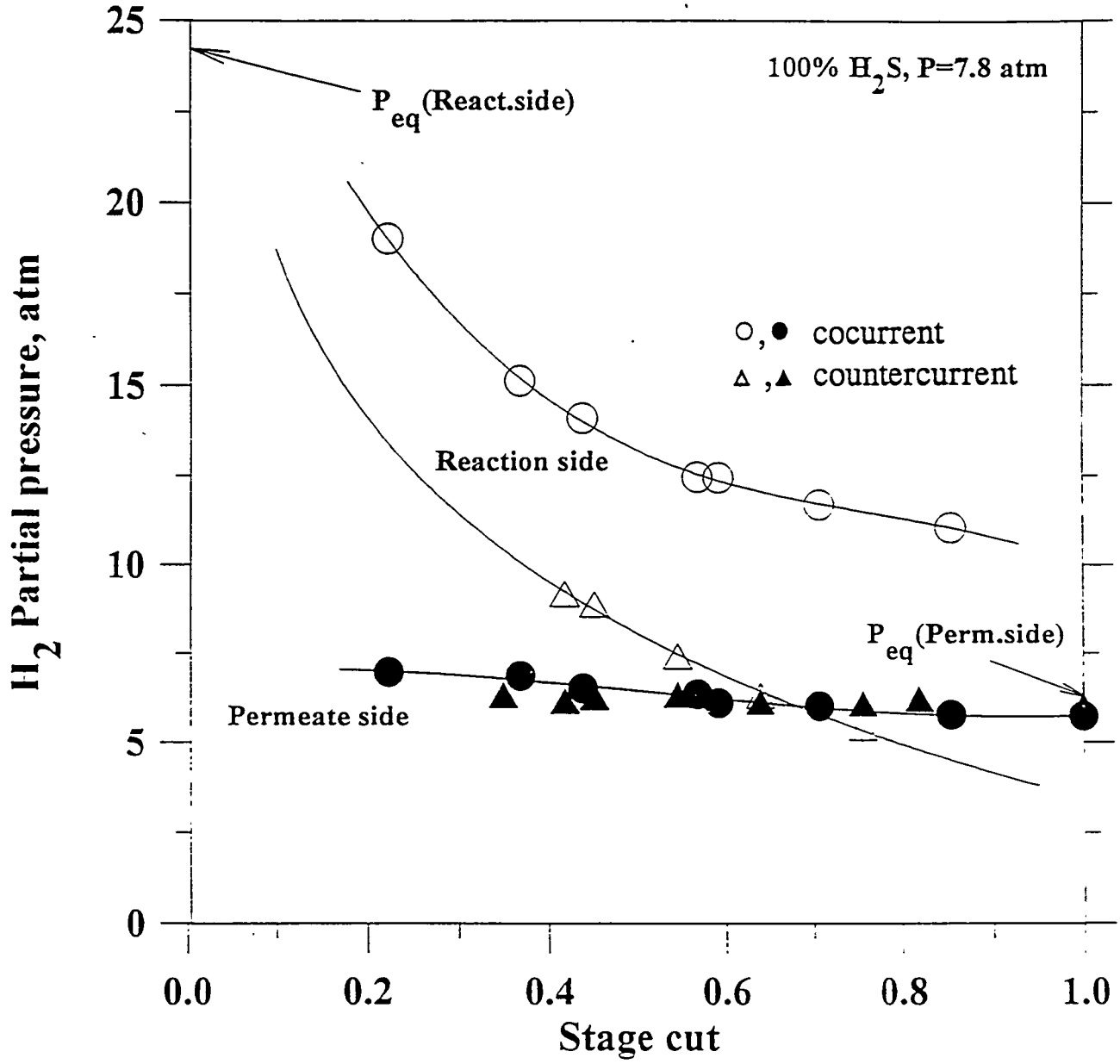

Figure 27(a). Partial pressure of H_2 in the cocurrent and countercurrent membrane reactors (100% H_2S).

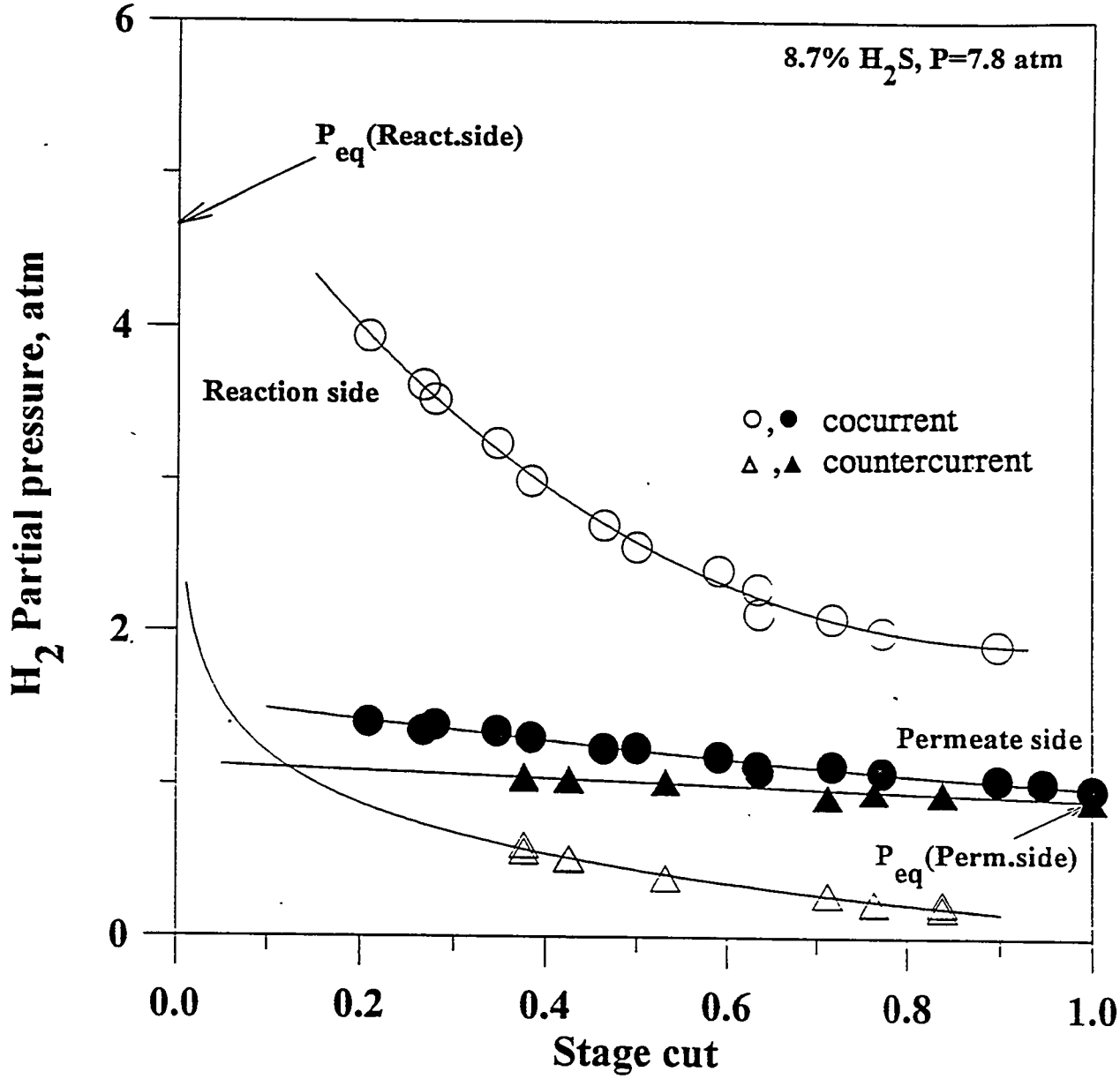

Figure 27(b). Partial pressure of H_2 in the cocurrent and countercurrent membrane reactors (8.6% H_2S).

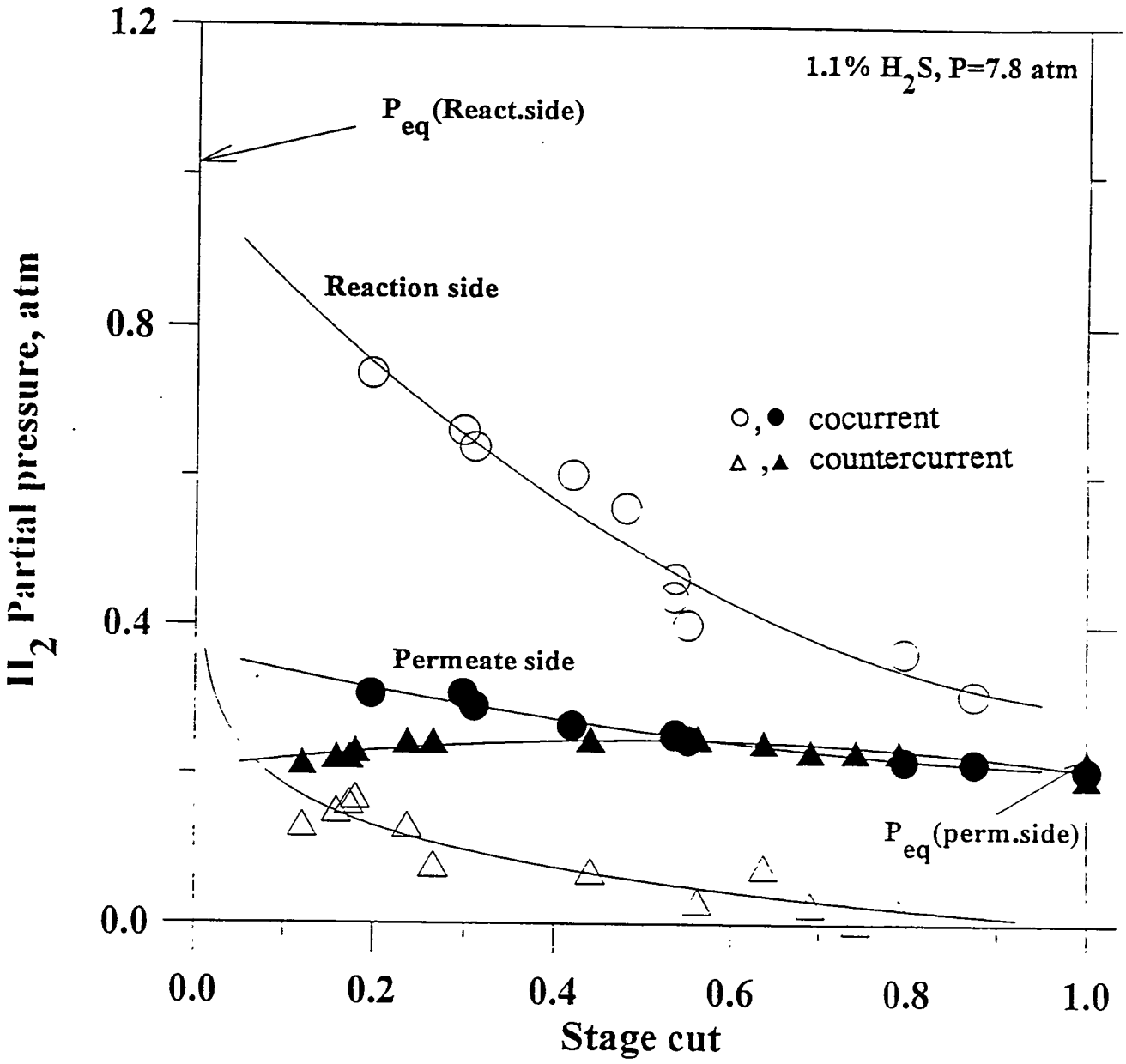

Figure 27(c). Partial pressure of H_2 in the cocurrent and countercurrent membrane reactors (1.1% H_2S).

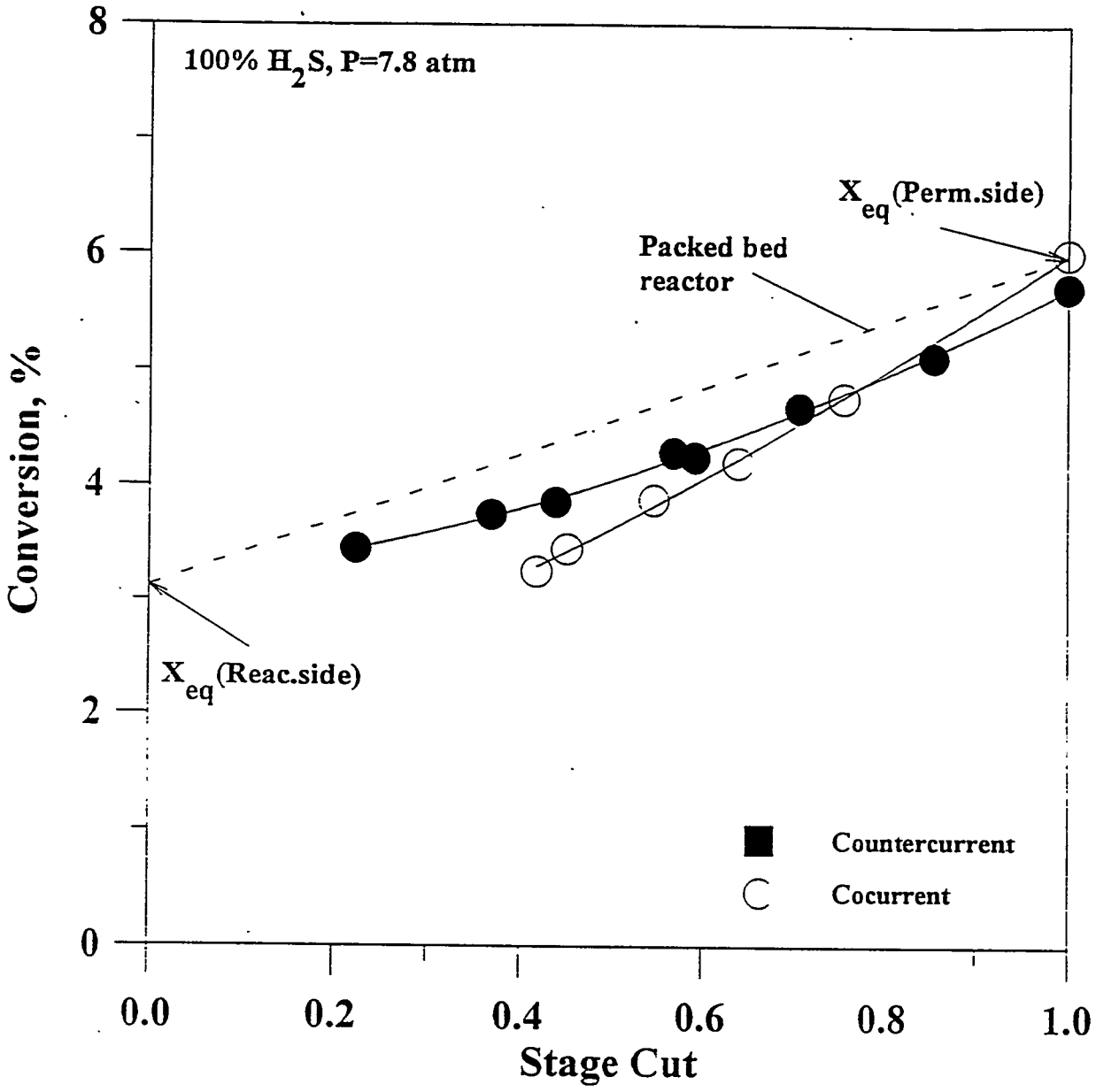

Figure 28(a). Conversion of H_2S in the cocurrent and countercurrent membrane reactors (100% H_2S).

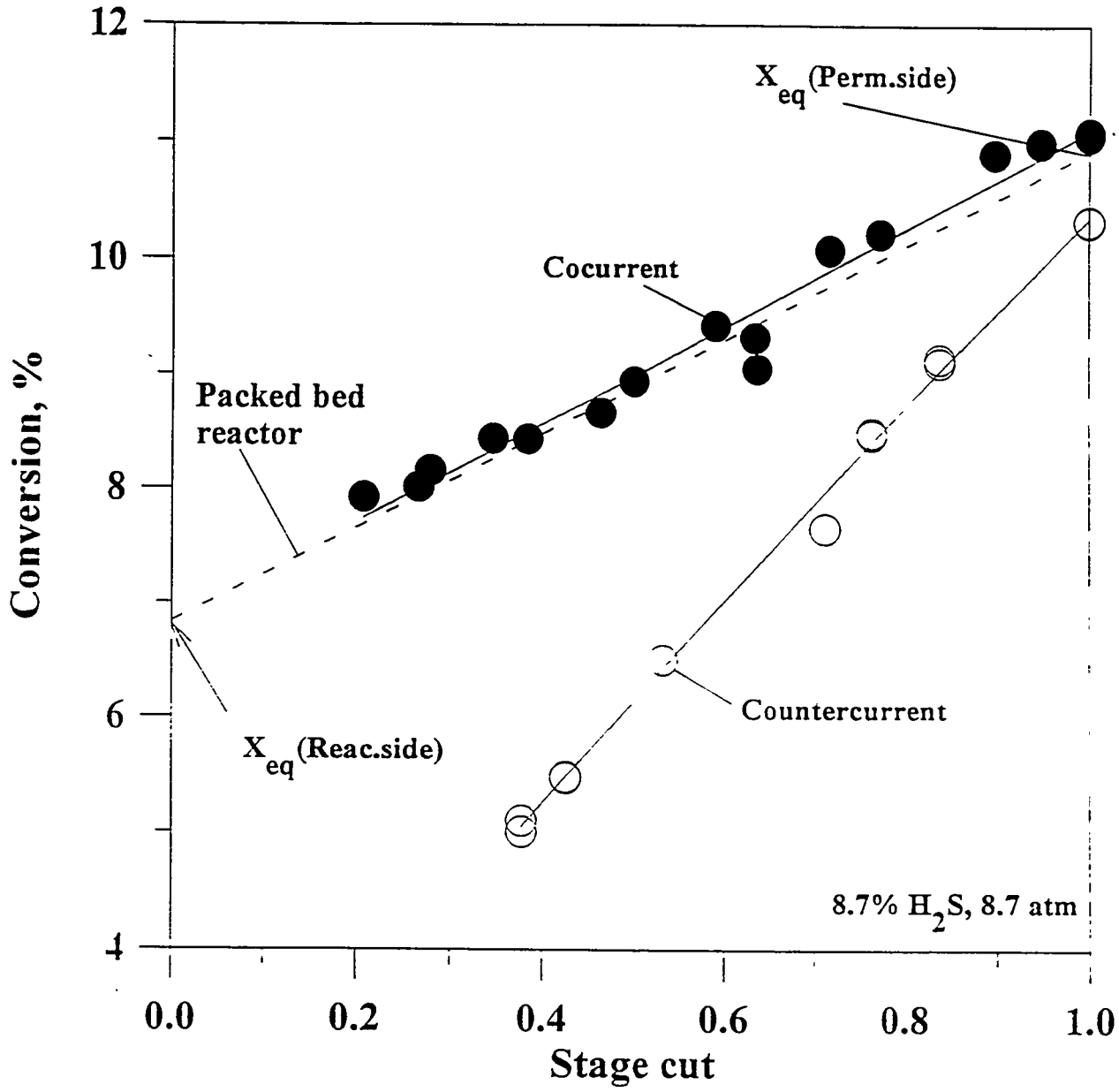

Figure 28(b). Conversion of H_2S in the cocurrent and countercurrent membrane reactors (8.6% H_2S).

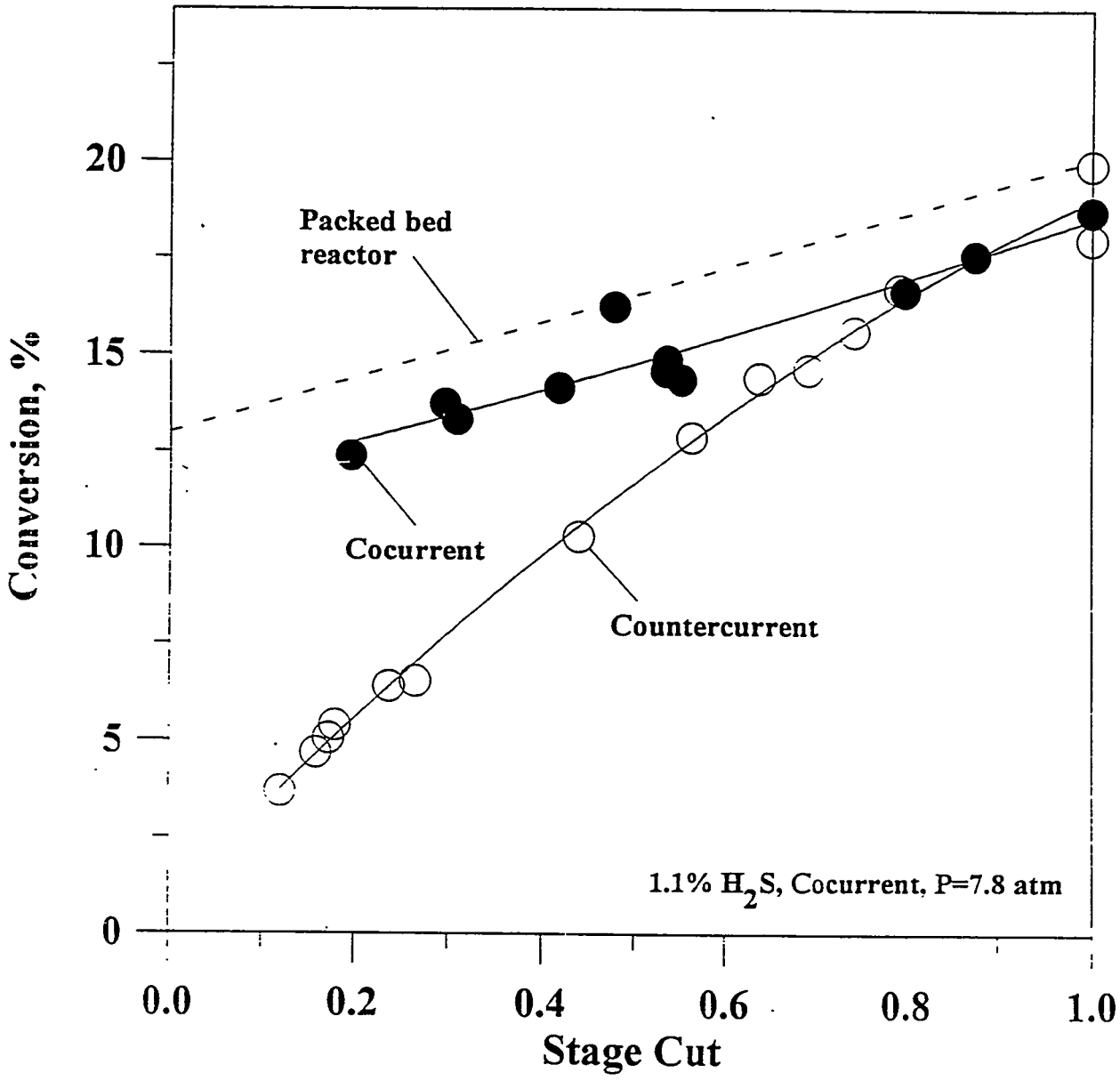

Figure 28(c). Conversion of H_2S in the cocurrent and countercurrent membrane reactors (1.1% H_2S).

I. Cocurrent Flow

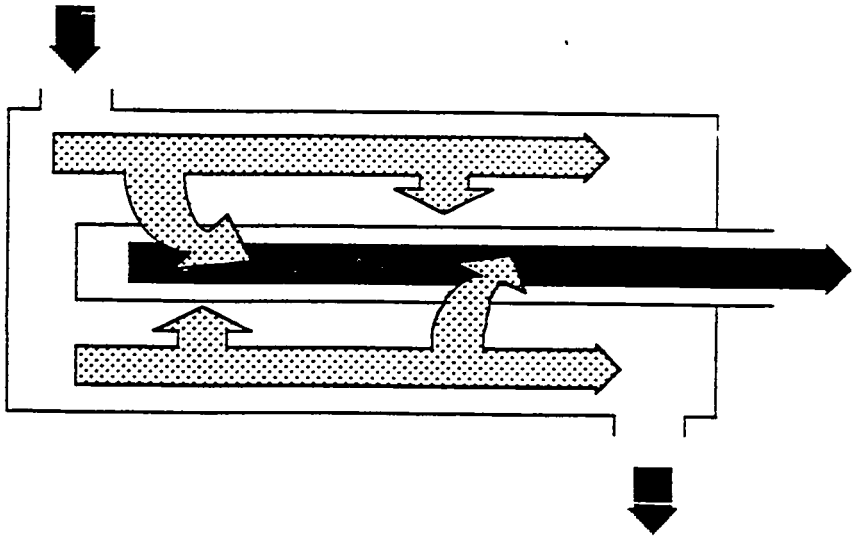

II. Countercurrent Flow

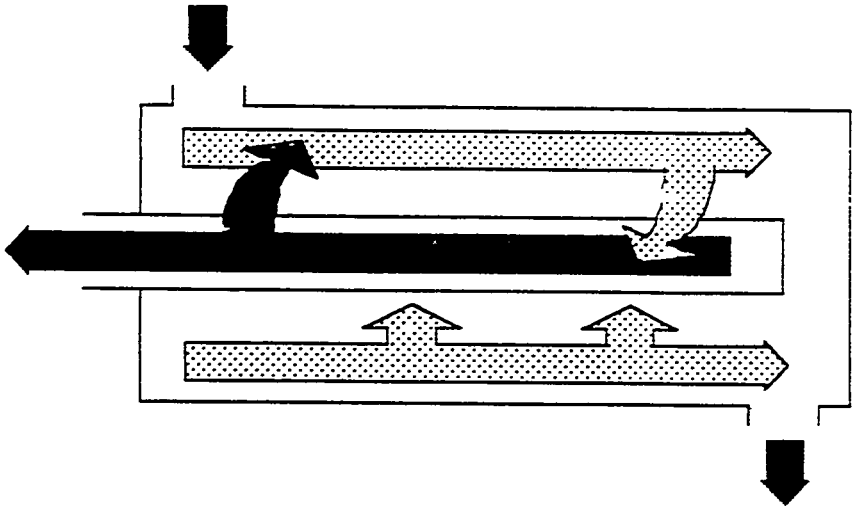

Figure 29. Graphical representation of H_2 flow patterns in the cocurrent and countercurrent membrane reactor configurations.

H_2 separation provides the best enhancement of the conversion in the membrane reactor. Theoretically, it is possible to get almost 100% conversion in a membrane reactor with such a membrane and a pure hydrogen on the permeate side. However, if the membrane with an infinite selectivity is used in the design of the membrane reactor surface area requirements for the membrane module increase dramatically thus making such a module commercially unacceptable.Therefore, even the high selectivities are required for the design of the membrane reactor an infinite selectivity of the membrane may not be justified from the economical standpoint.

Based on a good prediction ability of the developed model for the membrane reactor it was possible to use it for the optimization of the membrane reactor process of H_2S decomposition. The conversion in the membrane reactor is primarily affected by the membrane selectivity and pressure. Generally the membrane selectivity is difficult to control while the pressure in the membrane reactor system can be changed.

Modelling results for the decomposition of pure H_2S in the membrane reactor with the membranes of different selectivity for the H_2 separation are presented in Figure 30. When the permeate side pressure is fixed at 1 atm the conversion of H_2S cannot exceed a certain limit even when the membrane with very high selectivity (100 times the Knudsen selectivity) is used. The conversion is limited by the counterdiffusion of hydrogen from the permeate to the reaction side of the membrane reactor. Eventually, the partial pressures on the permeate and reaction sides become equal and further increase in the conversion is impossible. Therefore, the membrane selectivity itself does not provide high degree of the conversion in the membrane reactor.

The conversion can be increased if in addition to a highly selectivite membrane the pressure on the permeate side is lowered. Low pressure on the permeate side prevents the equilibration of the H_2 partial pressures on the permeate and reaction sides of the membrane reactor. In an ideal case the pressure on the permeate side should be zero to provide 100% conversion. When the pressure on the permeate side is lowered to 0.01 atm a considerable increase in the conversion is observed (Figure 31). Even when the permeate side pressure is so low the conversion does not reach even a 90% value. It is interesting to note that the conversion at the stage cut equal to 0.8 exceed the equilibrium conversion at the low pressure side of the membrane reactor. Thus, the excess pressure on the reaction side of the membrane reactor (7.8

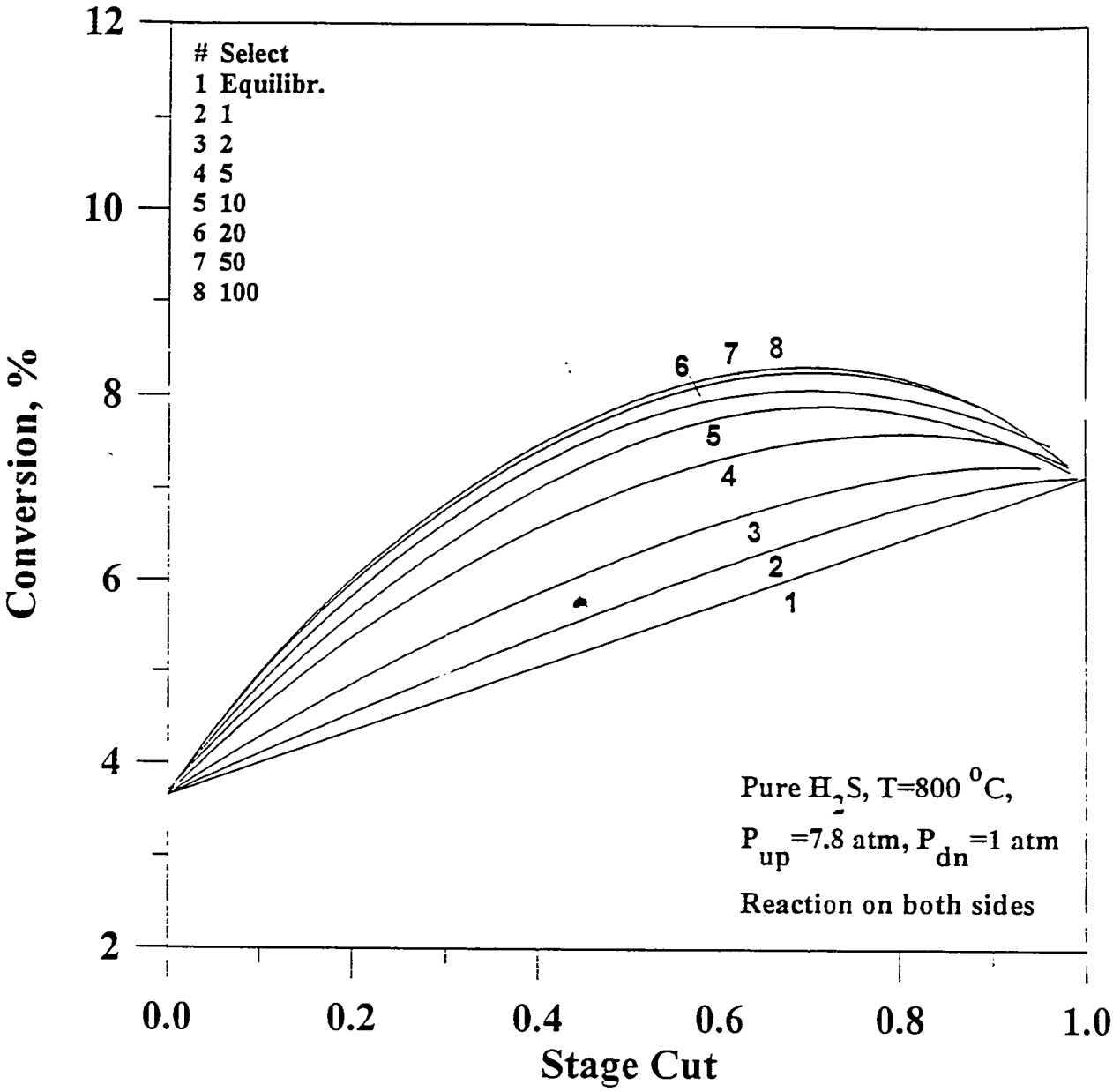

Figure 30. Conversion of pure H_2S in the membrane reactor at different membrane selectivities (p_{dn}=1 atm).

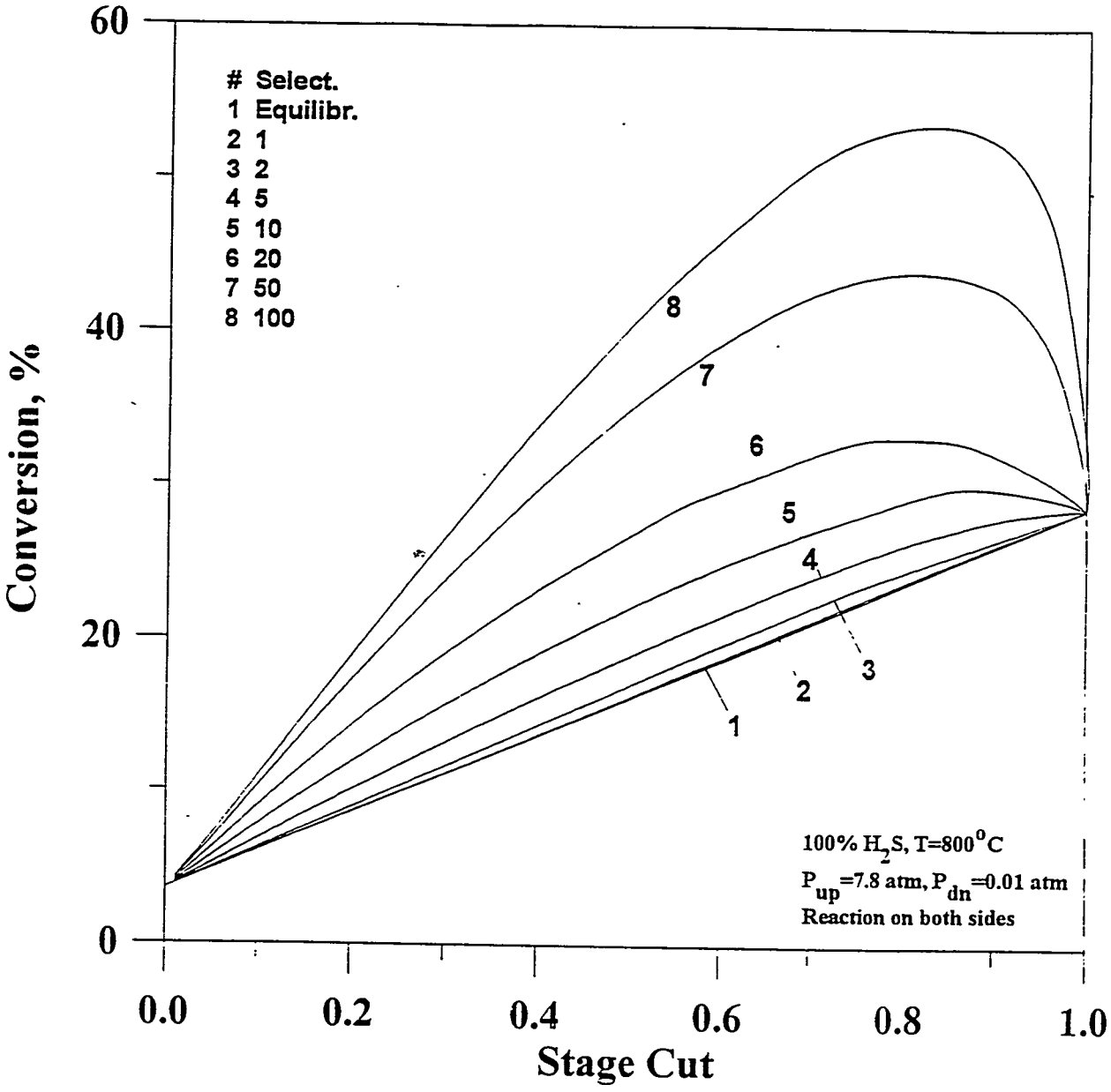

Figure 31. Conversion of pure H_2S in the membrane reactor at different membrane selectivities (p_{dn}=0.01 atm).

atm) allows the conversion to exceed the equilibrium conversion at the low pressure side.

Similar calculations were performed for the feed mixture with 500 ppm concentration of H_2S (Figures 32-33). The downstream pressure fixed at 1 atm prevented an increase in the conversion above 54% value. When the pressure at the permeate side was lowered to 0.01 atm the conversion increased up to 93% which is a very high value. This value is only slightly higher than the 91% equilibrium conversion that can be reached at the pressure equal to 0.01 atm in the conventional packed-bed reactor. The advantage of the membrane reactor however is that the 93% conversion was achieved at $\theta=0.1$. Therefore, ten times lesser volume of the feed has to be processed at low pressure in the membrane reactor than in the packed bed reactor in which 100% of the feed would be reacted at 0.01 atm.

It is possible in principle to achieve high conversion of H_2S in the membrane reactor if a combination of a highly selective membrane and a low pressure on the permeate side is utilized in the membrane reactor. For the IGCC applications even $\theta=0.1$ is probably too high to have a commercially efficient process.

5.7 Comparison of the packed bed and membrane reactors

For evaluation of the membrane reactor performance it is essential to have an adequate comparison of the conversion in the membrane reactor with the conversion in the packed bed reactor. However, it is extremely difficult to make an adequate comparison. The results of such comparisons can depend on various assumptions made. Therefore, a preliminary attempt is being made here to provide some comparison between the membrane reactor and the conventional packed-bed reactor. Further refinement of such comparison may be needed.

The pressure gradient across the membrane is always present in the membrane reactor to ensure the selective removal of one of the reaction products from the reaction zone. At different pressures, the conversion of the volume expansion reactions is different due to the effect of the pressure. Therefore, the conversion in the membrane reactor can not be compared simply with the conversion in the packed bed reactor with operation pressure equal to the operation pressure on the reaction side in the membrane reactor. However, an adequate comparison between the membrane reactor and the packed bed reactor can be made if the notion

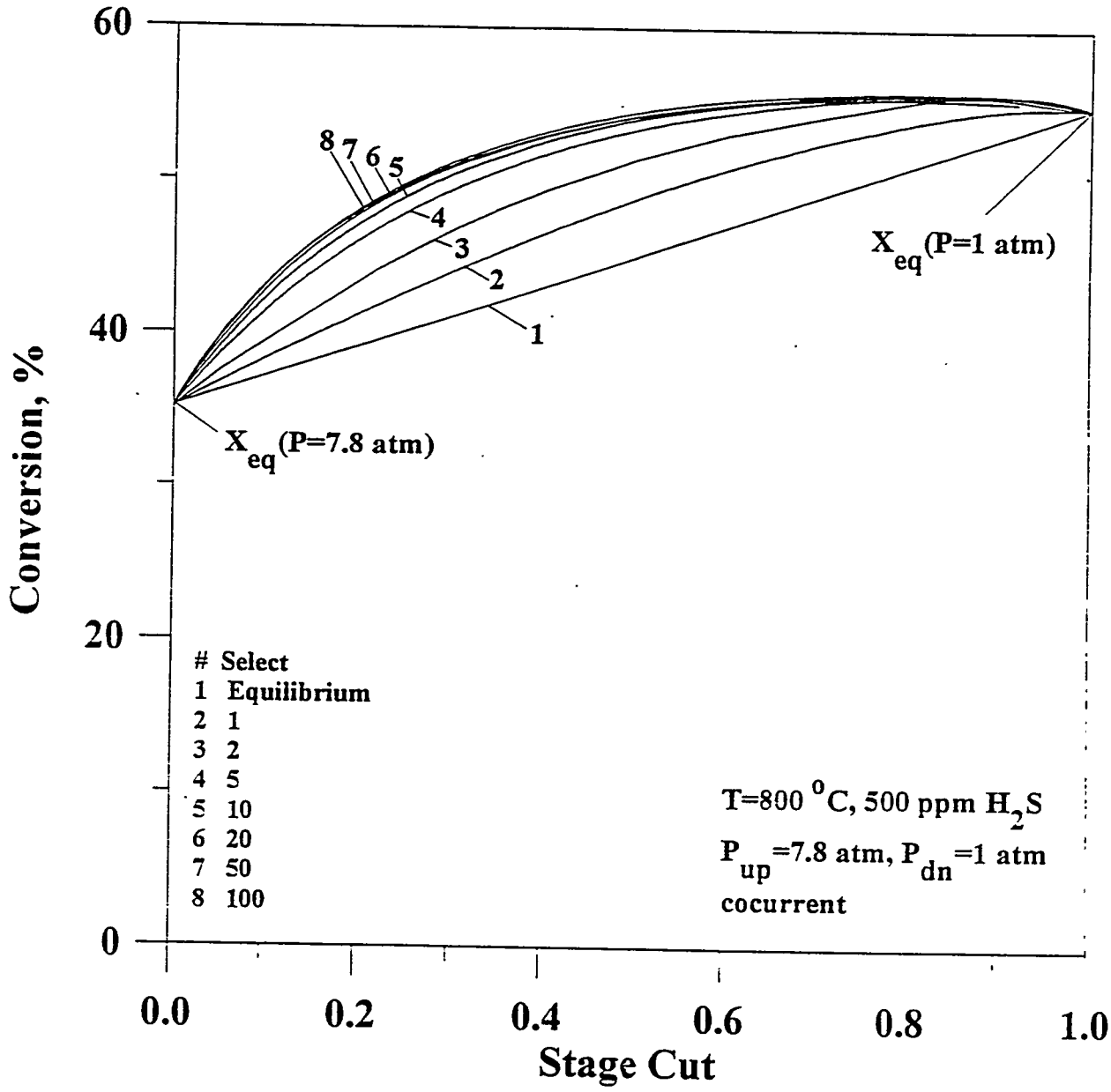

Figure 32. Conversion of 500 ppm H_2S gas mixture in the membrane reactor at different membrane selectivities (p_{dn}=1 atm).

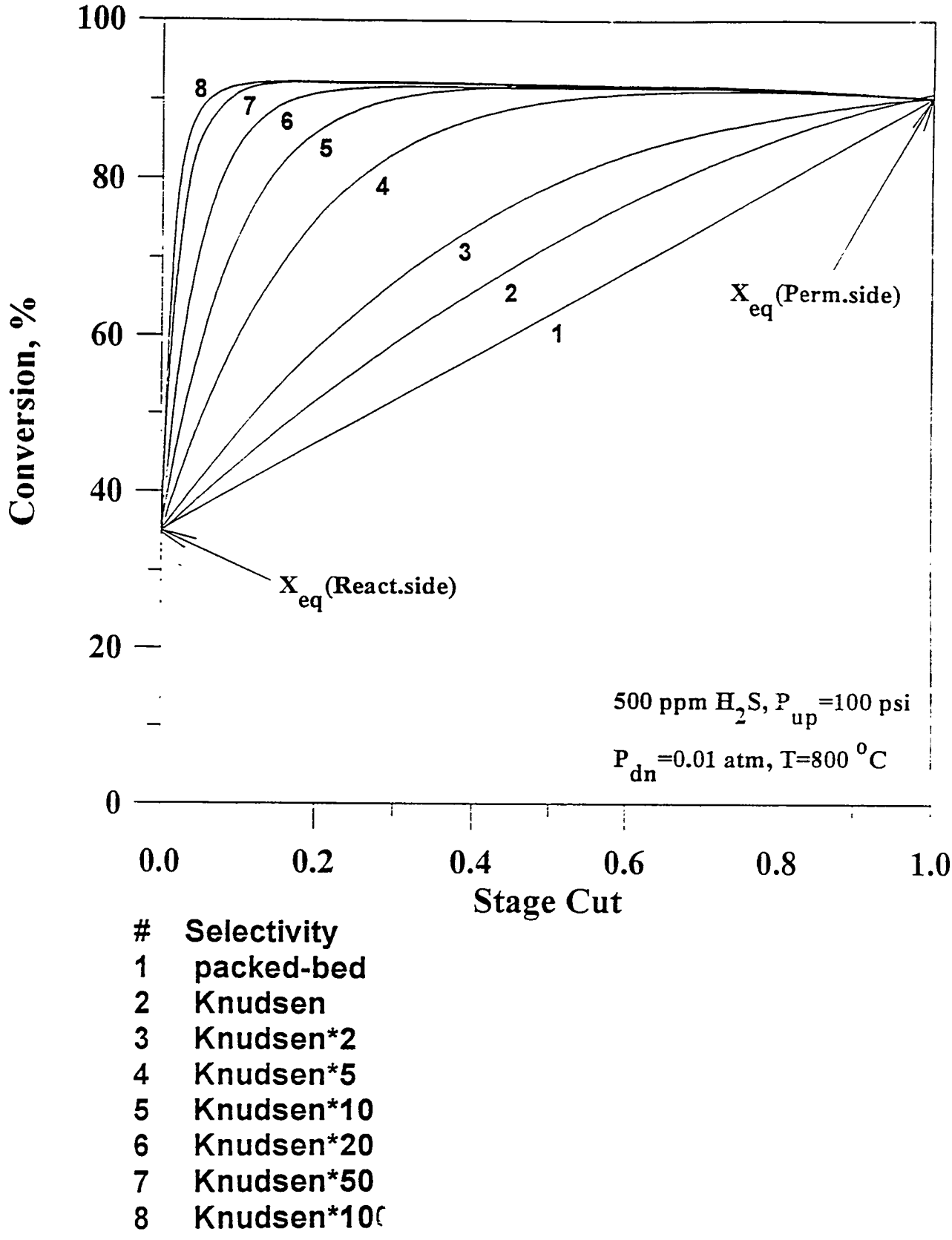

Figure 33. Conversion of 500 ppm H_2S gas mixture in the membrane reactor at different membrane selectivities (p_{dn}=0.01 atm).

of the stage cut is used. In this case the packed bed reactor similar to the membrane reactor is a reactor with two tubes operating at different pressures equal to the pressures on the reaction and permeate sides of the membrane reactor respectively. It is possible to assume that the fraction of the gas processed in each of the tubes is equal to θ in the tube with low pressure and $(1-\theta)$ in the tube with high pressure. Therefore, the total conversion in the packed bed reactor corresponding to the membrane reactor can be calculated in accordance with

$$X_{p-b}[\theta] = \theta X_{P_{down}} + (1-\theta) X_{P_{up}} \qquad (54)$$

Other more refined approaches to the comparison of the conversion in the packed bed and membrane reactors are also possible based on the energy balance. They are not considered in the present report.

Equation 54 is applicable to the ideal system in which the permeation from the reaction side to the permeate side occurs only within an isothermal region. If a temperature profile along the membrane reactor exists then corrections should be made to account for the permeation in the cold parts of the membrane reactor. For the experimental installation used in the experiments there are three temperature zones - zone I at room temperature, zone II at $T=775\pm10$ °C (mean temperature), and zone III at room temperature. In the cocurrent configuration in the zone I permeation of unreacted H_2S occurs to the permeate side of the membrane reactor. In the zone II H_2 produced during the course of the reaction is being selectively removed from the reaction side of the membrane reactor providing the shift in the reaction equilibrium. The process of the H_2 removal however is accompanied by simultaneous permeation of H_2S and S_2 due to low selectivity of the Vycor glass membrane. In the zone III the product mixture on the reaction side permeate selectively to the permeate side. The permeation is not accompanied by the simultaneous reaction in this case.

If the amounts of permeate in zones I and II equals to 2/3 of the total permeate flow and the permeate in zone III is equal to 1/3 then the modified version of Equation 54 can be written

as

$$X_{p\text{-}b}[\theta] = \frac{\theta\,(2X_{P_{down}} + X_{P_{up}})}{3} + (1-\theta)\,X_{P_{up}} \qquad (55)$$

Depending on the geometry of the particular membrane reactor and the temperature dependence of the permeability the fractions 2/3 and 1/3 should be recalculated each time.

The comparison between the experimental data on the total conversion in the membrane reactor and the conversion in the packed bed reactor calculated in accordance with Equation 55 is presented in Figures 34. The temperature of the packed bed reactor was assumed to be equal to 775 °C which is a mean temperature in the zone II of the membrane reactor.

It can be seen from Figure 34 that the equilibrium conversion predicted in accordance with Equation 55 changes similarly as the conversion in the membrane reactor for all of the gas compositions used in the study as well as for different pressures on the reaction side. The error in the calculated value of the conversion in the membrane reactor increases when the concentration of H_2S in the feed decreases due to sensitivity problems associated with the GC analysis. The highest experimental scatter in the results for the H_2S conversion was observed for the feed with the concentration of H_2S concentration equal to 500 ppm. At this low concentrations the GC detector system operates almost at its detection limit. Based on the present assumptions, it can be seen that the conversion in the membrane reactor is lower than the conversion in the packed bed reactor for all of the studied pressure and feed compositions. The predicted values of the conversion in the packed bed reactor are somewhat higher than the experimentally observed values for the conversion in the membrane reactor apparently due to the overestimation of the mean temperature in the membrane reactor.

Based on the present assumptions, the conversion of H_2S in the membrane reactor with Vycor glass membrane did not exceed the conversion in the packed-bed reactor operating under the similar process conditions because of the low membrane selectivity.

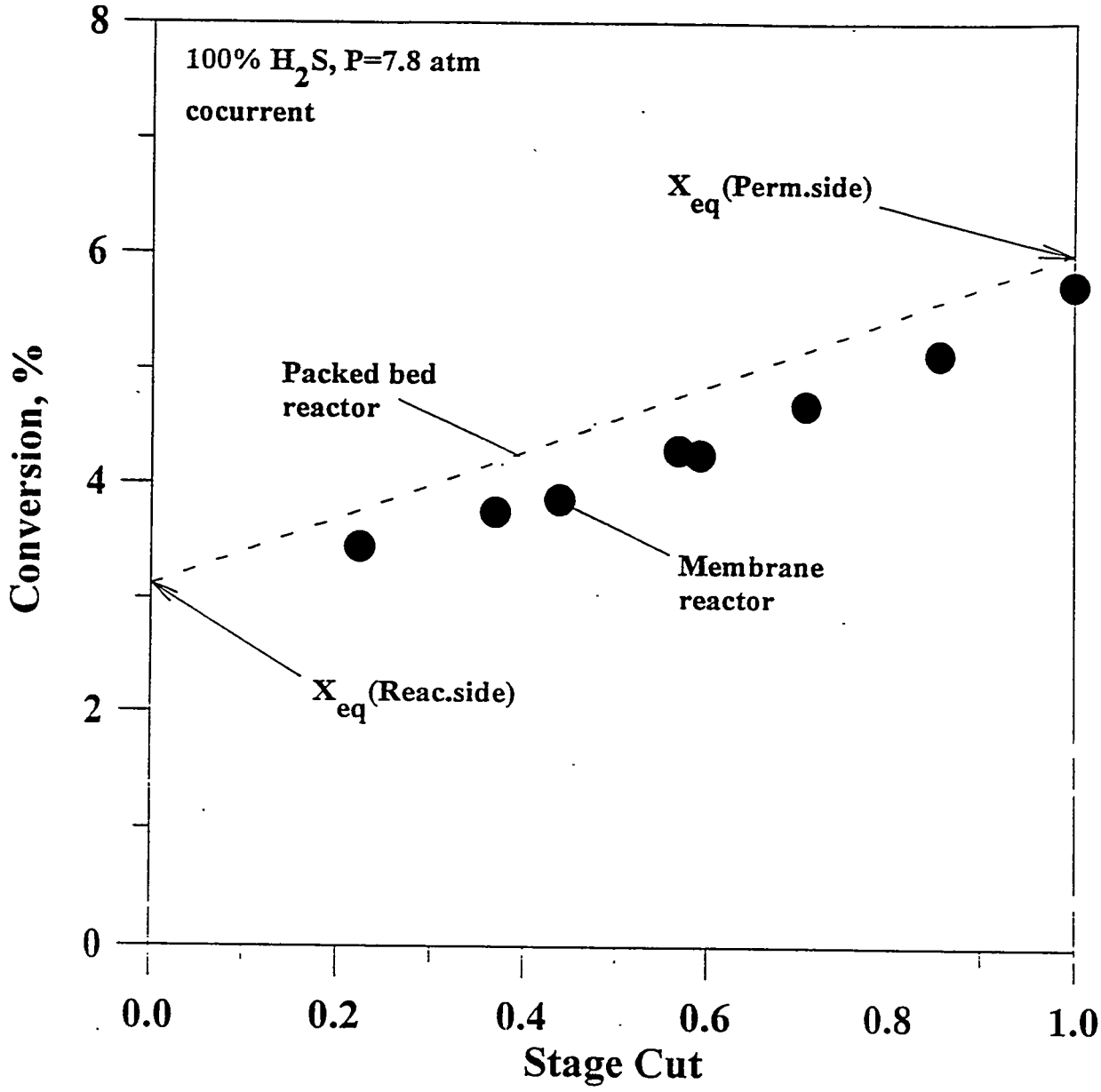

Figure 34(a). Comparison of the total conversion in the packed bed and membrane reactors (100% H_2S).

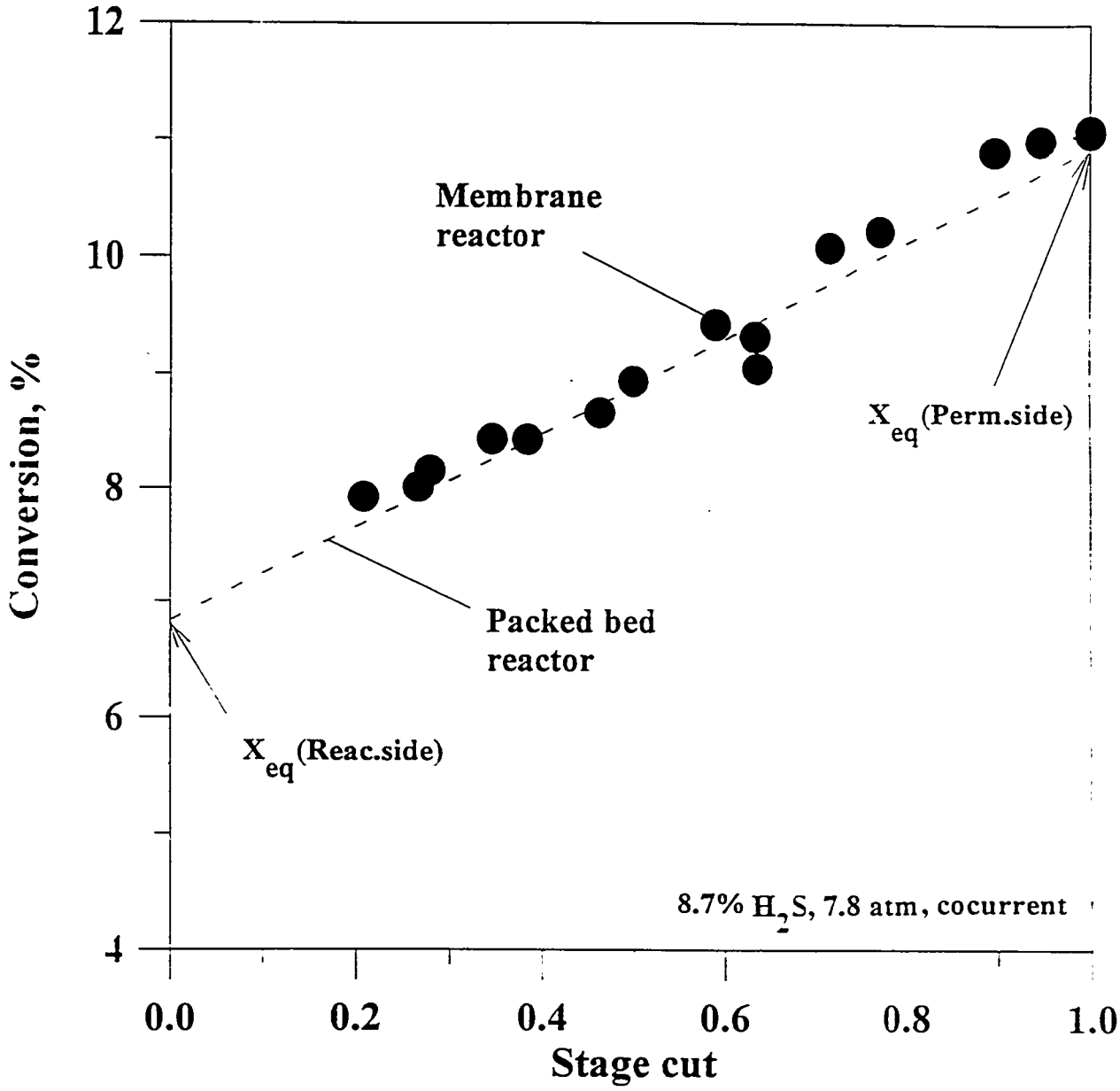

Figure 34(b). Comparison of the total conversion in the packed bed and membrane reactors (8.6% H_2S).

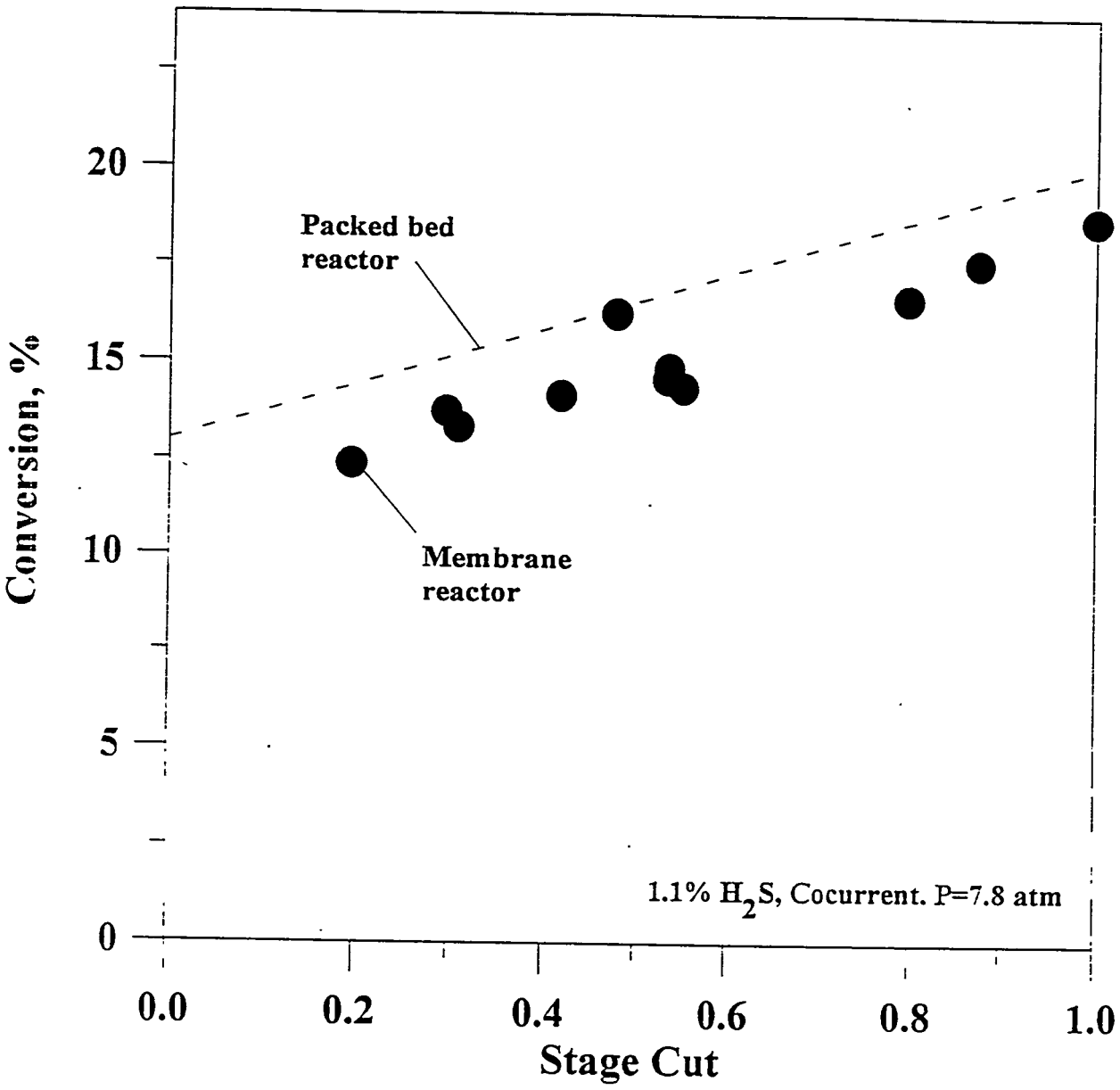

Figure 34(c). Comparison of the total conversion in the packed bed and membrane reactors (1.1% H_2S).

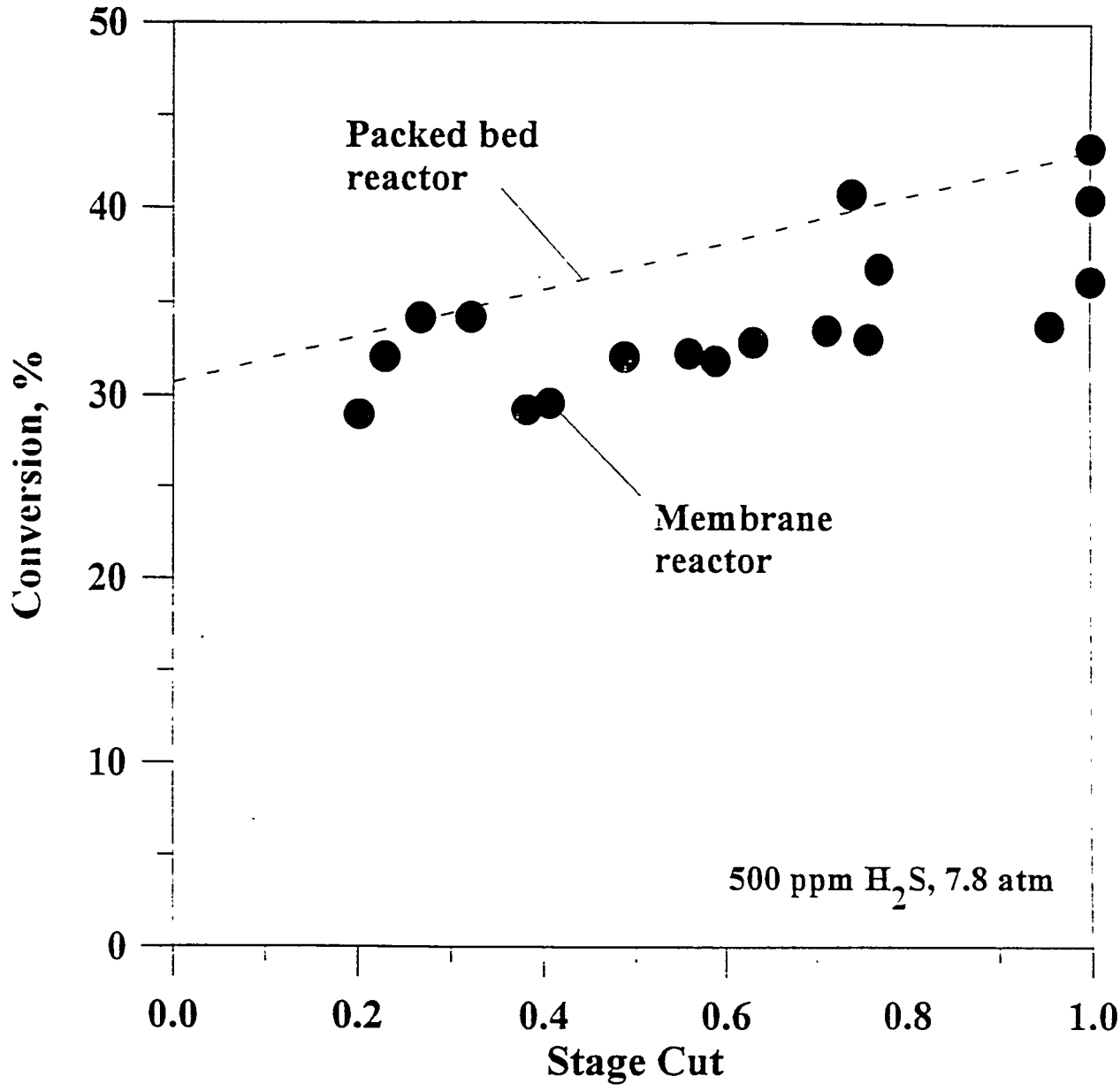

Figure 34(d). Comparison of the total conversion in the packed bed and membrane reactors (500 ppm H_2S).

VI. CONCLUSIONS

Experimental and theoretical analysis of the membrane reactor system for the reaction of H_2S decomposition was presented. The total conversion in the packed bed membrane reactor was studied as a function of the pressure ratio, the feed concentration, and the stage cut. The comparison between the packed bed reactor and the membrane reactor was made. The following conclusions are made.

* Feasibility of the membrane reactor process for decomposition of hydrogen sulfide was demonstrated.
* Experimental study of hydrogen sulfide decomposition in the membrane reactor was completed.
* Membrane reactor process was developed for the H_2S decomposition in the IGCC hot gas streams and experimentally tested in a wide range of process variables.
* A generalized model was developed for the simulation of the high temperature membrane reactor. It is predicted that the conversion in the membrane reactor may increase up to 90% if the highly selective membranes are employed in the membrane reactor design.
* The membrane reactor process is probably inefficient for the high temperature H_2S cleanup from the IGCC gas mixture.
* Knudsen selectivity is insufficient to yield an increase of the H_2S conversion in the membrane reactor.
* For an adequate comparison between the packed bed and the membrane reactor the shift in the reaction equilibrium on the permeate side should be accounted. An increase in the conversion for the volume expansion reactions may be due to the lowering of the pressure or dilution with the sweep gas on the permeate side of the membrane reactor.
* Permeability and selectivity of the molecular-sieve membrane were studied at elevated temperatures. The molecular-sieve glass membranes were found unstable at temperatures higher than 300 °C even though extremely high selectivities were observed at low temperatures.
* The Vycor glass silica membrane exhibited catalytic properties for the H_2S decomposition reaction.

* The experimental information collected during this project enabled, for the first time, develop a molecular-kinetic theory of gas diffusion in molecular-sieve gas separation membranes. It is now possible to predict on a quantitative basis the permeability and selectivity of the porous membranes and calculate their selectivity properties. This model can be used to make estimates of the possibility of utilizing the molecular-sieve membranes in different processes and systems without even necessity to prepare such a membrane.

* One of the findings during the project is that the porous membranes (e.g. Vycor glass) provide such a high surface area that the external mass transfer resistance is almost nonexistent for such catalytic systems. Compared to conventional packed bed reactors membrane based reactor systems may provide very efficient way of the reactor design. The surface areas of the membranes are very high (up to 500 m^2/g) and coupled with high transmembrane fluxes may considerably decrease the amounts of catalysts required for catalytic processes. For example no external mass transfer limitations were observed in the H_2S decomposition reaction inside the porous Vycor glass membrane while for the packed bed reactor some decrease of the conversion was observed due to the external mass transfer limitations.

VII. RECOMMENDATIONS

7.1 Molecular-sieve glass membranes

It was demonstrated that the molecular-sieve porous membranes are superior to any type of the gas separation membranes including polymeric, liquid, and porous (Knudsen type). The microporous membranes provide a unique combination of high productivity and selectivity. The selectivity factors observed in this membranes (10000 for He/CH_4) and high permeability (1000 Barrer for He) undoubtedly put this membrane among the best known commercial gas separation membranes. Apparently due to excessive Gibbs free energy the membranes were found unstable at temperatures higher than 300 °C. The study however demonstrated tremendous perspectives for utilization of the molecular-sieve membranes for the gas separation applications at temperatures below 300 °C, for example in petrochemical industry for separation of H_2 from hydrocarbons.

The thermal instability of the molecular-sieve glass membranes must be thoroughly investigated. Without understanding underlying reasons for the collapse of the porous structure at high temperatures it would be difficult to develop high temperature membranes.

Without a doubt future developments in the field of membrane gas separations lie in the development of microporous or dense inorganic membranes.

7.2 Membrane reactor

Comprehensive mathematical and experimental analysis of the membrane reactor demonstrated that under certain conditions the membrane reactor may provide high conversions at low stage cuts. These conditions include high membrane selectivity (100 times the Knudsen selectivity) and low pressure on the permeate side. It is not recommended to use sweep gas in any parts of the membrane reactor because hydrogen in the permeate will be diluted and could not be utilized. The conversion in the membrane reactor can increase only if highly selective membrane is used such as silica, Pd, or Pt and low pressures on the permeate side are kept. The conversion can be further increased if simultaneously a higher pressure on the reaction side is applied to lower the pressure ratio and to improve the membrane separation performance. Membranes with the Knudsen type of selectivity can not be used in the design of the membrane

reactor because even though they enable separation of H_2 from the reaction stream the extent of separation is not sufficient to provide significant increase of the conversion.

The membrane reactors are not well suited for the decomposition of low concentrations of H_2S in the IGCC gas streams. High content of H_2 in the feed suppresses the conversion of H_2S preventing successful conversion of H_2S in the membrane reactor. The feed stream, in principle, can be cleaned from H_2 by using the same highly selective Pd or Pt membranes. The surface area requirements for the process however are not clear because generally high levels of purification in membrane processes can be achieved only at a price of high membrane surface area.

The membrane reactor process seems perspective in the processes with high contents of the reactant material. It can be used in gas phase reactions the components of which is difficult to separate. The membrane reactor unit operation in this case provides simultaneous reaction and separation in a single technological unit.

One of the systems where the membrane reactors can be used for the decomposition of H_2S separated from natural gas. The membrane reactor may provide a one step process for the decomposition of H_2S into sulfur and hydrogen. It is a well known fact that a significant number of oil and gas fields are not being developed because of the high content of sulfuric components.

The membrane reactor technology is still under development and coupled with difficulties due to extreme conditions encountered in the industrial reaction processes. Further development of the new and improved membranes will allow one to design a highly selective and effective membrane reactors. Membrane reactors can not be commercialized with the existent commercial inorganic membranes.

Acknowledgements

The authors would like to acknowledge the financial support for this work provided by the U.S.Department of Energy, Morgantown Energy Technology Center, Morgantown, WV, under Contract No. DE-AC21-89MC26372. The authors also would like to acknowledge V. Venkataraman and D. Cicero for fruitful discussions and valuable comments during the course of the project.

REFERENCES

1. W.E. Pfefferle, U.S.Pat. 3,290,406 (1966)
2. J.E. Koresh, A. Sofer, The carbon molecular sieve membranes. General properties and the permeability of CH_4/N_2 mixture, Sep.Sci.Technol., 22 (1987) 973-982
3. A.B. Shelekhin, A.G. Dixon, Y.H. Ma, Adsorption, permeation, and diffusion of gases in microporous membranes. II. Permeation of gases in microporous glass membranes. J.Mem.Sci. 75 (1992) 233-244
4. D.J. Edlund, W.A. Pledger, Thermolysis of hydrogen sulfide in a metal-membrane reactor, J.Mem.Sci., 77 (1993) 255-264
5. V.M. Gryaznov, V.S. Smirnov, The reactions of hydrogenations on membrane catalysts, Russ.Chem.Rev. 43 (1974) 821-834
6. V.I. Lebedeva, V.M. Gryaznov, Effect of hydrogen removal through a membrane catalyst on the dehydrogenation of n-hexane, Izv.Akad.Nauk SSSR, Ser.Khim. 3 (1981 611-613
7. A.P. Mishchenko, M.E. Saryolova, V.M. Gryaznov, V.S. Smirnov, N.R. Roshan, V.P. Polyakova, Hydrogen permeability and catalytic activity of membranes made of palladium-copper alloys in relation to the dehydrogenation of 1,2-cyclohexanediol, Izv.Akad.Nauk SSSR, Ser.Khim., 7 (1977) 1620-1622
8. V.M. Gryaznov, Hydrogen permeable palladium membrane catalysts. An aid to the efficient production of ultra pure chemicals and pharmaceuticals, Plat.Met.Rev. 30 (1986a) 68-72
9. K. Mohan and R. Govind, Analysis of cocurrent membrane reactor, AIChE J., 32 (12) (1986) 2063.
10. N. Itoh, A membrane reactor using palladium, AIChE Journal, 33 (1987) 1576-1578
11. N. Itoh, W.-C. Xu, K. Haraya, Basic experimental study on palladium membrane reactors, 66 (1992) 149-155
12. S. Uemiya, N. Sato, H. Ando, T. Matsuda, E. Kikuchi, Steam reforming of methane in a hydrogen-permeable membrane reactor, Appl.Catal., 67 (1991) 223-230

13. D.J. Edlund, W.A. Pledger, Catalytic platinum-based membrane reactor for removal of H_2S from natural gas streams, submitted, J.Mem.Sci.

14. T. Okubo, K. Haruta, K. Kusakabe, S. Morooka, H. Anzai, S. Akiyama, Equilibrium shift of dehydrogenation at short space-time with hollow fiber ceramic membrane, Ind.Eng.Chem.Res. 30 (1991) 614-616

15. O. Shinji, M. Misono, Y. Yoneda, The dehydrogenation of cyclohexane by the use of a porous-glass reactor, Bull.Chem.Soc.Jpn., 55 (1982) 2760-2764

16. Z.D. Ziąka, R.G. Minet, T.T. Tsotsis, A high temperature catalytic membrane reactor for propane dehydrogenation, J.Mem.Sci., 77 (1993) 221-232

17. T. Kameyama, M. Dokiya, M. Fujishige, H. Yokokawa, K. Fukuda, Production of hydrogen sulfide by means of selective diffusion membranes, Int.J.Hydrogen Energy, 8 (1983) 5-13

18. T. Kameyama, M. Dokiya, M. Fujishige, H. Yokokawa, K. Fukuda, Possibility for effective production of hydrogen from hydrogen sulfide by means of a porous Vycor glass membrane, Ind.Eng.Chem.Fundam. 20 (1981) 97-99

19. A.B. Shelekhin, A.G. Dixon, Y.H. Ma, Theory of gas diffusion and permeation in molecular-sieve membranes, AIChE J., In print, 1994

20. A.B. Shelekhin, A.G. Dixon, Y.H. Ma, Adsorption, diffusion and permeation of gases in microporous membranes. III. Applications of percolation theory to interpretation of porosity, tortuosity, and surface area in microporous glass membranes. J.Mem.Sci., 83 (1993) 181-198

21. C.N. Satterfield, T.K. Sherwood, The role of diffusion in catalysis, Addison-Wesley Publishing Company, Inc., Reading, MA, 1963

22. R.L. June, A.T. Bell, D.N. Theodorou, Molecular dynamics study of methane and xenon in silicalite, J.Phys.Chem., 94 (1990) 8232

23 R.L. June, A.T. Bell, D.N. Theodorou, Transition-state studies of xenon and SF_6 diffusion in silicalite, J.Phys.Chem., 95 (1991) 8866

24. D.L. Roberts, I.C. Abraham, Y. Blum, J.D. Way, Gas separation with glass membranes, Final Report, DOE Contaract, No. DE-AC21-88MC25204, 8 May 1992

25. J. Xiao, J. Wei, Diffusion mechanism of hydrocarbons in zeolites - II. Analysis of experimental observations, Chem.Eng.Sci., 47 (1992) 1143

26. J.D. Cox, G. Pilcher, Thermochemistry of organic and organometallic compounds, Academic, London, 1970

27. W.L. McCabe, J.C. Smith, Unit operations of chemical engineering, The Tan Chiang Book Co., Taipei, Taiwan, 1976

28. V.E. Kaloidas, N.G. Papayannakos, Kinetic studies on the catalytic decomposition of hydrogen sulfide in a tubular reactor, Ind.Eng.Chem.Res. 30 (1991) 345-351

29. P.A. Tesner, M.S. Nemirovskii, D.N. Motyl, Kinetics of the thermal decomposition of hydrogen sulfide at 600-1200 °C, Kinetics and Catalysis, 31 (1991) 1081-1083

30. V.E. Kaloidas, N.G. Papayannakos, Kinetics of thermal, non-catalytic decomposition of hydrogen sulphide, 44 (1989) 2493-2500

31. M. Bhandarkar, A.B. Shelekhin, A.G. Dixon, Y.H. Ma, Adsorption, permeation, and diffusion of gases in microporous membranes. I. Adsorption of gases on microporous glass membranes. J.Mem.Sci., 75 (1992) 221-231

32. A.B. Shelekhin, A.G. Dixon, Y.H. Ma, Adsorption, permeation, and diffusion of gases in microporous membranes. III. Application of percolation theory to interpretation of porosity, tortuosity, and surface area in microporous glass membranes. J.Mem.Sci., 83 (1993) 181-198